Title
Phase Separation Phenomena in Hybrid Lipid/Block Copolymer Biomembranes

Author
Hamada, Naomi

Publication Date
2022

Peer reviewed|Thesis/dissertation

Phase Separation Phenomena in Hybrid Lipid/Block Copolymer Biomembranes

By

NAOMI HAMADA
DISSERTATION

Submitted in partial satisfaction of the requirements for the degree of

DOCTOR OF PHILOSOPHY

in

Chemical Engineering

in the

OFFICE OF GRADUATE STUDIES

of the

UNIVERSITY OF CALIFORNIA

DAVIS

Approved:

_____

Marjorie L. Longo, Chair

_____

Roland Faller

_____

Volkmar Heinrich

Committee in Charge

2022

Acknowledgements

This work could not have been accomplished without the guidance and encouragement of many people, and I am immensely thankful for them all.

First, I would like to acknowledge my advisor, Dr. Marjorie Longo. Thank you for the support, scientific input, and professional guidance over the past several years—none of this would have been possible without you. I would also like to thank Dr. Roland Faller and Dr. Volkmar Heinrich for being part of both my qualifying exam and dissertation committees, as well as for their input over the past few years. Thank you to my graduate school colleagues for your friendship and support, especially Dr. Sukriti Gakhar and Conary Meyer. I would also like to thank the DEB, especially Dr. Denneal Jamison-McClung, for encouraging me to explore new professional paths.

I would also like to thank my family. To my parents, Charles and Elizabeth Hamada, especially, thank you for encouraging me to develop my abilities to the fullest. Thank you also for encouraging and supporting me throughout many, many years of education. To my sister Natalie Hamada, thank you for your support and for being there to understand the graduate school experience too.

To Joseph Wan, thank you for patiently listening to me talk about this dissertation for what I am sure has felt like a very large number of years. Most of all, thank you for supporting and loving me as a person with your words and actions every day. I could not have done this without you.

Dissertation Abstract

Phase separation phenomena in hybrid lipid/block copolymer biomembranes

Lipids and amphiphilic block copolymers can be combined to form hybrid lipid/block copolymer membranes, which leverage both the biocompatibility of lipids and the tunability and mechanical stability of block copolymers. While lipid vesicles and nanoparticles have demonstrated clear success as drug delivery vehicles and hosts for reconstituted membrane proteins, the addition of block copolymers introduces the potential for further functionality, such as stimulus responsiveness and extended particle longevity. Multicomponent lipid biomembranes have been widely observed to phase separate into domains enriched in each component, and an understanding of the phase behavior of these membranes is crucial toward such applications. The presence of phase separation has been observed to impact the success of both membrane protein reconstitution and drug delivery. However, further work is necessary to investigate the phase behavior of hybrid lipid/block copolymer membranes.

In this work, we explore phase separation phenomena in hybrid lipid/block copolymer membranes. First, we mapped a phase diagram for the phospholipid DPPC and polybutadiene-block-polyethylene oxide (PBdPEO950) using fluorescence spectroscopy. Analysis of trends in the temperature dependence of membrane fluidity and hydration allowed solid-to-fluid phase transition temperatures to be identified and an apparent phase diagram to be mapped.

Fluorescence spectroscopy techniques were additionally extended to study phase separation phenomena in cholesterol-containing lipid POPC/egg sphingomyelin (SM) and hybrid

PBdPEO/egg SM membranes. Temperature break-point (T_{break}) values for nanometer scale vesicles were determined by decomposition of emission spectra of the fluorescent probe laurdan into three lognormal curves. T_{break} values were in good agreement with the one- to two-phase transition temperature observed by microscopy for micron-scale giant unilamellar vesicles. Low miscibility of PBdPEO and egg SM were observed, as well as stronger partitioning of cholesterol into PBdPEO than into POPC. Finally, we investigated the effects of incorporating a carboxyl-terminated PBdPEO copolymer into hybrid vesicles. T_{break} values displayed dependence on pH, Debye length, and vesicle composition consistent with an electrostatic repulsion contribution to vesicle phase behavior. Additionally, at Debye lengths comparable to those at physiologically relevant ionic strength, T_{break} at pH 5.9 was observed to be slightly higher than at pH 7.0 for vesicles containing significant amounts of carboxyl-terminated PBdPEO. Such electrostatic effects may have the ability to drive membrane phase separation in response to pH drops—such as those observed after endocytosis—in physiologically relevant conditions, suggesting the utility of such materials for drug delivery.

Table of Contents

Chapter 1 - Introduction

1.1 Lipid and hybrid biomembranes

1.1.1 Lipid biomembranes and single-component biomembrane properties

Lipid biomembranes play a crucial role in the structure and function of cells. In this biological context, lipid membranes act as an envelope for the contents of the cell. While the membranes themselves consist of a variety of lipids (including both phospholipids and sphingolipids [1]) and sterols, they are also richly decorated with sugars and proteins, as shown in the schematic in Figure 1. These proteins commonly span the hydrophobic thickness of the membrane; in this case, they are referred to as membrane proteins. Structurally, the cell membrane serves as a barrier between the interior contents and exterior environment of each cell, limiting the influx and exit of ions and large molecules. Functionally, cell membranes and the proteins residing within play roles in signal transduction and energy pathways [2].

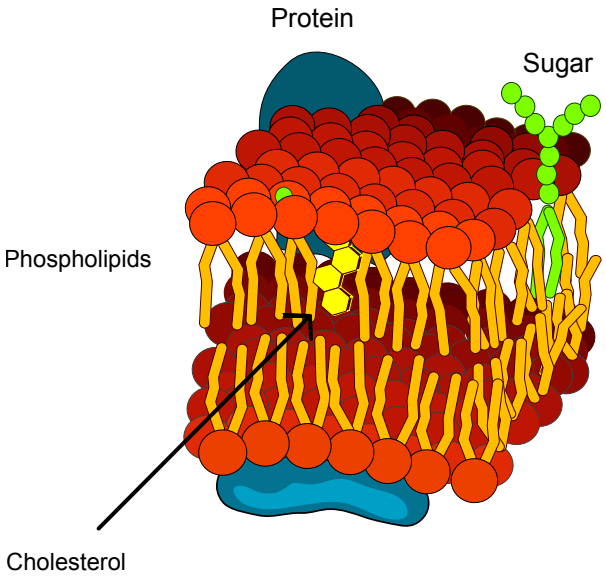

Figure 1. Schematic of some of the major components of a cell membrane. Modified from Wikipedia (https://creativecommons.org/licenses/by-sa/3.0/).

The bilayer structure of lipid membranes arises from the amphiphilicity of individual lipid molecules. Each lipid molecule consists of a hydrophilic headgroup and a pair of hydrophobic fatty acid chains (the "tails"). In the presence of water, this amphiphilic structure leads to self-assembly into a lipid bilayer driven by the hydrophobic effect.

Single-component lipid bilayers can exist in different phases, depending on the temperature and specific lipid structure. In the solid phase, often referred to as the gel or L_β phase, lipids are packed closely together, resulting in a strongly ordered structure with high rigidity and low lateral mobility. At a phase transition temperature specific to the given lipid species, the lipids undergo a transition from the solid phase to a less ordered fluid phase (the liquid crystalline or L_α phase), which displays decreased rigidity and high lateral mobility. Lipids existing in the solid phase at biologically relevant temperatures (i.e., ~20-50 ^oC) typically have saturated hydrocarbon tails, and lipids with longer hydrocarbon tails typically have greater phase transition temperatures. However, the presence of unsaturations (double bonds) in either or both of the fatty acid tails introduces a "kink" in the structure of the fatty acids. This disrupts the close packing associated with the solid phase and yields a lowered phase transition temperature, often well below room temperature.

The introduction of sterols (e.g., cholesterol) to a single-component lipid membrane strongly impacts the membrane phase behavior as well. Addition of sufficient amounts of a sterol to an L_β membrane results in a transition to the liquid ordered (L_o) phase, which displays significantly greater lateral mobility than the L_β phase, although the lipid tails still display closer packing and greater order than in the L_α phase [3].

1.1.2 Model membranes

Model membranes are commonly used to study specific properties of lipid membranes. Model membranes typically consist of a few well-defined components, allowing the investigation of specific questions in relative isolation. Two major types of model membranes include giant and large unilamellar vesicles (GUVs and LUVs).

Vesicles are spheres formed by lipid bilayers enclosing an aqueous volume. Unilamellar vesicles (Figure 2) are formed of a single lipid bilayer (as opposed to multilamellar vesicles, which consist of many bilayers stacked concentrically upon each other like the layers of an onion). GUVs and LUVs are distinguished by the vesicle diameter. GUVs are typically on the order of 1-100 µm in diameter, while LUVs range from ~100-1000 nm. GUVs are a common model membrane system when using microscopy to investigate the presence of domains in a membrane composed of a mixture of different lipids and/or sterols. LUVs, on the other hand, are typically too small to be observed in detail with a microscope. Instead, they are of interest because of their relevant size for both membrane protein reconstitution and drug delivery.

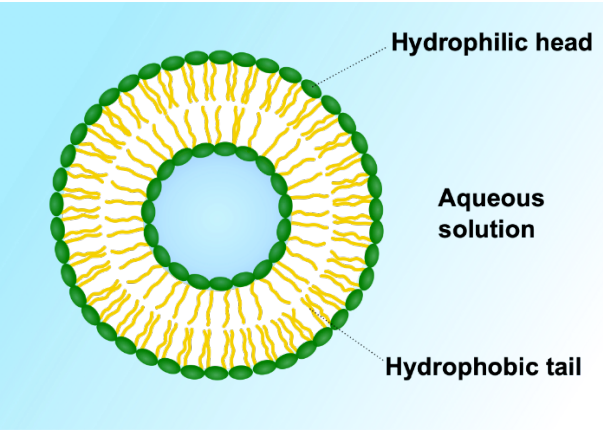

Figure 2. Schematic of a vesicle. While the image shown here depicts a unilamellar vesicle (consisting of a single lipid membrane), multilamellar vesicles consist of multiple concentric membranes, i.e., multiple lamellae. Image modified from Wikipedia (https://www.gnu.org/licenses/fdl-1.3.html).

1.1.3 Block copolymer membranes

To mimic the structure of lipid biomembranes, amphiphilic block copolymers have been of interest due to their similar ability to self-assemble into a bilayer-like structure. Block copolymers consist of at least two different "blocks" of repeating monomer units. An amphiphilic diblock copolymer consists of a block composed of hydrophobic monomers and a block composed of hydrophilic monomers. The ability of a particular block copolymer to form a bilayer is closely tied to the molecular weights of the hydrophilic and hydrophobic blocks. Block copolymers with a hydrophilic block composing roughly 35±10% of their total mass, comparable to the ratio for lipids, have been reported to be capable of forming polymer membranes [4]. Polymers with weight distributions falling outside of this range typically form either micelles or other aggregates.

A variety of block copolymers have been used to form membranes, including polydimethylsiloxane-block-polyethylene oxide (PDMS-PEO) [5,6] and polybutadiene-block-polyethylene oxide (PBdPEO) [7,8]. Block copolymers with a hydrophobic block with a low glass transition temperature, yielding a relatively fluid and disordered membrane at temperatures of biological interest, are often used for this purpose. The hydrophilic block PEO (also commonly referred to as polyethylene glycol, or PEG), is of especial interest for biological applications, based on the widespread use of PEG-bound lipids (PEG-lipids) to slow the opsonization of liposomal drug delivery vehicles [9].

The physical properties of block copolymer membranes have been observed to depend significantly on the block copolymer molecular weight. As the molecular weight of vesicle-forming block copolymers is increased, the thickness of the resulting membrane increases as well. Block copolymer membranes can be formed with thicknesses comparable to those of lipid

membranes (~5 nm) or much greater (20+ nm) [4]. Similarly, the lateral diffusion coefficient within the membrane [10] and membrane viscosity [11] have also been reported to increase as the polymer molecular weight increases.

1.1.4 Hybrid lipid/block copolymer membranes

Hybrid membranes formed of a combination of lipids and amphiphilic block copolymers have been of recent scientific interest, with the goal of leveraging the favorable characteristics of both lipid and block copolymer membranes—including the biocompatibility of lipid membranes and the tunability and chemical diversity of block copolymer membranes. Empirically, hybrid membranes have been observed to have favorable impacts when applied in certain biomedical or biological contexts. For example, incorporation of the membrane protein cytochrome bo_3 into hybrid vesicles composed of PBdPEO and the lipid palmitoyl oleoyl phosphatidylcholine (POPC) resulted in significant extension of the functional lifetime of the protein as compared to when vesicles composed of POPC alone were used [12]. Similarly, the yield of a mechanosensitive channel protein (MscL) via cell-free expression was greater when hybrid vesicles composed of a mixture of dioleoylphosphatidylcholine (DOPC) and PBdPEO were used rather than vesicles of only DOPC [13]. In this case, the authors observed that the area expansion modulus—which corresponds to the membrane interfacial tension—of hybrid vesicles was lower than that of lipid vesicles; in turn, this would reduce the energetic cost of bilayer expansion, perhaps facilitating the incorporation and subsequent structural integrity of the membrane protein [13,14]. Like multicomponent lipid membranes, hybrid membranes display composition- and temperature-dependent phase behavior, which will be further discussed in subsequent sections.

1.2 Multicomponent membrane phase behavior

1.2.1 Phase separation in lipid and hybrid vesicles

The cell membrane consists of a variety of sterols, low melting temperature, and high melting temperature lipids. Model membranes of such mixtures often display separation into phases enriched in each lipid component, with the lipid species tending to be in the more ordered phase partitioning away from lipids in the less ordered phase. One widely studied example of a phase-separating lipid mixture is DOPC, dipalmitoylphosphatidylcholine (DPPC), and cholesterol, the ternary phase diagram of which contains regions of coexisting solid, liquid disordered, and/or liquid ordered phases [15]. In comparison, two-component membranes consisting of a low T_m and a high T_m lipid typically display regions of coexisting solid and fluid phases enriched in the high T_m and low T_m lipids, respectively.

The incorporation of cholesterol into hybrid membranes has also been explored to a relatively limited extent, despite the importance of cholesterol in cell membranes and the frequent inclusion of cholesterol as a significant component of lipid-based drug delivery vehicles. The addition of 5 mol% cholesterol to PDMS- poly(2-methyl-2-oxazoline) (PMOXA) polymersomes was found to significantly decrease membrane thickness and increase membrane packing density [16]. Cholesterol-containing hybrid GUVs containing DPPC, cholesterol, and a 3800 g/mol PBdPEO block copolymer have been observed to display rounded domains similar to those displayed by lipid/cholesterol membranes in which the liquid ordered phase is present [7]. Similar behavior is displayed in Chapter 2 by GUVs composed of egg sphingomyelin (egg SM), cholesterol, and 950 g/mol PBdPEO [17]. In the latter example, relatively large amounts of cholesterol were needed to observe such phase behavior in comparison to the amounts incorporated into POPC/egg

SM/cholesterol GUVs, suggesting stronger partitioning of cholesterol into PBdPEO than into POPC.

1.2.2 Phase diagrams and phase separation phenomena in lipid and hybrid membranes

Mapping the phase diagrams of multicomponent membranes is of interest in the consideration of these materials for biomedical applications such as drug delivery or membrane protein reconstitution. The presence of phase separation in lipid vesicles has been suggested to impact their efficacy as drug delivery vehicles. For example, increased intracellular delivery of macromolecules has been observed for vesicles displaying domains enriched in a cationic lipid [18,19], in comparison to vesicles presenting a well-mixed surface. Similarly, the activity of certain membrane proteins has demonstrated dependence on the presence of domains within the membrane [20–23].

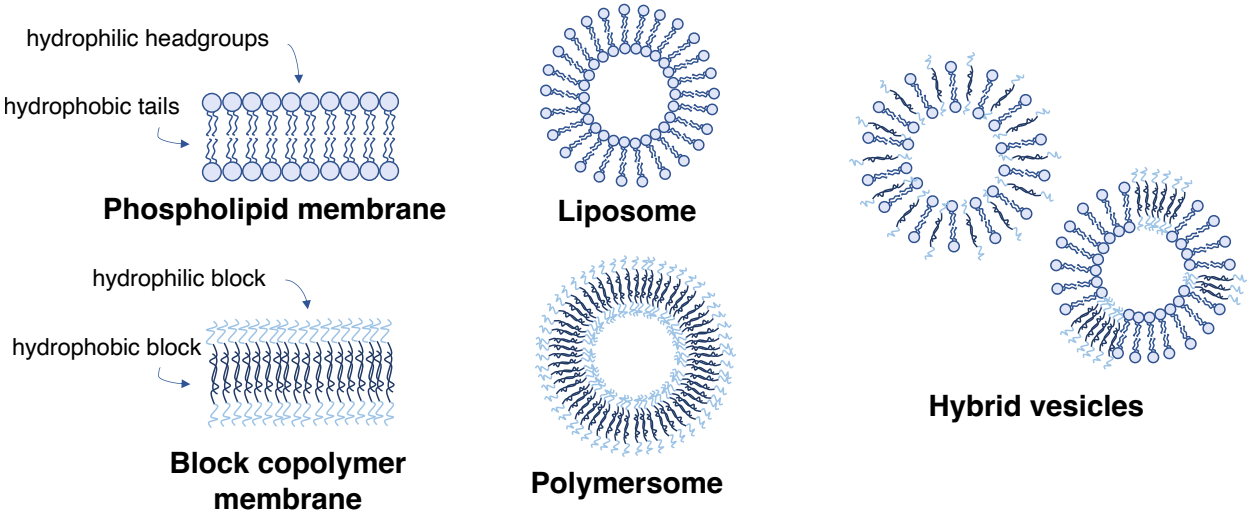

Figure 3. Phospholipids and block copolymers can form liposomes and polymersomes, respectively. When lipids and block copolymers are combined, the resulting hybrid vesicles may display either a well-mixed membrane or separate lipid-rich and polymer-rich domains, as shown in the schematic on the far right.

Hybrid membranes have also been established to be capable of both separation into lipid-rich and polymer-rich domains and mixing within in a single phase (Figure 3). Phase diagrams for hybrid

membranes, however, are far less widely studied, with investigations into hybrid membrane phase behavior commonly focusing on a handful of select compositions. The existing investigations in this area (including that in Chapter 2) have suggested that certain lipids and block copolymers, including PDMS-PEO and PBdPEO, mix less ideally and display broader phase coexistence regions than comparable phase-separating lipid mixtures such as DPPC/DOPC [6,24,25].

Phase separation may take place via either nucleation and growth or spinodal decomposition. Nucleation and growth is a first-order phase transition involving the rapid appearance (nucleation) of many small domains rich in the new phase after the thermodynamic barrier to formation of this phase is overcome [26]. The composition of this new phase differs significantly from that of the parent phase. Conversely, spinodal decomposition is a continuous (i.e., second-order) phase transition that takes place following a quench into the two-phase region near a critical point, where the two resulting phases initially share very similar compositions. Unlike nucleation and growth, spinodal decomposition is limited only by diffusion, not the presence of an initial energetic barrier to formation of the new phase [26]. The initial stages of spinodal decomposition involve systemic fluctuations which eventually coarsen in scale, eventually yielding two separate phases. In lipid GUVs, this typically appears as initial graininess across the surface of the GUV upon a decrease in temperature (i.e., a quench into the two-phase region), subsequently followed by coarsening into larger and more distinct domains [15].

Nucleation and growth is commonly described as a first-order phase transition mechanism, meaning that the formation of the new phase is completed very rapidly—theoretically instantaneously—although the coalescence of domains takes additional time. On the other hand, spinodal decomposition is typically thought of as a second-order phase transition mechanism, as the process of phase separation takes place continuously rather than instantaneously. Of interest is

the experimental determination of the mechanism by which phase separation might take place for a given composition. Langmuir surface pressure/area isotherms are expected to display a horizontal plateau during a first-order phase transition such as nucleation and growth, indicating a near-instantaneous change in the properties of the system. However, in the case of pure DPPC monolayers, for which the phase transition is expected to be first-order and to occur via nucleation and growth, this plateau instead slopes upward slightly [27], especially at higher compression rates. The authors suggest that although the observed phase transition ought to be strictly first-order, kinetic effects where domain growth (the rate of which is controlled by surface diffusion) impacts the mechanical properties of the membrane resulted in the upward slope of the plateau region [27]. Similar upward sloping of this plateau has been observed in the Langmuir surface pressure/area isotherms for polymer mixtures reported to display morphologies suggestive of spinodal decomposition during phase separation [28]. Spinodal decomposition is also a diffusion-limited process, differing from kinetically limited nucleation and growth in that there is no initial energetic barrier to formation of the new phase for the case of spinodal decomposition. In Chapter 3, we discuss the presence of either a gradual decrease or a sharp drop in the temperature dependence in the relative polarity of the fluorescent probe laurdan in hybrid membranes. We hypothesize that the plots displaying a gradual decrease may be the result of spinodal decomposition where diffusion limits the rate at which the phase transition is observed to take place, while the sharper drops may suggest phase separation via nucleation and growth.

1.3 Fluorescence microscopy and spectroscopy as tools to study membrane phase behavior

Fluorescence microscopy and spectroscopy are common techniques used to study the phase behavior of both lipid and hybrid membranes. While fluorescence microscopy is most commonly used for the observation of phase separation phenomena occurring in micron-scale vesicles or

membranes (e.g., in GUVs), fluorescence spectroscopy has been widely and effectively applied to study the phase behavior of lipid and hybrid vesicles on much smaller length scales [29–34].

1.3.1 Fluorescence microscopy

Fluorescence microscopy typically involves the incorporation of small amounts of a lipid-bound fluorophore into a lipid membrane. If multiple phases are present, such fluorescent lipids often strongly partition away from one of these phases. For example, the commonly used probe Texas Red DHPE partitions away from the more highly ordered solid and liquid ordered phases, preferentially residing instead in the less ordered, more fluid phase [35]. When used in multiphase GUVs, this partitioning results in microscopy images in which fluid phase domains appear bright and ordered phase domains appear dark, allowing the presence and morphology of domains in such GUVs to be visually ascertained. Liquid ordered phases often appear circular with smooth edges, while solid phases are typically patchy, hexagonal, or otherwise irregularly shaped [3,15].

1.3.2 Fluorescence spectroscopy

Fluorescent probes can provide valuable insight into the phase behavior of smaller vesicles, for which fluorescence microscopy cannot provide sufficient resolution. Diphenylhexatriene (DPH) and laurdan are two such commonly used fluorescent probes. DPH is hydrophobic and therefore partitions strongly into the hydrocarbon core of the membrane; the rotational freedom of DPH, expressed as an anisotropy value, depends strongly on the fluidity of the membrane [36]. For example, when incorporated into a portion of a membrane in an ordered phase, DPH is afforded limited rotational freedom, leading to higher anisotropy values. Trends in the temperature dependence of DPH anisotropy have been used to map phase diagrams of lipid mixtures [36] and to gain insight into the cooperativity of liposome phase transitions [30]. We also perform such

experiments to develop a phase diagram for DPPC/PBdPEO LUVs in Chapter 2, as well as to compare the phase behavior of these hybrid vesicles to that displayed by DPPC/DOPC.

Laurdan is another fluorescent probe commonly integrated into both lipid and hybrid membranes to study membrane phase behavior. As the polarity of the surrounding membrane increases, laurdan displays a red shift in its emission spectrum maximum [34]. Such increases in polarity are typically due to increased hydration permitted by a more disordered membrane. The relative polarity of the membrane is often quantified by calculation of a generalized polarization (GP) value, which compares the relative fluorescence emission intensities at two different wavelengths to determine the extent of the polarity-associated red shift [34]. Trends in the temperature dependence of laurdan GP have been widely used to gain insight into the phase behavior of lipid vesicles [34,37].

Additionally, several studies have suggested that the decomposition of laurdan emission spectra into multiple curves can provide additional insight into membrane phase behavior beyond that provided by laurdan GP [32,33,38]. These separate curves are expected to correspond to populations of laurdan molecules residing in membrane environments of varying hydration, with trends in the relative proportions of each population potentially providing information regarding trends in membrane phase behavior. This is especially useful for cholesterol-containing membranes, which display relatively weak trends in the dependence of laurdan GP values on temperature, in turn making it difficult to draw conclusions regarding membrane phase behavior using laurdan GP. In one such study, Puff et al. decomposed laurdan emission spectra from POPC/egg SM/cholesterol LUVs into three lognormal curves and found that trends in the temperature dependence of the ratios of the areas of the mid- and lowest-energy curves yielded temperature breakpoints in good agreement with the temperature of the first appearance of ordered

domains in GUVs upon cooling [33]. These authors found the results from laurdan emission spectrum decomposition to be in better agreement with GUV phase behavior, especially for vesicles containing greater amounts of cholesterol, than laurdan GP results. We apply and further develop this technique to study hybrid egg sphingomyelin/PBdPEO/cholesterol vesicles in Chapter 3.

1.4 Applications of lipid and hybrid membranes

Lipid and hybrid membranes are of interest for both membrane protein reconstitution and drug delivery. Understanding the phase behavior and surface morphology of lipid and hybrid membranes is important toward the design and optimization of these materials for such applications, and may further inform the relationship between material structure and function in these contexts.

Membrane proteins are of significant biomedical interest due to their participation in signal transduction, especially the amplification of external signals to yield an internal cell response. Indeed, drugs targeting a single class of membrane proteins, G-protein coupled receptors (GPCRs), comprise a major share (an estimated 27%) of the global pharmaceutical market [39]. However, elucidation of the structure of such membrane proteins or study of the function of isolated membrane proteins—crucial steps in the development of relevant pharmaceuticals—often involve the reconstitution of such proteins into artificial membranes. The use of nanolipoprotein particles (NLPs) and nanodiscs—small, discoidal lipid patches belted by an amphipathic protein or polymer—as well as lipid vesicles or supported bilayers has demonstrated great promise toward this end. The phase state and composition of the membrane have been observed to influence protein stability, motivating an understanding of membrane properties to optimize their application [20,23].

The use of hybrid lipid/block copolymer bilayers as hosts for the reconstitution of membrane proteins has additionally been observed to improve outcomes in comparison to the use of lipid-only or polymer-only membranes. Khan et al. added moderate amounts (25-50%) of a PBdPEO block copolymer to POPC vesicles and incorporated the membrane protein cytochrome *bo₃* [12]. They found that while cytochrome *bo₃* residing in hybrid vesicles retained >40% of its activity over a period of 41 days, using POPC vesicles resulted in a 97% reduction of protein activity over the same timeframe. Similarly, the incorporation of PBdPEO into DOPC vesicles resulted in an increased yield of properly folded membrane protein produced by cell-free expression, as compared to when DOPC-only vesicles were used [13].

Lipid vesicles and nanoparticles have been widely used for drug delivery, including the liposomal formulations of the chemotherapy Doxil and the antifungal Amphotericin B [9], as well as for the delivery of small molecules, DNA, and RNA both directly to cells [18,40,41] and systemically (e.g., mRNA-lipid nanoparticle (mRNA-LNP) Covid-19 vaccines).

Endosomal escape, however, remains a key barrier to drug delivery. Liposomes and mRNA-LNPs may enter cells via endocytosis. Once trapped in the endosome, however, these drug delivery vehicles are subjected to an acidic environment (pH ~5) and eventual enzymatic hydrolysis [42]. If endosomal escape is not achieved, the therapeutic payload will not be delivered. Among common strategies to promote endosomal escape are the inclusion of cell penetrating peptides [42] or cationic lipids [43]. Interestingly, the presence of phase separation in cationic lipid-containing vesicles enclosing a small molecule has been associated with enhanced delivery of the molecule to the cell cytoplasm [18,19]. This is suggested to be the result of phase separation concentrating the cationic lipids within domains, enhancing their ability to fuse with cell and endosomal membranes [18]. Such results additionally emphasize the value of investigating stimuli capable of

driving phase separation of the membranes of liposomal drug delivery vehicles, such as the drop in pH experienced upon endocytosis. In Chapter 4, we use fluorescence spectroscopy to study the effects of carboxyl terminated PBdPEO, which bears a single negative charge at physiological pH, on hybrid membrane phase behavior in a variety of pH and salt conditions. We investigate the ability of changes in pH (on the order of the drop in pH experienced upon endocytosis) to drive phase separation at physiologically relevant ionic strength and pH conditions.

1.5 References

[1] T. Harayama, H. Riezman, Understanding the diversity of membrane lipid composition, Nat. Rev. Mol. Cell Biol. 19 (2018) 281–296. https://doi.org/10.1038/nrm.2017.138.

[2] J.T. Groves, J. Kuriyan, Molecular mechanisms in signal transduction at the membrane, Nat. Struct. Mol. Biol. 17 (2010) 659–665. https://doi.org/10.1038/nsmb.1844.

[3] S.L. Veatch, S.L. Keller, Seeing spots: Complex phase behavior in simple membranes, Biochim. Biophys. Acta BBA - Mol. Cell Res. 1746 (2005) 172–185. https://doi.org/10.1016/j.bbamcr.2005.06.010.

[4] D.E. Discher, F. Ahmed, Polymersomes, Annu. Rev. Biomed. Eng. 8 (2006) 323–341. https://doi.org/10.1146/annurev.bioeng.8.061505.095838.

[5] T.P.T. Dao, A. Brûlet, F. Fernandes, M. Er-Rafik, K. Ferji, R. Schweins, J.-P. Chapel, A. Fedorov, M. Schmutz, M. Prieto, O. Sandre, J.-F. Le Meins, Mixing Block Copolymers with Phospholipids at the Nanoscale: From Hybrid Polymer/Lipid Wormlike Micelles to Vesicles Presenting Lipid Nanodomains, Langmuir. 33 (2017) 1705–1715. https://doi.org/10.1021/acs.langmuir.6b04478.

[6] D. Chen, M.M. Santore, Hybrid copolymer–phospholipid vesicles: phase separation resembling mixed phospholipid lamellae, but with mechanical stability and control, Soft Matter. 11 (2015) 2617–2626. https://doi.org/10.1039/C4SM02502D.

[7] J. Nam, T.K. Vanderlick, P.A. Beales, Formation and dissolution of phospholipid domains with varying textures in hybrid lipo-polymersomes, Soft Matter. 8 (2012) 7982–7988. https://doi.org/10.1039/c2sm25646k.

[8] C. Magnani, C. Montis, G. Mangiapia, A.-F. Mingotaud, C. Mingotaud, C. Roux, P. Joseph, D. Berti, B. Lonetti, Hybrid vesicles from lipids and block copolymers: Phase behavior from the micro- to the nano-scale, Colloids Surf. B Biointerfaces. 168 (2018) 18–28. https://doi.org/10.1016/j.colsurfb.2018.01.042.

[9] L. Sercombe, T. Veerati, F. Moheimani, S.Y. Wu, A.K. Sood, S. Hua, Advances and Challenges of Liposome Assisted Drug Delivery, Front. Pharmacol. 6 (2015). https://doi.org/10.3389/fphar.2015.00286.

[10] J.C.-M. Lee, M. Santore, F.S. Bates, D.E. Discher, From Membranes to Melts, Rouse to Reptation: Diffusion in Polymersome versus Lipid Bilayers, Macromolecules. 35 (2002) 323–326. https://doi.org/10.1021/ma0112063.

[11] H.A. Faizi, R. Dimova, P.M. Vlahovska, A vesicle microrheometer for high-throughput viscosity measurements of lipid and polymer membranes, Biophys. J. 121 (2022) 910–918. https://doi.org/10.1016/j.bpj.2022.02.015.

[12] S. Khan, M. Li, S.P. Muench, L.J.C. Jeuken, P.A. Beales, Durable proteo-hybrid vesicles for the extended functional lifetime of membrane proteins in bionanotechnology, Chem. Commun. 52 (2016) 11020–11023. https://doi.org/10.1039/C6CC04207D.

[13] M.L. Jacobs, M.A. Boyd, N.P. Kamat, Diblock copolymers enhance folding of a mechanosensitive membrane protein during cell-free expression, Proc. Natl. Acad. Sci. 116 (2019) veatch kl. https://doi.org/10.1073/pnas.1814775116.

[14] R. Catania, J. Machin, M. Rappolt, S.P. Muench, P.A. Beales, L.J.C. Jeuken, Detergent-Free Functionalization of Hybrid Vesicles with Membrane Proteins Using SMALPs, Macromolecules. 55 (2022) 3415–3422. https://doi.org/10.1021/acs.macromol.2c00326.

[15] S.L. Veatch, S.L. Keller, Separation of Liquid Phases in Giant Vesicles of Ternary Mixtures of Phospholipids and Cholesterol, Biophys. J. 85 (2003) 3074–3083. https://doi.org/10.1016/S0006-3495(03)74726-2.

[16] S. Winzen, M. Bernhardt, D. Schaeffel, A. Koch, M. Kappl, K. Koynov, K. Landfester, A. Kroeger, Submicron hybrid vesicles consisting of polymer – lipid and polymer – cholesterol blends, Soft Matter. 9 (2013) 5883–5890. https://doi.org/10.1039/C3SM50733E.

[17] N. Hamada, M.L. Longo, Characterization of phase separation phenomena in hybrid lipid/block copolymer/cholesterol bilayers using laurdan fluorescence with log-normal multipeak analysis, Biochim. Biophys. Acta BBA - Biomembr. 1864 (2022) 183887. https://doi.org/10.1016/j.bbamem.2022.183887.

[18] Z.I. Imam, L.E. Kenyon, G. Ashby, F. Nagib, M. Mendicino, C. Zhao, A.K. Gadok, J.C. Stachowiak, Phase-Separated Liposomes Enhance the Efficiency of Macromolecular Delivery to the Cellular Cytoplasm, Cell. Mol. Bioeng. 10 (2017) 387–403. https://doi.org/10.1007/s12195-017-0489-4.

[19] A.N. Trementozzi, Z.I. Imam, M. Mendicino, C.C. Hayden, J.C. Stachowiak, Liposome-Mediated Chemotherapeutic Delivery is Synergistically Enhanced by Ternary Lipid Compositions and Cationic Lipids, Langmuir ACS J. Surf. Colloids. 35 (2019) 12532–12542. https://doi.org/10.1021/acs.langmuir.9b01965.

[20] H. de Lima Santos, M.L. Lopes, B. Maggio, P. Ciancaglini, Na,K-ATPase reconstituted in liposomes: effects of lipid composition on hydrolytic activity and enzyme orientation, Colloids Surf. B Biointerfaces. 41 (2005) 239–248. https://doi.org/10.1016/j.colsurfb.2004.12.013.

[21] B. Cannon, M. Hermansson, S. Györke, P. Somerharju, J.A. Virtanen, K.H. Cheng, Regulation of Calcium Channel Activity by Lipid Domain Formation in Planar Lipid Bilayers, Biophys. J. 85 (2003) 933–942. https://doi.org/10.1016/S0006-3495(03)74532-9.

[22] T. Bhatia, F. Cornelius, J. Brewer, L.A. Bagatolli, A.C. Simonsen, J.H. Ipsen, O.G. Mouritsen, Spatial distribution and activity of Na+/K+-ATPase in lipid bilayer membranes with phase boundaries, Biochim. Biophys. Acta BBA - Biomembr. 1858 (2016) 1390–1399. https://doi.org/10.1016/j.bbamem.2016.03.015.

[23] Ü. Coskun, M. Grzybek, D. Drechsel, K. Simons, Regulation of human EGF receptor by lipids, Proc. Natl. Acad. Sci. 108 (2011) 9044–9048. https://doi.org/10.1073/pnas.1105666108.

[24] N. Hamada, S. Gakhar, M.L. Longo, Hybrid lipid/block copolymer vesicles display broad phase coexistence region, Biochim. Biophys. Acta BBA - Biomembr. 1863 (2021) 183552. https://doi.org/10.1016/j.bbamem.2021.183552.

[25] T.P.T. Dao, F. Fernandes, E. Ibarboure, K. Ferji, M. Prieto, O. Sandre, J.-F. Le Meins, Modulation of phase separation at the micron scale and nanoscale in giant polymer/lipid hybrid unilamellar vesicles (GHUVs), Soft Matter. 13 (2017) 627–637. https://doi.org/10.1039/C6SM01625A.

[26] C.M. Rosetti, A. Mangiarotti, N. Wilke, Sizes of lipid domains: What do we know from artificial lipid membranes? What are the possible shared features with membrane rafts in cells?, Biochim. Biophys. Acta BBA - Biomembr. 1859 (2017) 789–802. https://doi.org/10.1016/j.bbamem.2017.01.030.

[27] L.R. Arriaga, I. López-Montero, J. Ignés-Mullol, F. Monroy, Domain-Growth Kinetic Origin of Nonhorizontal Phase Coexistence Plateaux in Langmuir Monolayers: Compression Rigidity of a Raft-Like Lipid Distribution, J. Phys. Chem. B. 114 (2010) 4509–4520. https://doi.org/10.1021/jp9118953.

[28] G. Sato, S. Nishitsuji, J. Kumaki, Two-Dimensional Phase Separation of a Poly(methyl methacrylate)/Poly(l-lactide) Mixed Langmuir Monolayer via a Spinodal Decomposition Mechanism, J. Phys. Chem. B. 117 (2013) 9067–9072. https://doi.org/10.1021/jp403195g.

[29] F.A. Heberle, J.T. Buboltz, D. Stringer, G.W. Feigenson, Fluorescence methods to detect phase boundaries in lipid bilayer mixtures, Biochim. Biophys. Acta BBA - Mol. Cell Res. 1746 (2005) 186–192. https://doi.org/10.1016/j.bbamcr.2005.05.008.

[30] W.F. Zeno, S. Hilt, K.K. Aravagiri, S.H. Risbud, J.C. Voss, A.N. Parikh, M.L. Longo, Analysis of Lipid Phase Behavior and Protein Conformational Changes in Nanolipoprotein Particles upon Entrapment in Sol–Gel-Derived Silica, Langmuir. 30 (2014) 9780–9788. https://doi.org/10.1021/la5025058.

[31] T.P.T. Dao, F. Fernandes, M. Er-Rafik, R. Salva, M. Schmutz, A. Brûlet, M. Prieto, O. Sandre, J.-F. Le Meins, Phase Separation and Nanodomain Formation in Hybrid Polymer/Lipid Vesicles, ACS Macro Lett. 4 (2015) 182–186. https://doi.org/10.1021/mz500748f.

[32] N. Watanabe, Y. Goto, K. Suga, T.K.M. Nyholm, J.P. Slotte, H. Umakoshi, Solvatochromic Modeling of Laurdan for Multiple Polarity Analysis of Dihydrosphingomyelin Bilayer, Biophys. J. 116 (2019) 874–883. https://doi.org/10.1016/j.bpj.2019.01.030.

[33] N. Puff, G. Staneva, M.I. Angelova, M. Seigneuret, Improved Characterization of Raft-Mimicking Phase-Separation Phenomena in Lipid Bilayers Using Laurdan Fluorescence with Log-Normal Multipeak Analysis, Langmuir. 36 (2020) 4347–4356. https://doi.org/10.1021/acs.langmuir.0c00412.

[34] T. Parasassi, G. De Stasio, G. Ravagnan, R.M. Rusch, E. Gratton, Quantitation of lipid phases in phospholipid vesicles by the generalized polarization of Laurdan fluorescence, Biophys. J. 60 (1991) 179–189. https://doi.org/10.1016/S0006-3495(91)82041-0.

[35] J. Juhasz, J.H. Davis, F.J. Sharom, Fluorescent probe partitioning in giant unilamellar vesicles of 'lipid raft' mixtures, Biochem. J. 430 (2010) 415–423. https://doi.org/10.1042/BJ20100516.

[36] B.R. Lentz, Y. Barenholz, T.E. Thompson, Fluorescence depolarization studies of phase transitions and fluidity in phospholipid bilayers. 2. Two-component phosphatidylcholine liposomes, Biochemistry. 15 (1976) 4529–4537. https://doi.org/10.1021/bi00665a030.

[37] T. Parasassi, M. Di Stefano, M. Loiero, G. Ravagnan, E. Gratton, Influence of cholesterol on phospholipid bilayers phase domains as detected by Laurdan fluorescence., Biophys. J. 66 (1994) 120–132.

[38] A.D. Lúcio, C.C. Vequi-Suplicy, R.M. Fernandez, M.T. Lamy, Laurdan Spectrum Decomposition as a Tool for the Analysis of Surface Bilayer Structure and Polarity: a Study with DMPG, Peptides and Cholesterol, J. Fluoresc. 20 (2010) 473–482. https://doi.org/10.1007/s10895-009-0569-5.

[39] A.S. Hauser, M.M. Attwood, M. Rask-Andersen, H.B. Schiöth, D.E. Gloriam, Trends in GPCR drug discovery: new agents, targets and indications, Nat. Rev. Drug Discov. 16 (2017) 829–842. https://doi.org/10.1038/nrd.2017.178.

[40] S. Adams, P. Pathak, H. Shao, J.B. Lok, A. Pires-daSilva, Liposome-based transfection enhances RNAi and CRISPR-mediated mutagenesis in non-model nematode systems, Sci. Rep. 9 (2019) 483. https://doi.org/10.1038/s41598-018-37036-1.

[41] V.P. Torchilin, T.S. Levchenko, R. Rammohan, N. Volodina, B. Papahadjopoulos-Sternberg, G.G.M. D'Souza, Cell transfection in vitro and in vivo with nontoxic TAT peptide-liposome–DNA complexes, Proc. Natl. Acad. Sci. 100 (2003) 1972–1977. https://doi.org/10.1073/pnas.0435906100.

[42] A.K. Varkouhi, M. Scholte, G. Storm, H.J. Haisma, Endosomal escape pathways for delivery of biologicals, J. Controlled Release. 151 (2011) 220–228. https://doi.org/10.1016/j.jconrel.2010.11.004.

[43] G. Basha, T.I. Novobrantseva, N. Rosin, Y.Y.C. Tam, I.M. Hafez, M.K. Wong, T. Sugo, V.M. Ruda, J. Qin, B. Klebanov, M. Ciufolini, A. Akinc, Y.K. Tam, M.J. Hope, P.R. Cullis, Influence of Cationic Lipid Composition on Gene Silencing Properties of Lipid Nanoparticle Formulations of siRNA in Antigen-Presenting Cells, Mol. Ther. 19 (2011) 2186–2200. https://doi.org/10.1038/mt.2011.190.

Chapter 2- Hybrid lipid/block copolymer vesicles display broad phase coexistence region

Previously published in Biochimica et Biophysica Acta – Biomembranes 2021

*(*https://doi.org/10.1016/j.bbamem.2021.183552*)*

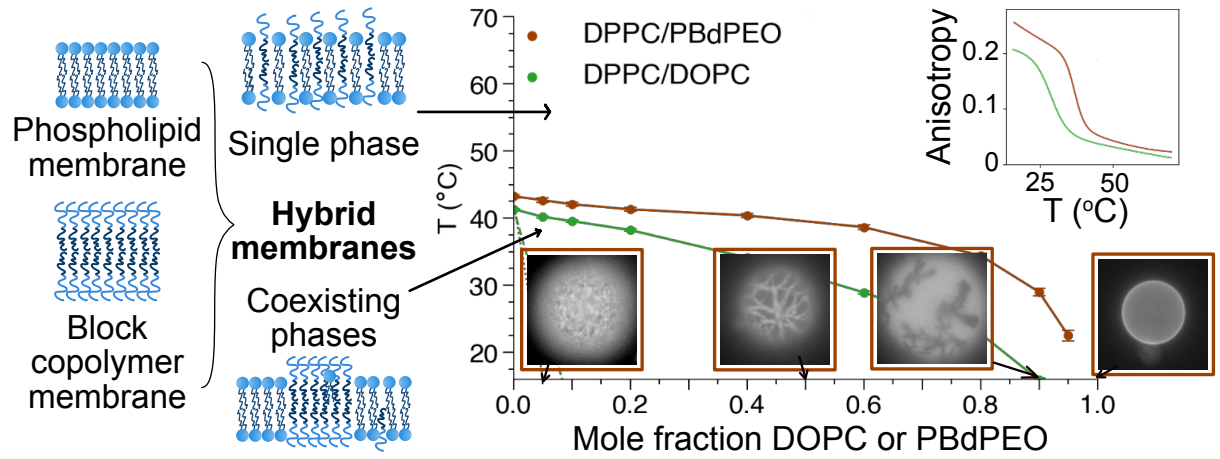

Abstract

The fluidity and polar environment of ~100 nm hybrid vesicles combining dipalmitoylphosphatidylcholine (DPPC) and poly(1,2-butadiene)-block-polyethylene oxide (PBd-PEO, average molecular weight 950 g/mol) were studied upon vesicle heating using the fluorescence spectroscopy techniques of DPH anisotropy and laurdan generalized polarization (GP). These techniques indicated PBd-PEO membranes are less ordered than solid DPPC, but slightly more ordered than fluid DPPC or dioleoylphosphatidylcholine (DOPC) membranes. We find the DPH anisotropy values are less than expected from additivity of the components' anisotropies in the fluid phase mixture of DPPC and PBd-PEO, inferring that DPPC strongly fluidizes the PBd-PEO. We use transitions in DPH anisotropy and laurdan GP to create a

temperature/composition phase diagram for DPPC/PBd-PEO which we find displays a significantly broader solid/fluid phase coexistence region than DPPC/DOPC, showing that DPPC partitions less readily into fluid PBd-PEO than into fluid DOPC. The existence of a broad solid/fluid phase coexistence region in DPPC/PBd-PEO vesicles is verified by Förster resonance energy transfer results and the visualization of phase separation in giant unilamellar vesicles containing up to 95% PBd-PEO and a single phase in 100% PBd-PEO vesicles at room temperature. These results add to the limited knowledge of phase behavior and phase diagrams of hybrid vesicles, and should be useful in understanding and tailoring membrane surface architecture toward biomedical applications such as drug delivery or membrane protein reconstitution.

2.2 Introduction

Hybrid vesicles, formed using amphiphilic block copolymers and lipids, combine the advantageous properties of both components and have gained the interest of the scientific community in recent years. While phospholipids are inherently biocompatible, block copolymers offer increased mechanical stability [1,2] and chemical diversity due to their tunable nature. These unique characteristics of hybrid vesicles make them desirable for potential applications in drug delivery and membrane protein reconstitution. Utilization of such hybrid vesicles for these applications requires an understanding of the membrane surface structure (*i.e.* the presence or absence of lipid- and polymer-rich phases), which may impact their efficacy towards the intended function. For example, it has been shown that phase-separated liposomes had an increased efficiency in escaping the endosome for intracellular delivery of cargo [3,4]. Similarly, the activity of certain membrane proteins reconstituted in lipid membranes has been shown to be dependent

on bilayer surface heterogeneity [5–8]. Therefore, it is essential to understand and tune the surface morphology of biomembranes for potential biomedical applications.

It is well established that lipid mixtures can demonstrate temperature and composition dependent phase separation driven by the hydrophobic thickness mismatch between different phases. Accordingly, an extensive body of work exists using methods including fluorescence microscopy [9], ^{2}H NMR [10], differential scanning calorimetry (DSC) [11], and fluorescence spectroscopy [12,13] to map the phase diagrams of lipid mixtures. In some recent studies, similar investigations have demonstrated the existence of separate lipid- and polymer- rich phases in hybrid vesicles [2,14–18]. However, the discussion on these phases has been limited to certain compositions and temperatures except for the work of Dao et al. [15] and Chen and Santore [2], which respectively present an apparent phase diagram for a 1-palmitoyl-2-oleoyl-glycero-3-phosphocholine (POPC)/polyethylene oxide-polydimethylsiloxane-polyethylene oxide (PEO-PDMS-PEO) copolymer mixture and a partial range of solid to fluid phase transition temperatures for a mixture of dipalmitoylphosphatidylcholine (DPPC) and a PDMS-PEO copolymer. Formation of hybrid giant unilamellar vesicles (GUVs) formed with polybutadiene-polyethylene oxide (PBd-PEO) block copolymers has demonstrated that certain combinations of the lipids DPPC or POPC with PBd-PEO can display either separate lipid- and polymer-rich domains, or a homogeneous membrane [14,16,19]. PBd-PEO hybrid membranes have also been shown to extend the functional lifetime of an incorporated membrane protein [20]. When used to form hybrid nano-sized vesicles, PDMS-based copolymers have been reported to form stable nanodomains at certain temperatures [21], but such behavior has not yet been fully explored for membranes containing polybutadiene-based copolymers. Thus, there exists an ongoing need to systematically investigate the phase behavior of lipid/polymer mixtures.

Development of a temperature/composition phase diagram mapping the behavior of hybrid vesicles formed using DPPC and poly(butadiene)-*block*-poly(ethylene oxide) (PBd-PEO) is therefore presented here. DPPC is a fully saturated lipid with a main solid-to-fluid phase transition temperature (T_{mid}) of ~41°C [11]. The PBd-PEO block copolymer used here had an average molecular weight of 950 g/mol (Bd(600)-EO(350)). This polymer is expected to demonstrate relatively fluid behavior across the range of temperatures explored due to the low glass transition temperature of its hydrophobic block [22]. Fluorescence spectroscopy and microscopy are combined to map the phase behavior of hybrid vesicles composed of DPPC and PBd-PEO. To construct an apparent temperature/composition phase diagram for DPPC/PBd-PEO vesicles, delimiting temperatures of large unilamellar vesicles are determined using the fluorescent probes diphenylhexatriene (DPH) and laurdan. Phase behavior is further evaluated by examining the efficiency of Förster resonance energy transfer (FRET).

Observing the temperature- and composition-dependent properties of DPH fluorescence anisotropy and laurdan generalized polarization (GP) values has been previously established as a method to map phase diagrams of lipid mixtures [12,23,24], but to the best of our knowledge has not been applied for this purpose to lipid/copolymer mixtures. Additionally, fluorescence microscopy is used to visualize domain formation in micron scale GUVs. The results presented here suggest the phase diagram for DPPC/PBd(600)-PEO(350) indeed consists of coexisting solid and fluid phases below the main phase transition temperature of the DPPC, and fluidizes above this temperature. These results for DPPC/PBd-PEO vesicles are also compared to DPPC/dioleoylphosphatidylcholine (DOPC) vesicles, which display a broad solid/fluid coexistence region. DOPC in the fluid phase is poorly miscible with solid DPPC. PBd-PEO and DPPC would be expected to demonstrate similarly poor miscibility due to the disordered nature of

PBd-PEO at room temperature. We will show that phase separation is observed across a greater range of compositions and temperatures for DPPC/PBd-PEO than DPPC/DOPC, and greater deviations from ideal mixing behavior are also observed within hybrid lipid/copolymer membranes.

2.3 Materials and Methods

2.3.1 Materials

Dipalmitoylphosphatidylcholine (DPPC), dioleoylphosphatidylcholine (DOPC), 1,2-dilinoleoylphosphatidylcholine (18:2 PC) and 1,2-dilinolenoylphosphatidylcholine (18:3 PC), 1,2-dipalmitoyl-sn-glycero-3-phosphoethanolamine-N-(7-nitro-2-1,3-benzoxadiazol-4-yl) (NBD-DPPE) and 1,2-dioleoyl-sn-glycero-3-phosphoethanolamine-N-(lissamine rhodamine B sulfonyl) (Rh-DOPE) in chloroform were purchased from Avanti Polar Lipids Inc. Poly(1,2-butadiene)-*block*-poly(ethylene oxide) (PBd-PEO) diblock copolymer with an average molecular weight of 950 g/mol (P41807C-BdEO, Bd(600)-*b*-EO(350), PDI = 1.06) was purchased from Polymer Source Inc. 1,6-diphenyl-1,3,5-hexatriene (DPH) was purchased from Acros Organics. 6-dodecanoyl-2-dimethylaminonaphthalene (laurdan) was purchased from AdipoGen Life Sciences. Texas Red DHPE was purchased from Biotium. All water used for experiments was purified with a Barnstead Nanopure System (Barnstead Thermolyne, Dubuque, IA) and had a resistivity ≥17.8 MΩ·cm.

2.3.2 Preparation of Hybrid Large Unilamellar Vesicles (LUVs)

DPPC and PBd-PEO stock solution aliquots at 25 mg/mL in chloroform were stored at -20 ºC. To achieve appropriate molar ratios of lipid and polymer mixtures (varying from 100 mol% DPPC to

100 mol% PBd-PEO), calculated volumes of stock solutions were combined in clean glass vials. Chloroform was evaporated under a gentle stream of N_2 to form a uniform dried lipid/polymer thin film. The vials were then kept under vacuum for 4-24 hours to remove any residual solvent. The lipid/polymer film was rehydrated to a total lipid+polymer concentration of 2 mg/mL using 20 mM Tris-HCl, 100 mM NaCl (pH 7.4) buffer. The hydrated lipid/polymer mixture was heated to 50-55 ^{o}C and then extruded through a 0.1 μm polycarbonate membrane using a mini extruder (Avanti). The temperature of the syringe-extruder assembly was maintained above the lipid phase transition temperature during this step. After extrusion, a dilute solution of hybrid vesicles (100X) was used to analyze size distribution using dynamic light scattering.

2.3.3 Fluorescence Anisotropy and Generalized Polarization Measurements

Phase behavior of the hybrid vesicles with temperature was studied using fluorescence anisotropy (r) of the fluorophore DPH. Hybrid vesicles at a concentration of 0.14 mg/ml were incubated with 5 μL of 200 μM DPH stock solution in ethanol for 45 minutes in the dark. This is a lipid:probe ratio of roughly 30:1. The anisotropy curve observed with a lipid:probe ratio of 500:1 in hybrid vesicles containing 60% PBd-PEO was consistent with that observed at a lipid:probe ratio of 30:1 (Figure S6). Fluorescence anisotropy was measured using a JASCO spectrofluorometer from 16°C to 70 °C at an interval of 2 °C. To obtain DPH anisotropy values, samples were measured at least 5 times at each temperature before ramping to the next temperature; reported DPH anisotropy values are the averages of these measurements. Each vesicle sample was heated only once and used to generate a single anisotropy or GP plot. The sample cuvette was incubated at each temperature for 3 minutes before taking the measurement. The excitation wavelength was 360 nm and the anisotropy value was measured at 440 nm. DPH anisotropy values are calculated using a

ratio of the difference in the parallel and perpendicular light intensity of the emission to the total intensity of the excitation light as shown in Equation (1),

$$r = \frac{I_{//} - I_{\perp}}{I_{//} + 2I_{\perp}} \qquad (1)$$

In order to track the fluidization of the membrane with temperature, least squares regression was used to fit observed anisotropy values to a sigmoidal function (Equation (2)). r_{max}, r_{min}, n, and T_{mid} are the maximum anisotropy value, minimum anisotropy value, a fitting parameter, and the inflection point of the sigmoidal function respectively. r_{max} and r_{min} establish the upper and lower limits of the anisotropy curve. A and B introduce a quadratic baseline to the function, which may better capture any asymmetry in the anisotropy curve with respect to temperature in the vicinity of T_{mid} for the mixture [25,26].

$$r(T) = \frac{r_{max} - r_{min}}{1 + e^{(T - T_{mid})n}} + r_{min} + AT + BT^2 \qquad (2)$$

This approach was also used to evaluate the fluidity indicated by DPH anisotropy for DPPC/DOPC, DPPC/18:2 PC, and DPPC/18:3 PC LUVs (prepared as in Section 2.2), providing a comparison to lipid systems for the phase behavior of hybrid DPPC/PBd-PEO LUVs. The T_{mid} values observed were relatively independent of vesicle type and preparation (Figure S4 and Table S1).

In addition to DPH anisotropy measurements, which indicate the fluidity of the membrane, the generalized polarization (GP) of laurdan provides information on the hydration of the membrane. Hybrid vesicles at a molar concentration of 0.1 mM were incubated with 5 μL of 200 μM laurdan stock solution in ethanol for 1 hour, yielding a lipid:probe ratio of 500:1. GP of the laurdan probe was measured for temperatures between 4° C and 70 °C at an interval of 2 °C with an incubation time of 3 minutes at each temperature. Steady-state emission spectra from vesicle samples were

collected at these temperatures between 380 nm – 500 nm upon excitation at 340 nm. Laurdan GP values are calculated using the difference in emission intensities at 440 and 490 nm and indicate the overall solvation of the membrane according to Equation (3),

$$GP = \frac{I_{440} - I_{490}}{I_{440} + I_{490}} \tag{3}$$

Least squares regression was used to fit observed GP values to a sigmoidal function (a modification of Equation (2) replacing the terms r_{max} and r_{min} with GP_{max} and GP_{min}, respectively):

$$GP(T) = \frac{GP_{max} - GP_{min}}{1 + e^{(T - T_{mid})n}} + GP_{min} + AT + BT^2 \tag{4}$$

2.3.4 Temperature Dependent Förster Resonance Energy Transfer (FRET)

Fluorescent probes NBD-DPPE and Rh-DOPE were included in the hybrid vesicles at 0.1 mol% and 2 mol% respectively. Both probes combined form a FRET pair with NBD-DPPE as donor and Rh-DOPE as the acceptor. Hybrid vesicles were diluted to a final concentration of 0.1 mM prior to fluorescence measurements. Steady-state fluorescence emission spectra of the donor, NBD-DPPE, was recorded in the presence (F), and absence (F_0) of the acceptor Rh-DOPE at temperatures between 4 °C and 70 °C. Samples were excited at 460 nm and the emission spectra were measured between 500 and 650 nm. NBD emission intensities were evaluated at 534 nm when calculating F and F_0. This experiment was also carried out as described above using DPPC/DOPC LUVs (prepared as in Section 2.2).

The fluorescent probes DPH (donor) and Rh-DOPE (acceptor) were also used as a separate FRET pair in hybrid vesicles at 0.2 mol% and 1 mol%, respectively. A stock solution of 200 μM DPH in ethanol was added to a 0.1 mM LUV suspension to achieve the desired concentration and allowed

to incubate in the dark for 45 minutes prior to fluorescence measurements. The volume of ethanol added was always less than 0.25% of the total diluted vesicle preparation. DPH was excited at 360 nm and its emission intensity recorded at 430 nm.

2.3.5 Preparation of Giant Unilamellar Vesicles (GUVs)

Giant unilamellar vesicles (GUVs) were prepared by electroformation. The desired amounts of DPPC, PBd-PEO, and Texas Red DHPE stocks in chloroform were combined in a clean glass conical vial and diluted to a final concentration of 0.5 mg/mL in 2:1 chloroform:methanol (by volume). A custom built electroformation chamber consisting of parallel platinum electrodes in a polytetrafluoroethylene housing was used. 25 µL of the stock solution was spread over each electrode using a gastight Hamilton syringe, and a gentle stream of N_2 was used to dry the electrodes. The chamber was placed under vacuum for 2-24 hours to remove any residual solvent. Glass coverslips were then fixed in place with vacuum grease over the chamber openings. The sealed chamber was filled with water and placed over a water bath of 50-55 ^{o}C. A function generator was connected to the electrodes. Vesicle formation was carried out at 3 V, using a frequency of 10 Hz for 30 minutes, 3 Hz for 15 minutes, 1 Hz for 7.5 minutes, and 0.5 Hz for 7.5 minutes. The chamber was then allowed to cool to room temperature prior to collection of GUVs. GUVs were stored in a plastic conical tube and imaged within 2 hours. A small aliquot of GUVs was added to an imaging chamber formed by a glass slide, silicone spacer, and no. 1.5 coverslip. Fluorescence microscopy images were collected using a Nikon Eclipse 80i equipped with a 60x oil immersion objective.

2.4 Results and Discussion

2.4.1 Fluorescence anisotropy and generalized polarization measurements

The fluorescent probes 1,6-diphenyl-1,3,5-hexatriene (DPH) and 6-dodecanoyl-2-dimethylaminonaphthalene (laurdan) were used to evaluate the phase behavior of hybrid dipalmitoylphosphatidylcholine (DPPC)/polybutadiene-*block*-polyethylene oxide (PBd-PEO) LUVs. Both DPH and laurdan partition strongly into LUV membranes [27,28] and provide insight regarding local membrane properties. LUVs were formed by extrusion and had average diameters ranging from 80-120 nm as measured by dynamic light scattering (Table S3). The compositions reported are mole percentages, unless otherwise specified.

DPH fluorescence anisotropy values depend strongly on the fluidity of the membrane into which DPH is incorporated, with high anisotropy values corresponding to a more solid, ordered membrane and low values to a more fluid, disordered membrane [12]. DPH steady state fluorescence anisotropy (DPH anisotropy) values were obtained across a range of temperatures crossing the main phase transition of DPPC, corresponding to the transition from an ordered solid phase to a disordered fluid phase [29]. These results are shown in Figure 1A for LUVs for a range of DPPC/PBd-PEO compositions. When measured across this range of temperatures DPH anisotropy behaved as a sigmoidal function, decreasing slowly far below and above the main phase transition of DPPC and rapidly in between. As a general trend, incorporating increasing amounts of PBd-PEO shifted this inflection point to lower temperatures, as expected due to the low glass transition temperature of PBd-PEO [22]. DPH anisotropy curves were also observed to be reversible with temperature (Figure S5) suggesting the temperature ramp rate used was appropriate.

As shown in Figure 1A, DPH anisotropy values for pure PBd-PEO LUVs do not have the characteristic sigmoidal curve with increasing temperature. This suggests the absence of a phase transition within the observed temperature range, although DPH anisotropy still demonstrates significant dependence on temperature due to an increase in membrane fluidity as the temperature increases [30]. A similar temperature dependence has been previously observed in fluid palmitoyl-oleoyl-phosphatidylcholine (POPC) vesicles [23] and observed by us in pure dioleoylphosphatidylcholine (DOPC) LUVs (Figure S1) above their main phase transition temperatures.

The dependence of DPH anisotropy on temperature and composition in DPPC/PBd-PEO LUVs also follows similar trends to those observed in DPPC/DOPC LUVs (Figure S1), measured in order to have a comparison to a well-studied binary lipid system [10,12]. DPH anisotropy values at temperatures below the inflection point vary more with composition in DPPC/DOPC vesicles than in DPPC/PBd-PEO vesicles (from 0.28-0.10 and 0.28-0.20, respectively, at 16 ºC as the mole fraction of DPPC, x_{DPPC}, varies from 1 → 0). This suggests DOPC forms a much more fluid membrane than PBd-PEO, despite the disordered state of PBd-PEO. Previous work has suggested pure block copolymer membranes have a higher effective viscosity than pure lipid membranes, as determined by comparing experimentally obtained lateral diffusion coefficients of both species to theoretical predictions [31]. This could be attributed to increased drag at the block copolymer bilayer midplane due to entanglements between the hydrophobic tails of copolymers in opposing monolayers [32]. Indeed, DPH anisotropy values at temperatures above the inflection point vary less with composition in DPPC/DOPC vesicles than in DPPC/PBd-PEO vesicles (from 0.02-0.03 and 0.02-0.05 respectively, at 70 ºC as x_{DPPC} goes from 1 → 0). This suggests both fluid DPPC and fluid DOPC form a more fluid membrane than PBd-PEO.

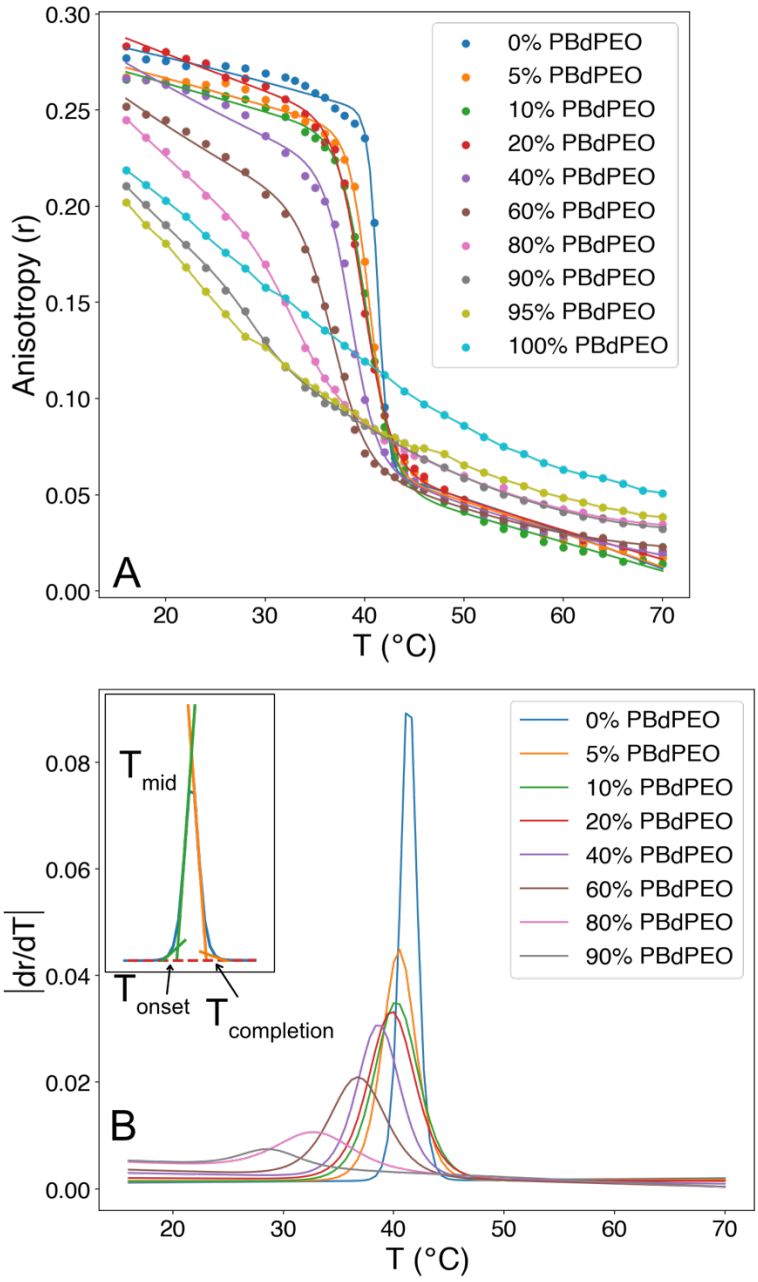

Figure 1. A. Temperature dependence of DPH anisotropy (r) values in hybrid DPPC/PBd-PEO LUVs. Plotted points correspond to measured data; lines show regressed fits to Equation (2), except for 95% and 100% PBd-PEO, as Equation (2) could not be regressed for these compositions due to the lack of clear inflection point. Plotted lines for 95% and 100% PBd-PEO are not the result of any fit. B. The absolute values of the first derivative with respect to temperature of the regressed DPH anisotropy curves. The onset and completion points of the sigmoidal curves were evaluated as shown in the inset: the mean of the intersection with the baseline of lines tangent to the points of steepest slope and of greatest curvature was taken as Tonset (green) or Tcompletion (orange). The value of the midpoint temperature, Tmid, was obtained by regression of Equation (2). Inset sample composition is 0% PBd-PEO (100% DPPC).

To assess the onset (T_{onset}), inflection point (T_{mid}), and completion temperatures ($T_{completion}$) for the sigmoidal portions of the curves, the observed anisotropy values at each composition were regressed against Equation (2) (Figure 1A), directly giving T_{mid}. The derivative of Equation (2) was evaluated with respect to temperature (Figure 1B). Because of the sigmoidal shape of the DPH anisotropy curves, this yielded peak-shaped functions with baseline values corresponding to the small slopes of the DPH anisotropy curves. The points at which the slope begins to deviate sharply from and returns to its baseline values (*i.e.* the start and the end of the peak) correspond T_{onset} and $T_{completion}$. To determine these points, tangent lines were constructed along the peaks shown in Figure 1B [33]. Representative tangent constructions are shown in Figure S9. The onset and completion temperatures were taken to be the averages of the intersection of two left-side tangents and two right-side tangents with the baseline of each peak respectively, analogous to the procedure followed to find transition onset and completion temperatures using differential scanning calorimetry (DSC). For pure DPPC LUVs, this yielded a phase transition width of ~5.5 ^{o}C and regression against Equation (2) yielded a T_{mid} of 41.4±0.2 ^{o}C (measured by the inflection point in the sigmoidal fit), consistent with values obtained by DSC [11,30,34]. Statistical analysis is discussed in the Supplementary Material.

Experimental DPH anisotropy values were compared to the theoretical values using a weighted average, which we will refer to as ideal anisotropy, for different LUV compositions. Ideal anisotropy values were calculated as a weighted sum of the anisotropy values for pure DPPC and pure PBd-PEO LUVs (further discussed in the Supplementary Material). Deviations from ideal anisotropy ($\Delta r/r$) (Figure 2) were then calculated by dividing the difference between observed and ideal anisotropy values by the ideal anisotropy value [35]. Such deviations from ideal anisotropy could be the result of multiple factors. If both DPPC and PBd-PEO coexist within a single phase,

deviations from ideal fluidity would suggest the lipid and polymer interact extensively enough to have a fluidizing or an ordering effect on each other. However, if separate DPPC-rich and PBd-PEO-rich phases coexist, interactions with partitioned PBd-PEO or DPPC, respectively, in these phases or contributions of the edges of phase-separated domains could also result in deviations from ideal fluidity.

At temperatures below $T_{completion}$ for LUVs containing ~20-80% PBd-PEO, DPH anisotropy values generally demonstrate small positive deviations from ideal anisotropy, indicating a less fluid membrane than expected. Assuming DPPC-rich solid and PBd-PEO-rich liquid phases coexist below $T_{completion}$, these smaller deviations from ideal anisotropy are not the result of extensive interaction of DPPC and PBd-PEO within one single phase. DPPC might be inducing greater ordering of PBd-PEO by partitioning into the PBd-PEO rich phase and/or by interacting with PBd-PEO partitioning into the DPPC-rich phase. It is also possible that deviations from ideal behavior could be a result of increased ordering at the domain edges.

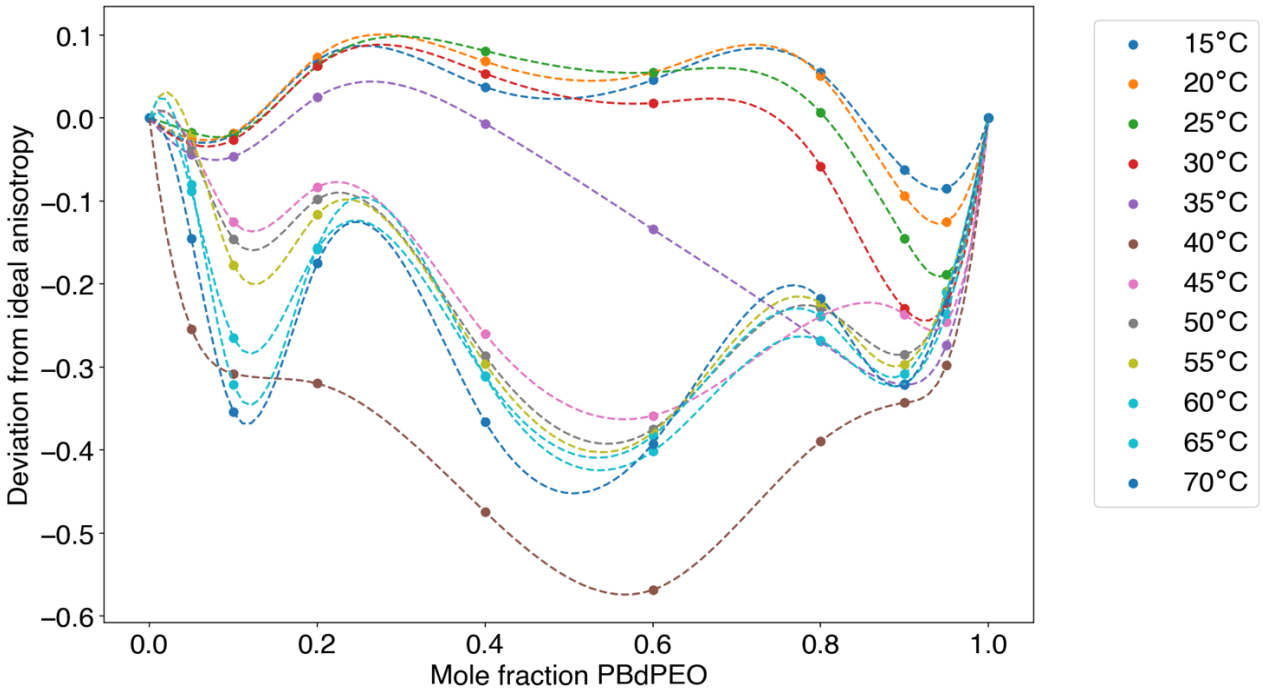

Figure 2. Deviations from ideal anisotropy (Δr/r) at select temperatures as a function of DPPC/PBd-PEO LUV composition. Points were calculated as described in the text; dashed lines are cubic splines fit to calculated values.

Above $T_{completion}$, primarily larger, negative deviations from ideal anisotropy are observed, indicating fluid DPPC may have a disordering effect on PBd-PEO. Indeed, above its T_{mid}, pure DPPC displays a lower anisotropy value and greater fluidity than pure PBd-PEO at the same temperatures. The presence of appreciable deviations from ideal anisotropy across this range of temperatures also suggests DPPC and PBd-PEO are able to interact with each other, in turn suggesting the existence of a single fluid phase above $T_{completion}$. While such trends are not as clear above $T_{completion}$ for DPPC/DOPC LUVs (Figure S7), which consist of a single fluid phase above $T_{completion}$ [10], this may be due to the small difference in the fluidities of pure DPPC and pure DOPC membranes above T_{mid}. A limited dependence of membrane fluidity on composition, and thus weaker deviations from ideal fluidity, would therefore be expected. However, the greater difference in the fluidities of pure DPPC and pure PBd-PEO at these temperatures might facilitate the observation of greater deviations from ideal anisotropy.

For LUVs made with more than 90% PBd-PEO, T_{mid} values could not be resolved due to the absence of clear inflection points in the anisotropy curves; measured anisotropy values for LUVs with these compositions could not be regressed to the expression in Equation (2). In addition, T_{onset} and $T_{completion}$ could not be clearly resolved for LUVs containing more than 80% PBd-PEO. This motivated the use of laurdan generalized polarization (GP) to provide further data for phase diagram construction, including compositions for which onset, completion, and midpoint temperatures could not be resolved using DPH anisotropy.

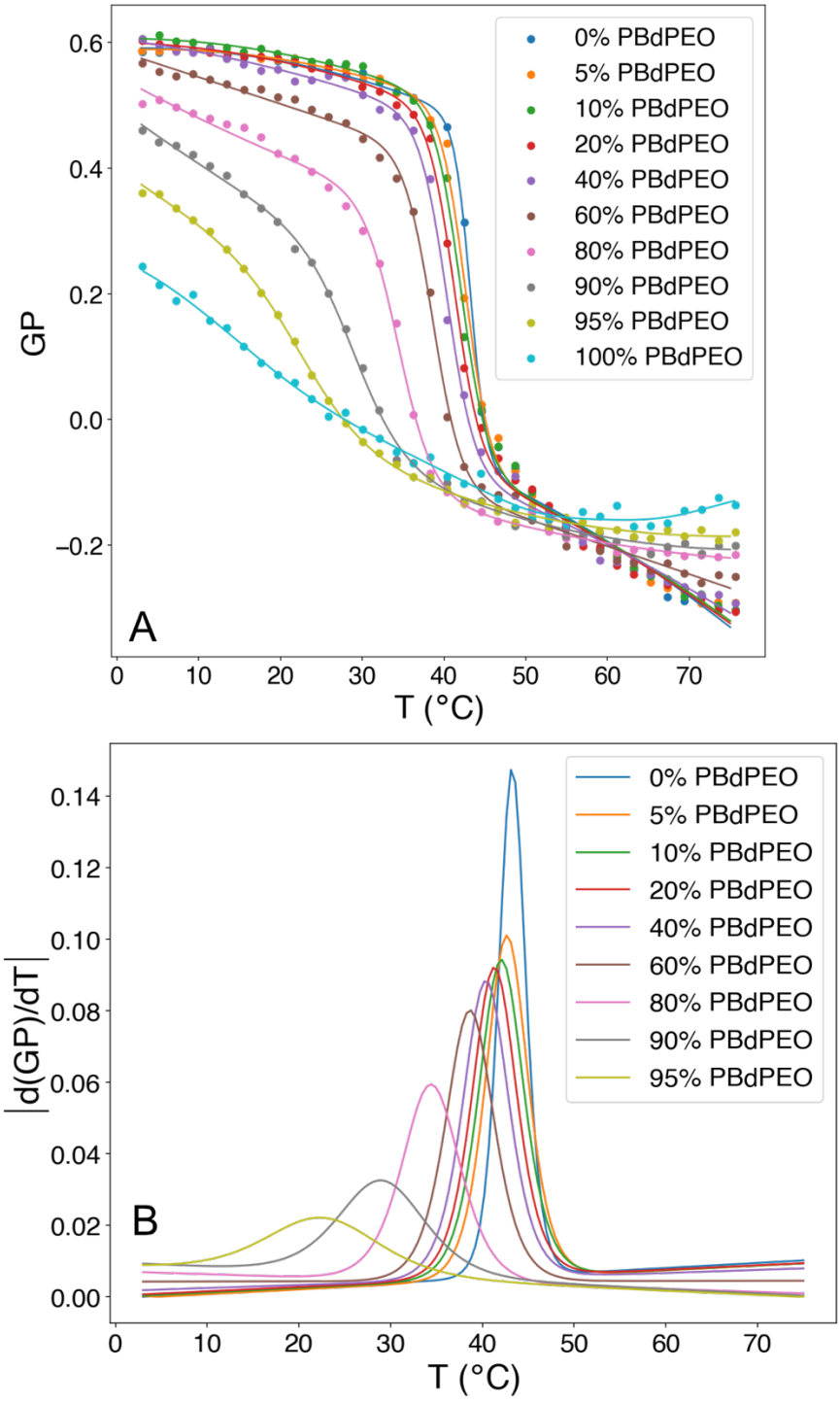

Figure 3. A. Generalized polarization (GP) of laurdan, corresponding to membrane polarity, as a function of temperature and vesicle composition. GP values were regressed against Equation (4), except for 100% PBd-PEO, for which no regression could be completed due to the lack of inflection point. Plotted line for 100% PBd-PEO is not the result of any fit. B. Absolute values of the derivatives of the regressed curves in A with respect to temperature.

Laurdan GP values in DPPC/PBd-PEO LUVs were calculated using Equation (3). Laurdan displays a red-shifted emission peak in more polar environments [24]. In the case of a lipid membrane undergoing a solid-to-fluid phase transition, an increase in polarity is due to the increase in membrane fluidity permitting increased hydration and thus increased polarity [24]. The dependence of laurdan GP on temperature and vesicle composition indicated similar results to those obtained by evaluating DPH anisotropy values as seen in Figure 3A. GP behaves as a sigmoidal function of temperature. As greater amounts of PBd-PEO were incorporated, the inflection point of the GP curves shifted to lower temperatures. No phase transition was evident for the pure PBd-PEO membrane. The inflection point of the plot of GP versus temperature corresponds to T_{mid}. T_{mid} values were evaluated by regression against a sigmoidal function (Equation (4)). T_{onset} and $T_{completion}$ values were determined as described for DPH anisotropy values (Figure S10). For 100% PBd-PEO LUVs, the observed GP values could not be regressed due to the lack of a clear inflection point, so the plotted line in Figure 3A is included only to guide the eye. T_{mid}, T_{onset}, and $T_{completion}$ could be evaluated for compositions ranging from 0-95% PBd-PEO, suggesting greater sensitivity of laurdan than DPH. A much broader transition was observed with laurdan for the pure DPPC LUVs (~9.3 ºC), as shown in Figure 3B, than when DPH was used as the fluorescent probe. However, neither laurdan nor DPH has been found to significantly perturb membrane phase transition behavior [36,37], suggesting this difference does not reflect a true broadening of the phase transition. The $T_{completion}$ values observed were approximately 3 ºC higher than those obtained from analysis of DPH fluorescence anisotropy.

2.4.2 Temperature dependence of FRET efficiency

To obtain further evidence regarding the presence or absence of separate DPPC-rich and PBd-PEO-rich phases in LUVs, the efficiency of FRET between the donor 1,2-dipalmitoyl-sn-glycero-

3-phosphoethanolamine-N-(7-nitro-2-1,3-benzoxadiazol-4-yl) (NBD-DPPE) and the acceptor 1,2-dioleoyl-sn-glycero-3-phosphoethanolamine-N-(lissamine rhodamine B sulfonyl) (Rh-DOPE) was evaluated. The Förster radius (R_0) of the NBD/Rh fluorophore pair is approximately 5 nm [38]. Domains smaller than the Förster radius cannot be resolved by FRET and result in a FRET profile indistinguishable from that of a randomly mixed membrane. NBD-DPPE has been found to prefer the ordered phase in DPPC/DOPC/cholesterol mixtures [39], while Rh-DOPE partitions preferentially into the disordered phase due to exclusion of its unsaturated acyl tails from the highly ordered solid phase [40,41]. In the case of fluid/solid phase coexistence, NBD-DPPE and Rh-DOPE would therefore be separated, reducing the efficiency of FRET. Additionally, attempts to conjugate a fluorescent probe to PBd-PEO were unsuccessful, further motivating the use of Rh-DOPE for FRET experiments. To account for the decrease in fluorescence emission intensity often observed with NBD probes at increasing temperature, FRET efficiency was evaluated over a range of temperatures as F/F_0, where F and F_0 are the donor emission intensity in the presence and absence of acceptor, respectively. FRET efficiency is thus $1-F/F_0$ [42]. Observed trends in F/F_0 are the result of changes in the average proximity of NBD and Rh. For two fluorophores expected to prefer different phases, a higher value of F/F_0 (lower FRET efficiency) would be expected in the case of separate domains. As the ordered phase transitions and the membrane mixes, F/F_0 decreases, resulting in a sigmoidal curve. Each F/F_0 curve was fit with a smoothed cubic spline and the inflection point of the curve was estimated visually to determine T_{mid}. T_{mid} corresponds to the midpoint of the transition from ordered domains large enough to reduce FRET efficiency to domains smaller than the Förster radius of the donor/acceptor pair.

DPPC/PBd-PEO LUVs containing large amounts of PBd-PEO (60-90%) demonstrated a sigmoidal dependence of F/F_0 on temperature (Figure 4), suggesting the coexistence of separate

DPPC-rich and PBd-PEO-rich phases, where ordered DPPC-rich domains decrease in size as the temperature is increased. The inflection points of the F/F_0 curves for these LUVs occur at temperatures as much as 10 °C below the T_{mid} values indicated by DPH anisotropy and laurdan GP curves. As mentioned above, the T_{mid} indicated by FRET represents the midpoint of the temperature range across which ordered domains become too small to be resolved by FRET. Pathak and London have previously reported discrepancies between values of T_{mid} observed with FRET and DPH anisotropy in lipid mixtures. They attributed this to the longer-range nature of FRET interactions (in comparison to DPH anisotropy, which reflects the immediate environment of the probe) [38,43].

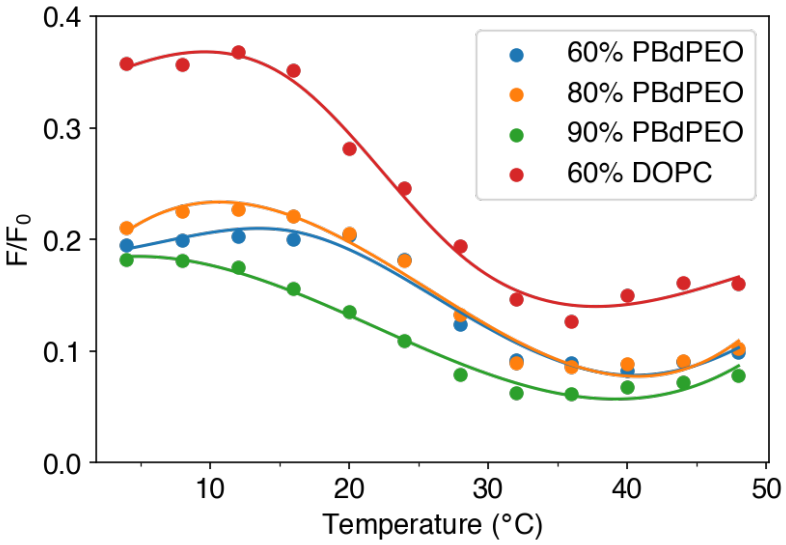

Figure 4. Efficiency of FRET between NBD-DPPE (0.1 mol%) and Rh-DOPE (2 mol%) in DPPC/PBd-PEO and DPPC/DOPC LUVs. Plotted lines are smoothed cubic splines fit to observed F/F0 values.

FRET efficiency between NBD and Rh was also evaluated in DPPC/DOPC LUVs containing 60% DOPC (Figure 4) for comparison. While DPH anisotropy indicates a T_{mid} of 29 °C for LUVs of this composition (Figure S1), FRET indicates a T_{mid} of ~26 °C. For LUVs containing the same amount of PBd-PEO instead of DOPC, FRET indicates a similar T_{mid} of ~27°C (although DPH

anisotropy indicates a higher T_{mid} for LUVs containing 60% PBd-PEO than for those containing 60% DOPC).

To further investigate the extent of domain coexistence in LUVs containing lower concentrations of PBd-PEO, NBD-DPPE was replaced by DPH as the FRET donor to Rh-DOPE (Figure 5). DPH is expected to partition equally between fluid and solid phases, and the DPH/Rh pair has been reported to have a Förster radius of ~3.6 nm [38]. A sigmoidal F/F_0 curve was observed for LUVs containing 40% PBd-PEO, suggesting coexistence of DPPC-rich and PBd-PEO-rich phases. The inflection point of this curve, corresponding to T_{mid}, was roughly 33.9 ^oC. This is 4-5 ^oC below the T_{mid} indicated by DPH anisotropy and laurdan GP—in closer agreement than the 8-10 ^oC difference between T_{mid} observed in our hybrid membranes with the NBD/Rh FRET pair. Indeed, FRET pairs with smaller Förster radii, which can detect smaller domains, report higher values of T_{mid} [38,43]. In relation to this work, the size of nanodomains in a sphingomyelin/POPC/cholesterol mixture was inferred by comparing the efficiencies of FRET between donor/acceptor pairs with different Förster radii [44].

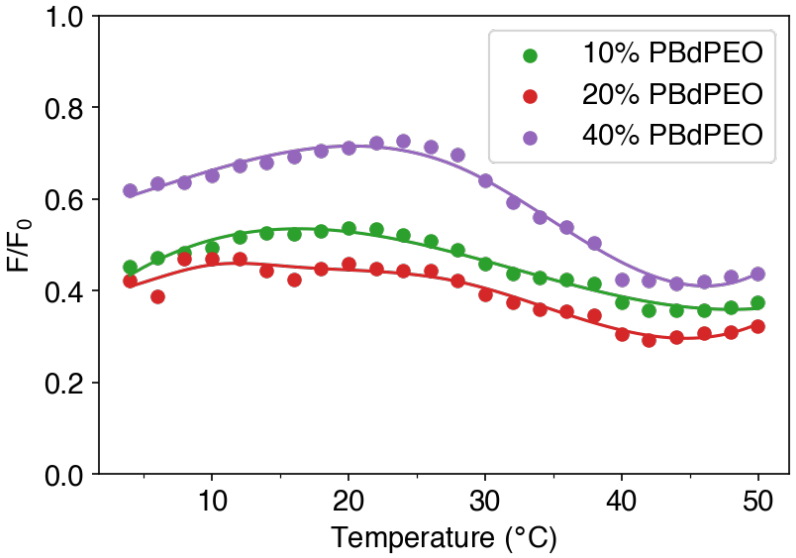

Figure 5. Efficiency of FRET between DPH (0.2 mol%) and Rh-DOPE (1 mol%) in LUVs made with 10 mol%, 20 mol%, and 40 mol% PBd-PEO between 4 and 50 oC. Plotted lines are smoothed cubic splines fit to each set of F/F0 values.

Above T_{mid}, the low F/F_0 values observed suggest DPPC and PBd-PEO mix to form a single fluid phase, rather than demonstrating fluid-fluid phase separation (as has been reported for a different lipid/copolymer mixture) [18]. The block copolymer used in this work is expected to have a hydrophobic thickness of ~3 nm [45,46], comparable to that of a fluid lipid membrane. Observation of a single fluid phase above T_{mid} is thus reasonable, as the hydrophobic thickness mismatch between fluid DPPC and PBd-PEO is minimal.

The sigmoidal shape of the F/F_0 curve indicative of a phase transition is largely absent for LUVs containing lower amounts of PBd-PEO (10% and 20%). LUVs containing lower amounts of PBd-PEO have relatively little of the disordered phase, so it is likely that an appreciable amount of Rh-DOPE may also partition into the ordered DPPC-rich phase. This would result in premature quenching of the FRET donor and little change in FRET efficiency once the membrane eventually transitions.

We additionally investigated the effect of Rh-DOPE on the observed T_{mid} in order to ensure the discrepancy between T_{mid} values reported by FRET and DPH anisotropy/laurdan GP is not an artifact from the probe incorporation in the hybrid bilayer. DPH anisotropy and laurdan GP were used to assess T_{mid} in DPPC/PBd-PEO LUVs made with and without Rh-DOPE at the concentrations used for the FRET experiments described above (Figure S8). DPH anisotropy and laurdan GP reported an increase in T_{mid} of 0.5-1.3 ^{o}C upon inclusion of 1% Rh-DOPE, and 0.9-2.2 ^{o}C upon inclusion of 2% Rh-DOPE (Table S2), which cannot explain the much lower T_{mid} values reported by FRET in comparison to DPH anisotropy/laurdan GP. Therefore, as discussed earlier, it seems likely that the lower T_{mid} measured using FRET indicates the presence of nanodomains.

2.4.3 DPPC/PBd-PEO phase diagram and comparisons to GUV behavior.

T_{onset}, T_{mid}, and $T_{completion}$ obtained from analysis of DPH anisotropy, laurdan GP, and FRET experiments are summarized in Figure 6A. The $T_{completion}$ line indicates the endpoint of solid/fluid phase coexistence, i.e. the liquidus boundary. At temperatures above $T_{completion}$, solid/fluid phase coexistence gives way to full fluidization of the membrane. The fact that the liquidus line is relatively horizontal between 0% and 60% PBd-PEO suggests the possibility of a coexisting DPPC-rich fluid phase with a PBd-PEO rich fluid phase above this line. Although we label this region as one phase, i.e. F(L+P), based on analysis in the previous sections, this is actually still an open question. The solidus boundary on the left side of the phase diagram has been sketched in to mirror the weak partitioning of DPPC into the PBd-PEO-rich phase seen on the right side of the liquidus line. Both DPH and laurdan results indicate a broad solid/fluid coexistence region (S(L) + F(P)) corresponding to solid DPPC lipid-rich and fluid PBd-PEO polymer-rich phases. The liquidus line has the same shape when plotted with respect to the mass fraction of PBd-PEO (Figure

6B) which accounts for the possible impact of polymer polydispersity on the actual molar composition.

For comparison, ideal phase transition temperatures for a range of compositions were also sketched by calculating the freezing point depression of DPPC in an ideal mixture of DPPC and PBd-PEO. The molal freezing point depression constant (cryoscopic constant) was calculated based on an enthalpy of fusion of 8.7 kcal/mol [11] and a van't Hoff factor of 0.5 to account for registry of solid DPPC domains across the bilayer. The large difference in the shape of this line in comparison to the $T_{completion}$ and T_{mid} lines of DPPC/PBd-PEO is a further indication of the non-ideality of the DPPC/PBd-PEO system.

We would expect that the bottom side of the solidus boundary exists at a temperature well below 0 °C as appropriate for PBd-PEO. Therefore, the T_{onset} line is not a solidus line. Indeed, Lentz et al. [12] show a line under the liquidus line, and of the same shape, for DOPC/DPPC membranes measured by DPH anisotropy and interpret it as well within the solid/fluid coexistence region. Based upon their work, it appears that DPH is most sensitive to the fluidity change that takes place in the membrane as it approaches and then crosses the solid/fluid to fluid boundary. Laurdan GP appears to be behaving similarly, as the T_{onset} line closely follows the shape of the $T_{completion}$ line. In contrast, FRET analysis reveals a shift in solid-phase domain size which may be why T_{mid} by FRET (purple stars) may not be following the downward trend of the liquidus line in comparison to T_{mid} for the DPH anisotropy and laurdan GP results, which clearly follow that trend.

Representative fluorescence microscopy images of hybrid GUVs in room-temperature (22 °C ± °2 C) water are shown in Figure 6C, corresponding to the labeled points in Figure 6A. GUVs were formed at 50-55 °C and allowed to cool freely to room temperature (a process typically

requiring ~45 minutes) before being diluted into room temperature water and imaged. GUVs containing as much as 95% PBd-PEO (Figure 6C) demonstrate clear phase separation indicated by the partitioning of the fluorescently labeled lipid Texas Red DHPE away from solid DPPC-rich (dark) and into fluid PBd-PEO-rich (bright) domains. GUVs containing small amounts of DPPC display irregularly shaped dark domains characteristic of the solid DPPC-rich phase. 50% PBd-PEO GUVs display dark DPPC-rich domains surrounded by bright, interconnected PBd-PEO-rich stripes (Figure 6C) in approximately equal proportions consistent with the composition on the phase diagram. Previous work studying hybrid lipid/block copolymer GUVs has suggested that at ≥ 50% DPPC such dark DPPC-rich stripes consist of the gel ($L_{\beta'}$) phase, while patchy domains have been attributed to kinetic trapping of the ripple ($P_{\beta'}$) phase [2]. Pure PBd-PEO GUVs do not demonstrate such phase separation, but instead appear to consist of a single fluid phase (Figure 6C). This is consistent with the absence of a phase transition indicated by DPH anisotropy and laurdan GP within this temperature range.

The Hildebrand solubility parameter of the polymer hydrophobic block, poly(1,2)-butadiene [47], is reported to be 15.9 $(J/cm^3)^{1/2}$. This solubility parameter is similar for alkanes, typically ranging from ~14-16 $(J/cm^3)^{1/2}$ [48], suggesting the strong tendency for DPPC and PBd-PEO to phase separate does not arise from a fundamental insolubility of the hydrophobic portions of the two components with respect to each other. The PBd-PEO copolymer used in this work has an average molecular weight of 950 g/mol, lighter than those previously studied throughout the literature, which generally range from 1800 to at least 3800 g/mol [16,19,20]. While a smaller hydrophobic mismatch would therefore be expected between DPPC and the lighter PBd-PEO used in this work, as opposed to the heavier copolymers, an extensive two-phase coexistence regime is still observed.

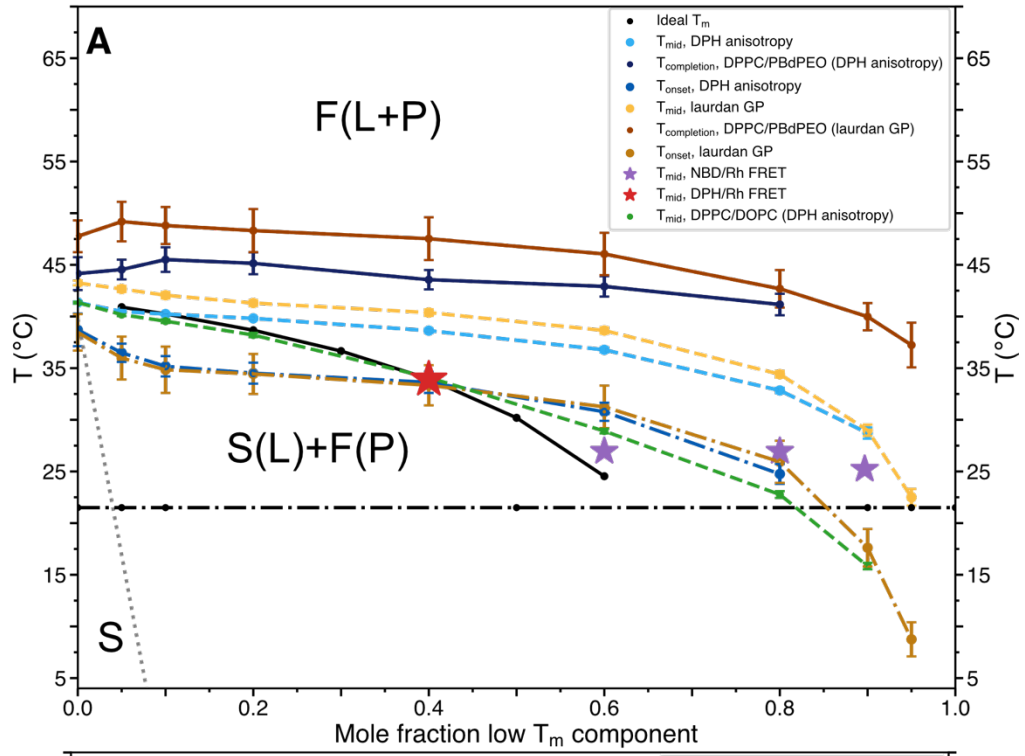
A
F(L+P)
S(L)+F(P)
S
Ideal T_m
T_{mid}, DPH anisotropy
$T_{completion}$, DPPC/PBdPEO (DPH anisotropy)
T_{onset}, DPH anisotropy
T_{mid}, laurdan GP
$T_{completion}$, DPPC/PBdPEO (laurdan GP)
T_{onset}, laurdan GP
T_{mid}, NBD/Rh FRET
T_{mid}, DPH/Rh FRET
T_{mid}, DPPC/DOPC (DPH anisotropy)
T (°C)
Mole fraction low T_m component

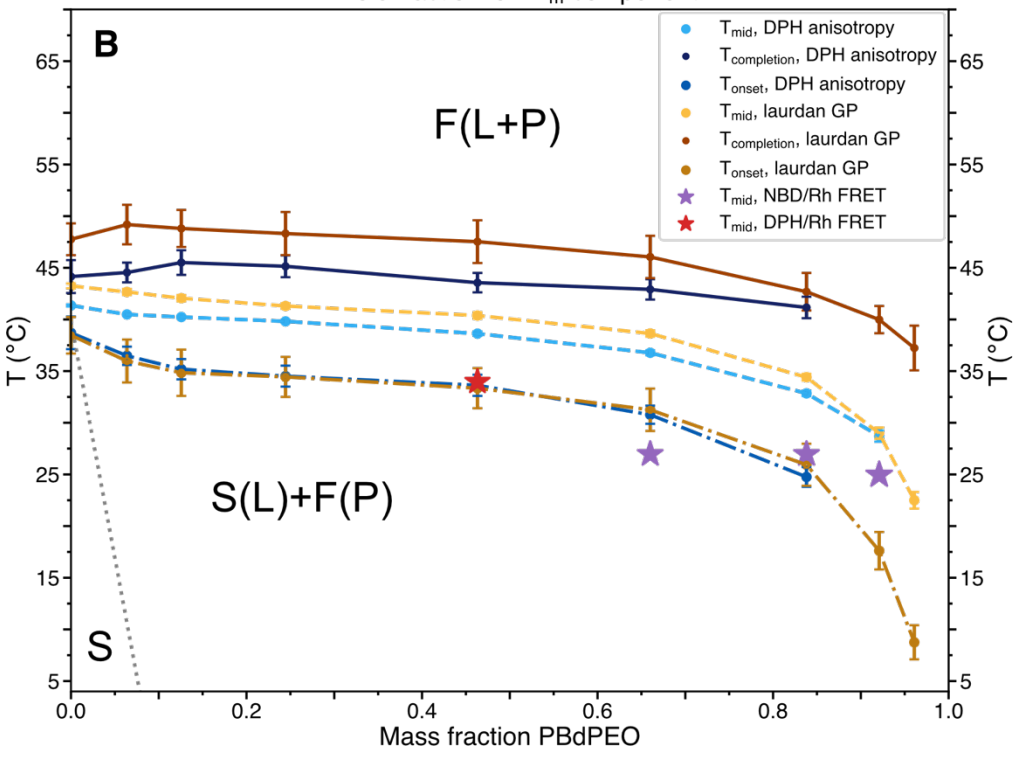
B
F(L+P)
S(L)+F(P)
S
T_{mid}, DPH anisotropy
$T_{completion}$, DPH anisotropy
T_{onset}, DPH anisotropy
T_{mid}, laurdan GP
$T_{completion}$, laurdan GP
T_{onset}, laurdan GP
T_{mid}, NBD/Rh FRET
T_{mid}, DPH/Rh FRET
T (°C)
Mass fraction PBdPEO

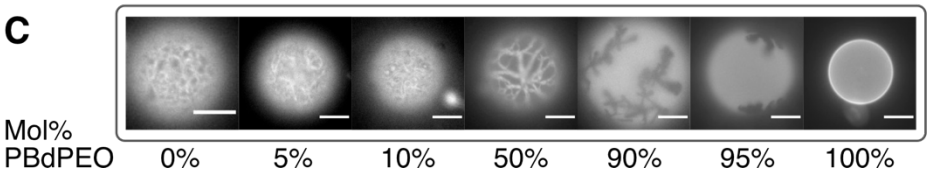
C
Mol%
PBdPEO
0%
5%
10%
50%
90%
95%
100%

Figure 6. A. A summary of the onset (T_{onset}), inflection (T_{mid}), and completion ($T_{completion}$) temperatures of the sigmoidal curves indicated by DPH anisotropy, laurdan GP, and FRET between NBD-DPPE/Rh-DOPE or DPH/Rh-DOPE. All data corresponds to DPPC/PBd-PEO vesicles unless otherwise indicated; dashed green line corresponds to DPPC/DOPC vesicles. L and P indicate DPPC lipid-rich and PBd-PEO polymer-rich, respectively; S and F indicate solid and fluid phases. Points obtained by analysis of DPH anisotropy are shown in blue, while points obtained by analysis of laurdan GP are in orange; connecting lines are drawn to guide the eye and not the result of any applied fits. Uncertainty values for 0% PBd-PEO DPH anisotropy data were determined by doubling the propagated standard deviation error for T_{mid} from independent regression of data from 3 samples against Equation (2). All other error bars represent twice the standard deviation error for the value of T_{mid} returned from regression of measured data from one sample against Equation (2) or (4). For $T_{completion}$ and T_{onset}, error bounds were determined as the difference between the intersection of tangent lines to the points of steepest slope and of greatest curvature for the absolute value of the first derivative of the anisotropy or GP values for each composition. For 0% PBd-PEO, this uncertainty was propagated for 3 samples; for all other samples, plotted values represent data from one sample. Dotted gray line is an estimate of the left side of the solidus line. B. Same data as presented in Figure 6A, but with respect to the mass fraction of PBd-PEO instead of the mole fraction. C. Fluorescence microscopy images obtained at room temperature of GUVs labeled with 0.25 mol% Texas Red DHPE, corresponding to the appropriate points on the dot-dashed line in A. Scale bars represent 10 μm.

Of note, while DPH anisotropy and laurdan GP suggest DPPC/PBd-PEO bilayers display an extensive solid/fluid phase coexistence region, it is difficult to visually determine whether the inhomogeneity of hybrid GUVs containing smaller amounts of PBd-PEO (*e.g.* 5-10%) is due to phase separation or to the uneven partitioning of Texas Red DHPE (perhaps into the grain boundaries between regions of microcrystalline DPPC-rich solid phase). Indeed, pure DPPC GUVs demonstrate visible inhomogeneity (Figure 6C), likely for the latter reason.

We also constructed a phase diagram for DPPC/DOPC from our anisotropy data for comparison purposes (Figure S2) that is in good agreement with that of Lentz et al. [12], when converted to the microviscosity scale used in their work (Figure S3). For DPPC/PBd-PEO LUVs, $T_{completion}$ decreases only slightly as up to 90% PBd-PEO is added to DPPC, then begins to drop more rapidly as 95% PBd-PEO is approached. In contrast, for DPPC/DOPC LUVs $T_{completion}$ decreases only slightly as up to just 40% DOPC is added to DPPC, as shown in Figure S2. Beyond this point, $T_{completion}$ then decreases more rapidly as the amount of DPPC decreases for DPPC/DOPC LUVs than for DPPC/PBd-PEO LUVs. Therefore, solid DPPC-rich domains coexist with fluid PBd-PEO-rich domains across a larger range of compositions and temperatures than with fluid DOPC-rich domains as shown in Figure S2. For example, DPPC/PBd-PEO membranes contain coexisting

solid and fluid phases across nearly all compositions at room temperature as shown in Figure 6, compared to the narrower range of compositions for DPPC/DOPC (Figure S2). Overall, this comparison shows that while DPPC and PBd-PEO can coexist within hybrid membranes, DPPC partitions less readily into fluid PBd-PEO than into fluid DOPC. Despite this, DPPC appears to have a measurable ordering effect on PBd-PEO based upon the positive deviation from ideal DPH anisotropy discussed in Section 3.1. Moreover, the shape of the T_{mid} line for DPPC/DOPC, shown in Figure 6A for comparison, follows the ideal freezing point depression line remarkably more closely than for DPPC/PBd-PEO.

We then replaced DOPC with a phosphatidylcholine lipid with two unsaturations in each chain (18:2 PC) and subsequently with a lipid with three unsaturations in each chain (18:3 PC). For mixtures of DPPC and polyunsaturated lipids (DPPC/18:2 PC and DPPC/18:3 PC), the $T_{completion}$ values indicated by DPH anisotropy are very similar to those observed for DPPC/DOPC (Figure S2). Similar to the addition of DOPC, $T_{completion}$ displays slight decreases as up to 40% of either 18:2 PC or 18:3 PC is added, then decreases more rapidly as more 18:2 PC or 18:3 PC is added. This emphasizes the extensive nature of the DPPC/PBd-PEO phase coexistence region in comparison to the phase behavior observed for mixtures of solely lipids.

2.5 Conclusions

A combination of fluorescence spectroscopy and microscopy was used to study fluidity and construct a phase diagram for DPPC/PBd-PEO. Fluorescence spectroscopy was also employed to study fluidity and outline a phase diagram for DPPC/DOPC, which was found to be in good agreement with previously published phase diagrams [10,12]. This provided a basis for

comparison between the phase behavior of a hybrid lipid/block copolymer membrane and a well-studied lipid system. The liquidus temperatures of DPPC/PBd-PEO display a generally similar dependence on composition to those of DPPC/DOPC, with the liquidus temperature of the mixture decreasing as the amount of the component with the lower phase transition temperature increases. However, DPPC/PBd-PEO displays an expanded solid/fluid phase coexistence region and mixing behavior that is less ideal in comparison to DPPC/DOPC. Solid DPPC partitions less readily into the PBd-PEO-rich fluid phase than into the DOPC-rich fluid phase. While strong negative deviations from ideal anisotropy show that that in the fluid region of the phase diagram, fluid DPPC strongly enhances the fluidity of PBd-PEO. Moreover, in the solid-fluid coexistence region, DPPC has a measurable ordering influence on PBd-PEO despite the weak partitioning of DPPC into the PBd-PEO-rich phase. These behaviors reflect that PBd-PEO demonstrates greater fluidity than a solid lipid membrane, but slightly lower fluidity than a fluid lipid membrane. The phase information and diagram developed here may be useful for the design of hybrid biomembranes for drug delivery vehicles or membrane protein reconstitution, given the importance of understanding the membrane phase state for such applications.

2.6 Acknowledgements

This material is based upon work supported by the National Science Foundation under Grant No. DMR – 1806366.

2.7 References

[1] B.M. Discher, Y.-Y. Won, D.S. Ege, J.C.-M. Lee, F.S. Bates, D.E. Discher, D.A. Hammer, Polymersomes: Tough Vesicles Made from Diblock Copolymers, Science. 284 (1999) 1143–1146. https://doi.org/10.1126/science.284.5417.1143.

[2] D. Chen, M.M. Santore, Hybrid copolymer–phospholipid vesicles: phase separation resembling mixed phospholipid lamellae, but with mechanical stability and control, Soft Matter. 11 (2015) 2617–2626. https://doi.org/10.1039/C4SM02502D.

[3] Z.I. Imam, L.E. Kenyon, G. Ashby, F. Nagib, M. Mendicino, C. Zhao, A.K. Gadok, J.C. Stachowiak, Phase-Separated Liposomes Enhance the Efficiency of Macromolecular Delivery to the Cellular Cytoplasm, Cel. Mol. Bioeng. 10 (2017) 387–403. https://doi.org/10.1007/s12195-017-0489-4.

[4] R. Koynova, L. Wang, R.C. MacDonald, Synergy in Lipofection by Cationic Lipid Mixtures: Superior Activity at the Gel−Liquid Crystalline Phase Transition, J. Phys. Chem. B. 111 (2007) 7786–7795. https://doi.org/10.1021/jp071286y.

[5] H. de Lima Santos, M.L. Lopes, B. Maggio, P. Ciancaglini, Na,K-ATPase reconstituted in liposomes: effects of lipid composition on hydrolytic activity and enzyme orientation, Colloids and Surfaces B: Biointerfaces. 41 (2005) 239–248. https://doi.org/10.1016/j.colsurfb.2004.12.013.

[6] T. Bhatia, F. Cornelius, J. Brewer, L.A. Bagatolli, A.C. Simonsen, J.H. Ipsen, O.G. Mouritsen, Spatial distribution and activity of Na+/K+-ATPase in lipid bilayer membranes with phase boundaries, Biochimica et Biophysica Acta (BBA) - Biomembranes. 1858 (2016) 1390–1399. https://doi.org/10.1016/j.bbamem.2016.03.015.

[7] B. Cannon, M. Hermansson, S. Györke, P. Somerharju, J.A. Virtanen, K.H. Cheng, Regulation of Calcium Channel Activity by Lipid Domain Formation in Planar Lipid Bilayers, Biophysical Journal. 85 (2003) 933–942. https://doi.org/10.1016/S0006-3495(03)74532-9.

[8] Ü. Coskun, M. Grzybek, D. Drechsel, K. Simons, Regulation of human EGF receptor by lipids, PNAS. 108 (2011) 9044–9048. https://doi.org/10.1073/pnas.1105666108.

[9] S.L. Veatch, S.L. Keller, Separation of Liquid Phases in Giant Vesicles of Ternary Mixtures of Phospholipids and Cholesterol, Biophysical Journal. 85 (2003) 3074–3083. https://doi.org/10.1016/S0006-3495(03)74726-2.

[10] M.L. Schmidt, L. Ziani, M. Boudreau, J.H. Davis, Phase equilibria in DOPC/DPPC: Conversion from gel to subgel in two component mixtures, The Journal of Chemical Physics. 131 (2009) 175103. https://doi.org/10.1063/1.3258077.

[11] S. Mabrey, J.M. Sturtevant, Investigation of phase transitions of lipids and lipid mixtures by sensitivity differential scanning calorimetry, PNAS. 73 (1976) 3862–3866. https://doi.org/10.1073/pnas.73.11.3862.

[12] B.R. Lentz, Y. Barenholz, T.E. Thompson, Fluorescence depolarization studies of phase transitions and fluidity in phospholipid bilayers. 2. Two-component phosphatidylcholine liposomes, Biochemistry. 15 (1976) 4529–4537. https://doi.org/10.1021/bi00665a030.

[13] F.A. Heberle, J.T. Buboltz, D. Stringer, G.W. Feigenson, Fluorescence methods to detect phase boundaries in lipid bilayer mixtures, Biochimica et Biophysica Acta (BBA) - Molecular Cell Research. 1746 (2005) 186–192. https://doi.org/10.1016/j.bbamcr.2005.05.008.

[14] J. Nam, T.K. Vanderlick, P.A. Beales, Formation and dissolution of phospholipid domains with varying textures in hybrid lipo-polymersomes, Soft Matter. 8 (2012) 7982–7988. https://doi.org/10.1039/c2sm25646k.

[15] T.P.T. Dao, F. Fernandes, E. Ibarboure, K. Ferji, M. Prieto, O. Sandre, J.-F. Le Meins, Modulation of phase separation at the micron scale and nanoscale in giant polymer/lipid hybrid unilamellar vesicles (GHUVs), Soft Matter. 13 (2017) 627–637. https://doi.org/10.1039/C6SM01625A.

[16] C. Magnani, C. Montis, G. Mangiapia, A.-F. Mingotaud, C. Mingotaud, C. Roux, P. Joseph, D. Berti, B. Lonetti, Hybrid vesicles from lipids and block copolymers: Phase behavior from the micro- to the nano-scale, Colloids and Surfaces B: Biointerfaces. 168 (2018) 18–28. https://doi.org/10.1016/j.colsurfb.2018.01.042.

[17] M. Schulz, D. Glatte, A. Meister, P. Scholtysek, A. Kerth, A. Blume, K. Bacia, W.H. Binder, Hybrid lipid/polymer giant unilamellar vesicles: effects of incorporated biocompatible PIB–PEO block copolymers on vesicle properties, Soft Matter. 7 (2011) 8100–8110. https://doi.org/10.1039/C1SM05725A.

[18] T.P.T. Dao, F. Fernandes, M. Er-Rafik, R. Salva, M. Schmutz, A. Brûlet, M. Prieto, O. Sandre, J.-F. Le Meins, Phase Separation and Nanodomain Formation in Hybrid Polymer/Lipid Vesicles, ACS Macro Lett. 4 (2015) 182–186. https://doi.org/10.1021/mz500748f.

[19] J. Nam, P.A. Beales, T.K. Vanderlick, Giant Phospholipid/Block Copolymer Hybrid Vesicles: Mixing Behavior and Domain Formation, Langmuir. 27 (2011) 1–6. https://doi.org/10.1021/la103428g.

[20] S. Khan, M. Li, S.P. Muench, L.J.C. Jeuken, P.A. Beales, Durable proteo-hybrid vesicles for the extended functional lifetime of membrane proteins in bionanotechnology, Chem. Commun. 52 (2016) 11020–11023. https://doi.org/10.1039/C6CC04207D.

[21] T.P.T. Dao, A. Brûlet, F. Fernandes, M. Er-Rafik, K. Ferji, R. Schweins, J.-P. Chapel, A. Fedorov, M. Schmutz, M. Prieto, O. Sandre, J.-F. Le Meins, Mixing Block Copolymers with Phospholipids at the Nanoscale: From Hybrid Polymer/Lipid Wormlike Micelles to Vesicles Presenting Lipid Nanodomains, Langmuir. 33 (2017) 1705–1715. https://doi.org/10.1021/acs.langmuir.6b04478.

[22] A.F. Halasa, J.M. Massie, Polybutadiene, in: Kirk-Othmer Encyclopedia of Chemical Technology, John Wiley & Sons, Inc, 2000. https://doi.org/10.1002/0471238961.1615122508011201.a01.

[23] R.F.M. de Almeida, A. Fedorov, M. Prieto, Sphingomyelin/Phosphatidylcholine/Cholesterol Phase Diagram: Boundaries and Composition of Lipid Rafts, Biophysical Journal. 85 (2003) 2406–2416. https://doi.org/10.1016/S0006-3495(03)74664-5.

[24] T. Parasassi, G. De Stasio, A. d'Ubaldo, E. Gratton, Phase fluctuation in phospholipid membranes revealed by Laurdan fluorescence, Biophysical Journal. 57 (1990) 1179–1186. https://doi.org/10.1016/S0006-3495(90)82637-0.

[25] S.C. Nelson, S.K. Neeley, E.D. Melonakos, J.D. Bell, D.D. Busath, Fluorescence anisotropy of diphenylhexatriene and its cationic Trimethylamino derivative in liquid dipalmitoylphosphatidylcholine liposomes: opposing responses to isoflurane, BMC Biophys. 5 (2012) 5. https://doi.org/10.1186/2046-1682-5-5.

[26] W.F. Zeno, S. Hilt, K.K. Aravagiri, S.H. Risbud, J.C. Voss, A.N. Parikh, M.L. Longo, Analysis of Lipid Phase Behavior and Protein Conformational Changes in Nanolipoprotein Particles upon Entrapment in Sol–Gel-Derived Silica, Langmuir. 30 (2014) 9780–9788. https://doi.org/10.1021/la5025058.

[27] M. Shinitzky, Y. Barenholz, Dynamics of the Hydrocarbon Layer in Liposomes of Lecithin and Sphingomyelin Containing Dicetylphosphate, J. Biol. Chem. 249 (1974) 2652–2657.

[28] T. Parasassi, G. De Stasio, G. Ravagnan, R.M. Rusch, E. Gratton, Quantitation of lipid phases in phospholipid vesicles by the generalized polarization of Laurdan fluorescence, Biophysical Journal. 60 (1991) 179–189. https://doi.org/10.1016/S0006-3495(91)82041-0.

[29] M.R. Vist, J.H. Davis, Phase equilibria of cholesterol/dipalmitoylphosphatidylcholine mixtures: deuterium nuclear magnetic resonance and differential scanning calorimetry, Biochemistry. 29 (1990) 451–464. https://doi.org/10.1021/bi00454a021.

[30] B.R. Lentz, Y. Barenholz, T.E. Thompson, Fluorescence depolarization studies of phase transitions and fluidity in phospholipid bilayers. 1. Single component phosphatidylcholine liposomes, Biochemistry. 15 (1976) 4521–4528. https://doi.org/10.1021/bi00665a029.

[31] J.C.-M. Lee, M. Santore, F.S. Bates, D.E. Discher, From Membranes to Melts, Rouse to Reptation: Diffusion in Polymersome versus Lipid Bilayers, Macromolecules. 35 (2002) 323–326. https://doi.org/10.1021/ma0112063.

[32] R. Dimova, U. Seifert, B. Pouligny, S. Förster, H.-G. Döbereiner, Hyperviscous diblock copolymer vesicles, Eur. Phys. J. E. 7 (2002) 241–250. https://doi.org/10.1140/epje/i200101032.

[33] J. Ehrig, E.P. Petrov, P. Schwille, Phase separation and near-critical fluctuations in two-component lipid membranes: Monte Carlo simulations on experimentally relevant scales, New J. Phys. 13 (2011) 045019. https://doi.org/10.1088/1367-2630/13/4/045019.

[34] R.L. Biltonen, D. Lichtenberg, The use of differential scanning calorimetry as a tool to characterize liposome preparations, Chemistry and Physics of Lipids. 64 (1993) 129–142. https://doi.org/10.1016/0009-3084(93)90062-8.

[35] M.M. Lozano, M.L. Longo, Complex formation and other phase transformations mapped in saturated phosphatidylcholine/DSPE-PEG2000 monolayers, Soft Matter. 5 (2009) 1822. https://doi.org/10.1039/b820070j.

[36] J. Repáková, J.M. Holopainen, M.R. Morrow, M.C. McDonald, P. Čapková, I. Vattulainen, Influence of DPH on the Structure and Dynamics of a DPPC Bilayer, Biophysical Journal. 88 (2005) 3398–3410. https://doi.org/10.1529/biophysj.104.055533.

[37] S.S.W. Leung, J. Thewalt, Link between Fluorescent Probe Partitioning and Molecular Order of Liquid Ordered-Liquid Disordered Membranes, J. Phys. Chem. B. 121 (2017) 1176–1185. https://doi.org/10.1021/acs.jpcb.6b09325.

[38] P. Pathak, E. London, The Effect of Membrane Lipid Composition on the Formation of Lipid Ultrananodomains, Biophysical Journal. 109 (2015) 1630–1638. https://doi.org/10.1016/j.bpj.2015.08.029.

[39] J. Juhasz, J.H. Davis, F.J. Sharom, Fluorescent probe partitioning in giant unilamellar vesicles of 'lipid raft' mixtures, Biochem. J. 430 (2010) 415–423. https://doi.org/10.1042/BJ20100516.

[40] T. Baumgart, G. Hunt, E.R. Farkas, W.W. Webb, G.W. Feigenson, Fluorescence probe partitioning between Lo/Ld phases in lipid membranes, Biochimica et Biophysica Acta (BBA) - Biomembranes. 1768 (2007) 2182–2194. https://doi.org/10.1016/j.bbamem.2007.05.012.

[41] P. Sengupta, A. Hammond, D. Holowka, B. Baird, Structural determinants for partitioning of lipids and proteins between coexisting fluid phases in giant plasma membrane vesicles, Biochimica et Biophysica Acta (BBA) - Biomembranes. 1778 (2008) 20–32. https://doi.org/10.1016/j.bbamem.2007.08.028.

[42] B.K.-K. Fung, L. Stryer, Surface density determination in membranes by fluorescence energy transfer, Biochemistry. 17 (1978) 5241–5248. https://doi.org/10.1021/bi00617a025.

[43] P. Pathak, E. London, Measurement of Lipid Nanodomain (Raft) Formation and Size in Sphingomyelin/POPC/Cholesterol Vesicles Shows TX-100 and Transmembrane Helices Increase Domain Size by Coalescing Preexisting Nanodomains But Do Not Induce Domain Formation, Biophysical Journal. 101 (2011) 2417–2425. https://doi.org/10.1016/j.bpj.2011.08.059.

[44] R.S. Petruzielo, F.A. Heberle, P. Drazba, J. Katsaras, G.W. Feigenson, Phase behavior and domain size in sphingomyelin-containing lipid bilayers, Biochimica et Biophysica Acta (BBA) - Biomembranes. 1828 (2013) 1302–1313. https://doi.org/10.1016/j.bbamem.2013.01.007.

[45] G. Srinivas, D.E. Discher, M.L. Klein, Self-assembly and properties of diblock copolymers by coarse-grain molecular dynamics, Nat. Mater. 3 (2004) 638–644. https://doi.org/10.1038/nmat1185.

[46] D.R. Barden, H. Vashisth, Parameterization and atomistic simulations of biomimetic membranes, Faraday Discuss. 209 (2018) 161–178. https://doi.org/10.1039/C8FD00047F.

[47] A.F.M. Barton, Handbook of Polymer-Liquid Interaction Parameters and Solubility Parameters, CRC Press, 1990.

[48] A.F.M. Barton, CRC Handbook of Solubility Parameters and Other Cohesion Parameters, 2nd ed., Routledge, 2017. https://doi.org/10.1201/9781315140575.

2.8 Supplementary Material

2.8.1 Comparisons to DPPC/DOPC

DPH anisotropy values and the absolute value of their derivatives in DPPC/DOPC LUVs were evaluated as a function of temperature (

Figure S1A and S1B) to provide a comparison to DPPC/PBd-PEO LUVs.

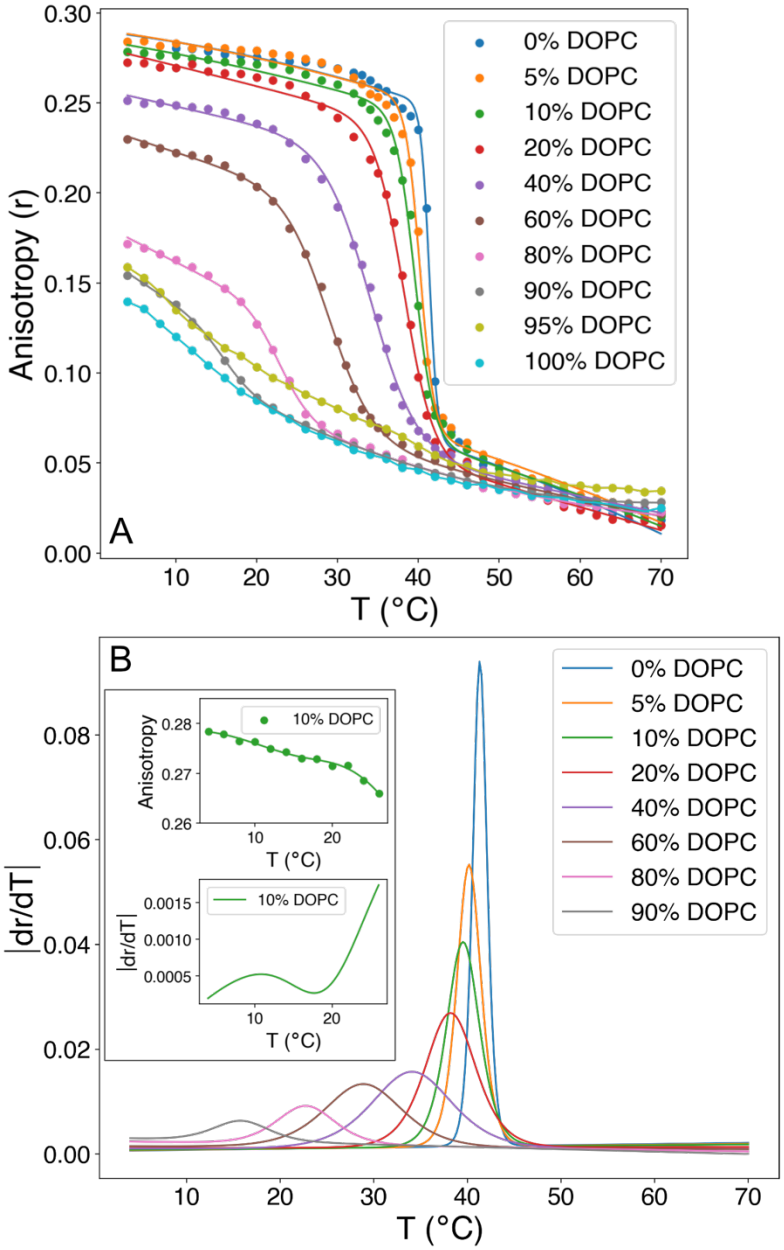

Figure S1. A. Anisotropy (r) of DPH in DPPC/DOPC LUVs as a function of temperature. Plotted lines show sigmoidal fit to measured anisotropy values as described in the main text (Section 2.3), except for LUVs containing 95% or 100% DOPC. Equation 2 (main text, Section 2.3) could not be regressed for these compositions due to the lack of clear inflection point. Plotted lines for 95% and 100% DOPC are not the result of any fit. B. Absolute values of the derivatives of the regressed curves in A with respect to temperature. Inset shows the same sigmoidal fit applied to 10% DOPC LUVs from 4-26 °C, the temperature range within which the transition of DOPC from the solid to the fluid phase is expected. The fit yielded a T_{mid} of 10.9 °C, corresponding to the maximum of the absolute value of the first derivative of the fit with respect to temperature.

Figure S2 compares $T_{completion}$ of DPPC/DOPC, DPPC/18:2 PC, DPPC/18:3 PC, and DPPC/PBd-PEO vesicles. S, S+F, and F indicate regions where solid, solid and fluid, and fluid phases exist or

coexist. Solid domains are DPPC-rich. $T_{completion}$ was obtained from DPH anisotropy for DPPC/DOPC, DPPC/18:2 PC, and DPPC/18:3 PC LUVs and from DPH anisotropy and laurdan GP for DPPC/PBd-PEO LUVs.

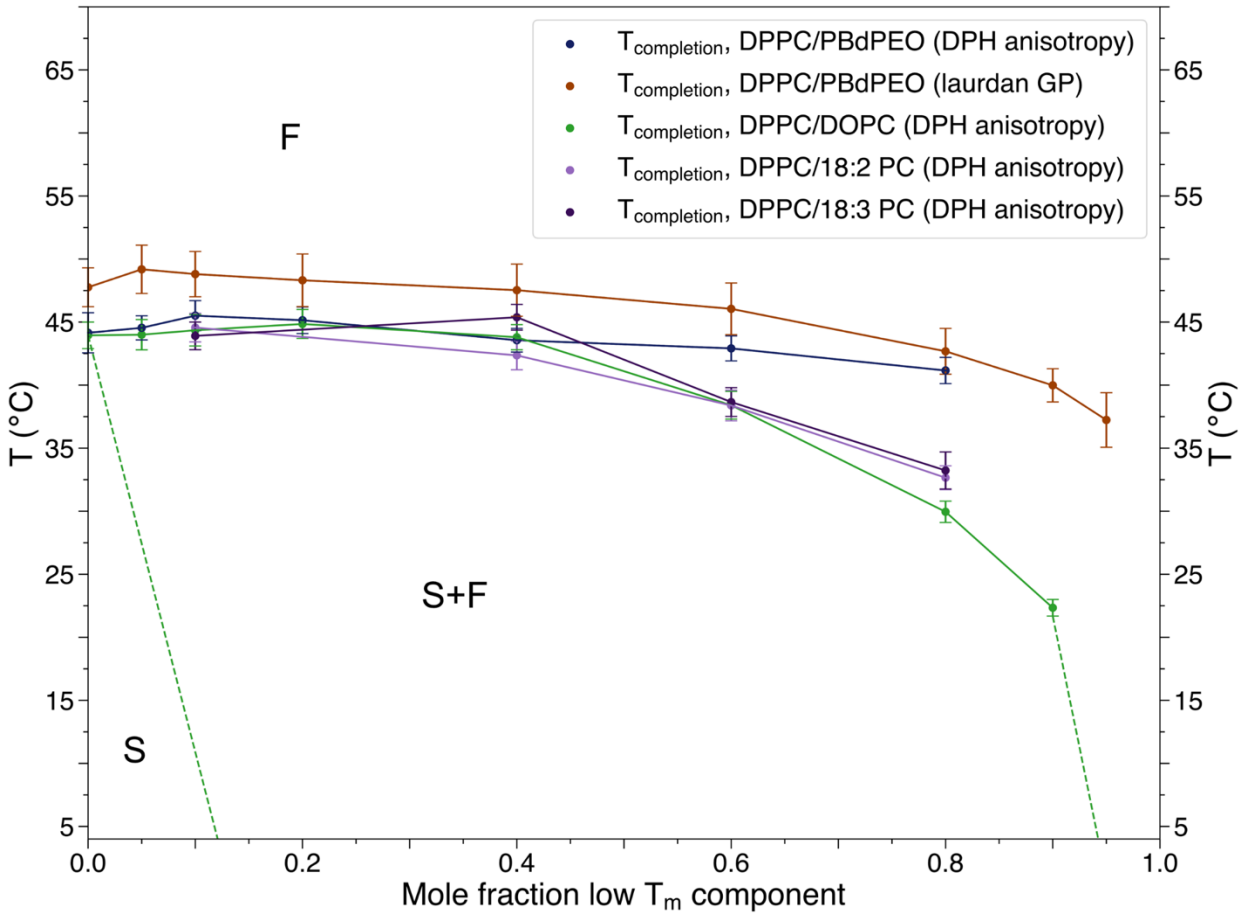

Figure S2. Comparison between $T_{completion}$ for DPPC/DOPC, DPPC/18:2 PC, DPPC/18:3 PC, and DPPC/PBd-PEO LUVs. The x-axis corresponds to the mole fraction of DOPC for DPPC/DOPC LUVs, or to the mole fraction of PBd-PEO for PBd-PEO/DPPC LUVs. The left dashed green line represents the left side of the DPPC/DOPC solidus line based on the T_{mid} of 10.9 °C as an estimate for the solidus transition in 10% DOPC LUVs (see lower inset of Figure S1B). The right dashed green line is an estimated continuation of the DPPC/DOPC liquidus line, drawn based on a solid-fluid transition temperatureof -20 ºC for pure DOPC [1,2]. Error bounds for $T_{completion}$ were determined as the difference between the intersection of tangent lines to the points of steepest slope and of greatest curvature for the absolute value of the first derivative of the anisotropy or GP values for each composition. For 100% DPPC, this uncertainty was propagated for 3 samples; for all other samples, plotted values represent data from one sample. Error bars correspond to two times the propagated standard deviation error from three samples (100% DPPC DPH anisotropy data) or two times the standard deviation error from one sample (all other data) for the value of T_{mid} returned from regression of measured DPH anisotropy or GP values against a sigmoidal function as described in "Methods" in the main text (Section 2.3).

For comparison, the data presented in Figure S1 using LUVs were also analyzed using the calculations described by Lentz et al. [2,3] (Figure S3). Using this method, the delimiting

temperatures of the phase transition correspond to breakpoints in the dependence of the apparent viscosity of the membrane. According to the phase diagram of Lentz et al. [2], the onset (T_{low}) and completion (T_{high}) temperatures decrease nearly linearly with vesicle composition for multilamellar vesicles (MLVs). However, three delimiting temperatures were reported for small unilamellar vesicles (SUVs) of each composition. For SUVs, the completion temperature decreases first slowly, then more rapidly as increasing amounts of DOPC are incorporated.

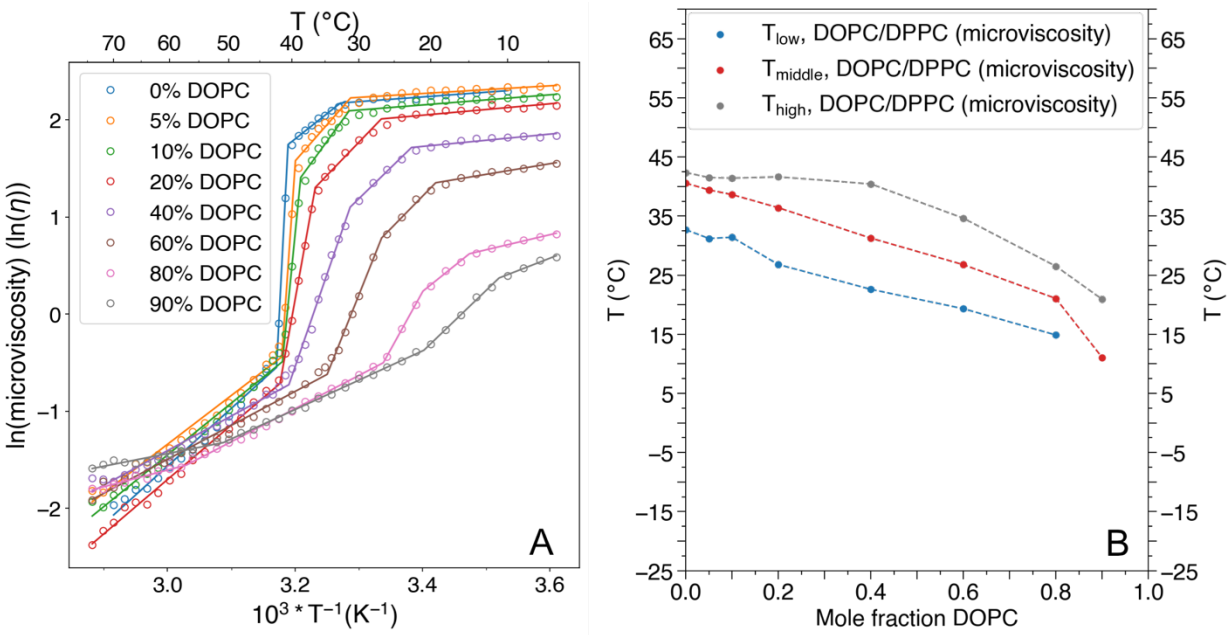

Figure S3. A. Temperature dependence of the natural logarithm of the apparent microviscosity of DPPC/DOPC LUVs, calculated as previously described [2,3] from the data shown in Figure S1. B. Breakpoints in the temperature dependence of microviscosity values shown in A, corresponding to the method previously used [2] to assess the delimiting temperatures of the phase transition.

Applying the methods of Lentz et al. [2,3] to the data in Figure S1 yielded Figure S3A. The profiles in Figure S3B shared characteristics with the phase diagrams published by Lentz et al. [2] for MLVs and for SUVs. Three distinct breakpoints (T_{low}, T_{middle}, T_{high}) in the dependence of apparent membrane viscosity with temperature were evident in the vicinity of the phase transition for the LUVs examined here, similar to the trends previously reported for SUVs. The shape of the completion temperature line was similar to that previously reported for SUVs. However, the shape

of the onset line was most similar to that previously reported for MLVs. Therefore, the profiles shared properties with both the MLV and SUV phase diagrams, perhaps due to the characteristics LUVs share with both MLVs and SUVs (i.e. reduced curvature strain in comparison to SUVs and unilamellarity, respectively). Similarly, the completion temperatures in Figure S3A are within a couple of degrees of those previously reported for SUVs below 60% DOPC and MLVs above 60% DOPC.

2.8.2 Effects of vesicle preparation and measurement methods on T_{mid}

The effects of various sample preparation methods on T_{mid} were investigated (Figure S4) at both 80% and 90% DOPC in DPPC/DOPC vesicles. Vesicle type and preparation methods vary across both of the previously published phase diagrams and the work presented here. Schmidt et al. constructed a phase diagram using MLVs in potassium phosphate buffer prepared from ethanol (EtOH)-based lipid stock solution [1], while Lentz et al. reported phase diagrams for MLVs and SUVs prepared from chloroform-based lipid stock solutions in a potassium chloride solution [2]. Factors such as vesicle suspension medium [4,5] and vesicle curvature and lamellarity [6,7] have been previously reported to impact bilayer mechanical properties and phase behavior to varying extents. The factors investigated here were therefore: vesicle type (LUV or MLV), lipid stock solution solvent (chloroform or EtOH), rehydration medium (20 mM Tris/100 mM NaCl buffer or water), LUV preparation method (freeze-thawed prior to extrusion, or extruded after hydration at ~50 ^{o}C), direction of temperature ramp during measurement (heating or cooling), and DPH:lipid ratio (1:30 or 1:500). If it is stated that vesicles were passed through freeze-thaw cycles prior to extrusion, lipid thin films of the desired composition were prepared as described in “Methods” in the main text (Section 2.2), hydrated at 50 ^{o}C, and subjected to five freeze-thaw cycles (5 minutes at -65 ^{o}C, 5 minutes at 50 ^{o}C). LUVs were then prepared by extrusion.

Slight variations in T_{mid} were observed for vesicles of differing lamellarity and sample preparation methods (

Table S1), and it is possible that some of the factors investigated may genuinely impact T_{mid}. For example, vesicle preparation in water instead of Tris/NaCl buffer generally corresponded to a slightly increased T_{mid}, suggesting the choice of buffer may have some effect on phase behavior. Very slight differences between T_{mid} values for DPPC vesicles of varying curvature and lamellarity have also been previously reported [6], and similar behavior is observed here as well. When averaged across preparation methods, 80% DOPC LUVs had a T_{mid} of (23.02±0.30) ºC, while 80% DOPC MLVs had a T_{mid} of (22.87±0.90) ºC. Similarly, 90% DOPC LUVs had a T_{mid} of (17.50±1.16) ºC, while 90% DOPC MLVs had a T_{mid} of (17.50±1.18) ºC. Further work would be required to draw definitive conclusions, however, as the standard deviation of T_{mid} observed here for both compositions (~0.6-1.2 ºC) is consistent with a variation in vesicle composition of ~1-2% (within the range of experimental error) due to the strong dependence of T_{mid} on composition for vesicles containing large amounts of DOPC. This suggests the T_{mid} reported in this work did not depend strongly on the sample preparation methods used, though slight variation is still possible.

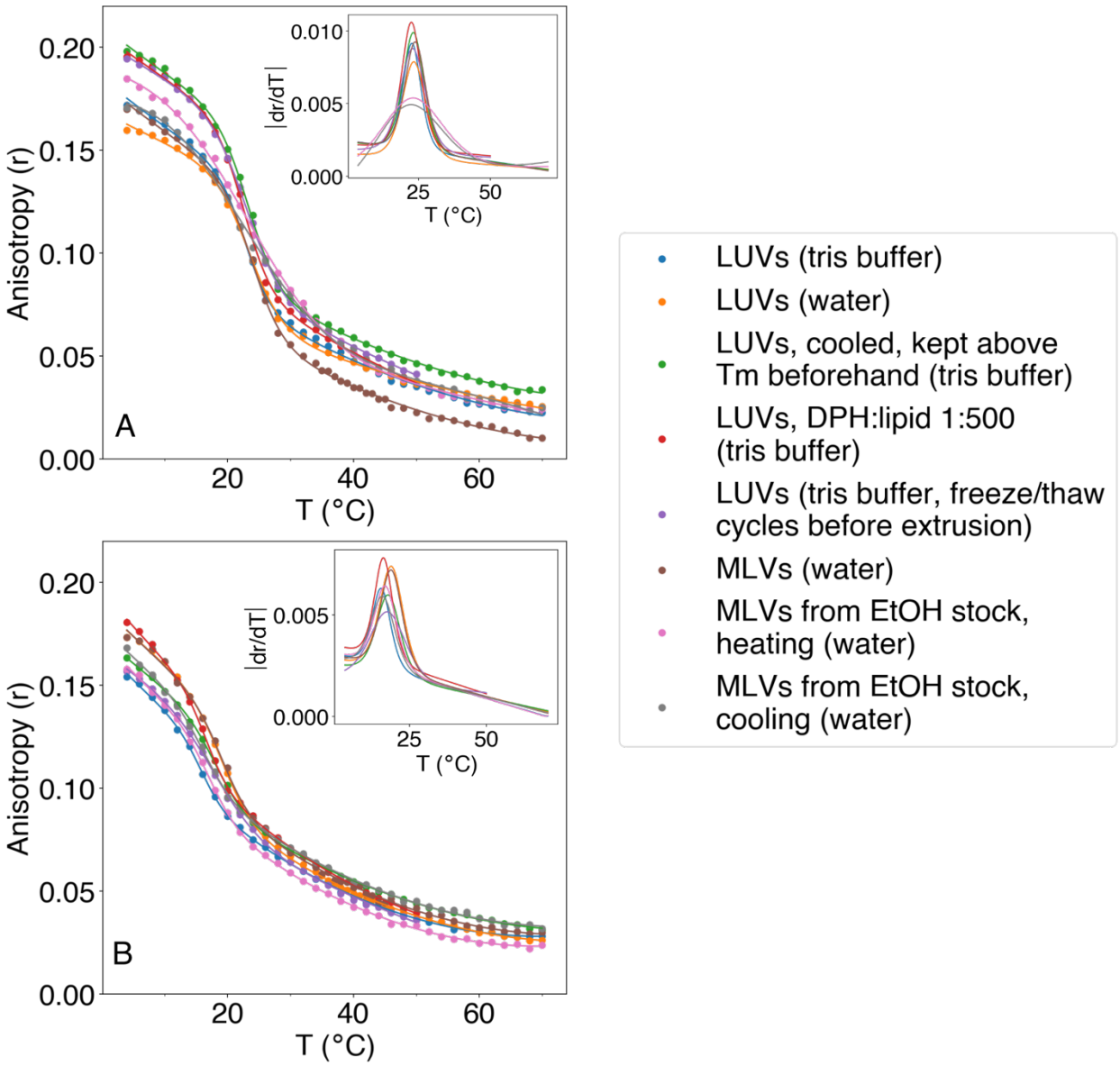

Figure S4. Dependence of DPH anisotropy values on vesicle preparation methods and lamellarity for DPPC/DOPC vesicles containing A. 80% DOPC or B. 90% DOPC. Insets show absolute values of the first derivatives of each DPH anisotropy curve with respect to temperature.

Table S1. Vesicle preparation conditions and corresponding T_{mid} values for DPPC/DOPC vesicles containing either 80% or 90% DOPC. A DPH:lipid ratio of 1:30 was used for all samples unless otherwise specified. Final row reports mean T_{mid} value and standard deviation.

Sample	**80% DOPC, T_{mid} (°C)**	**90% DOPC, T_{mid} (°C)**
LUVs in 20 mM Tris/100 mM NaCl (chloroform lipid stock, measured from 4-70 °C)	22.8	15.8
LUVs in water (chloroform lipid stock, measured from 4-70 °C)	23.4	19.1
MLVs in water (chloroform lipid stock, measured from 4-70 °C)	23.9	19.1
MLVs in water (EtOH lipid stock, measured from 4-70 °C)	23.0	17.1
MLVs in water (EtOH lipid stock, measured from 70-4 °C)	21.7	16.3
LUVs in 20 mM Tris/100 mM NaCl (chloroform lipid stock; extruded from freeze-thawed MLVs and measured from 4-70 °C)	23.0	17.9
LUVs in 20 mM Tris/100 mM NaCl (chloroform lipid stock; maintained above T_{mid} until use and measured from 70-4 °C)	23.3	18.1
LUVs in 20 mM Tris/100 mM NaCl (chloroform lipid stock; measured from 4-70 °C; DPH:lipid ratio 1:500)	22.6	16.6
Average	22.96±0.62	17.50±1.16

Figure S5 demonstrates the reversibility of DPH anisotropy with temperature in 40:60 DPPC:PBd-PEO LUVs. The difference in T_{mid} observed between heating and cooling cycles was small (0.4 °C), suggesting the temperature ramp rate used for fluorescence experiments was sufficiently slow to permit sample equilibration.

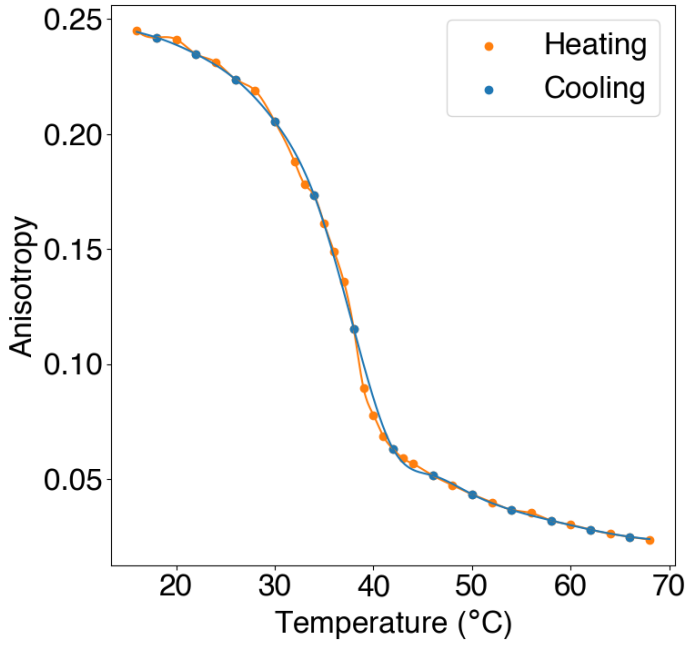

Figure S5. DPH anisotropy in 40:60 DPPC:PBd-PEO LUVs. Sample was heated from 16-70 °C to obtain "Heating" curve, then cooled at the same rate from 70-16 °C to obtain "Cooling" curve.

DPH anisotropy in hybrid LUVs containing different DPH:lipid/polymer ratios was also evaluated to ensure DPH concentration did not significantly affect the observed behavior (Figure S6). DPH:(DPPC+PBd-PEO) ratios of 1:30 and 1:500 were evaluated for 80:20 DPPC:PBd-PEO LUVs. The observed T_{mid} agreed within 0.4 °C, suggesting no significant alteration of membrane behavior between the two DPH concentrations.

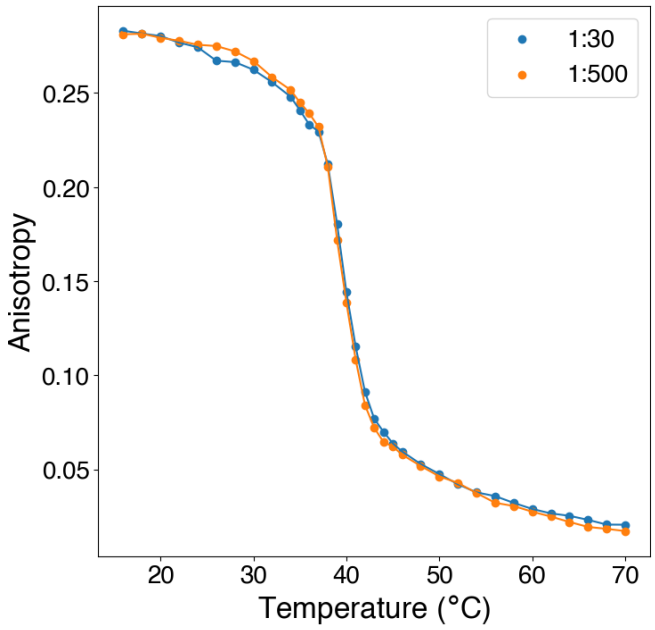

Figure S6. Comparison between DPH anisotropy curves obtained with different DPH:(DPPC+PBd-PEO) molar ratios. Legend indicates this ratio. Data shown for 80:20 DPPC:PBd-PEO LUVs.

2.8.3 Deviations from ideal fluidity

To gain further insight into the dependence of membrane fluidity on vesicle composition, the deviation of DPH anisotropy values from those predicted for the case of ideal mixing was determined [8]. Ideal anisotropy values (r_{ideal}) were calculated as functions of temperature and composition as shown in Equation (S5), corresponding to the weighted sum of the anisotropy values observed in the pure DPPC (r_{DPPC}) and pure PBd-PEO (r_{PBdPEO}) LUVs. x_{DPPC} and x_{PBdPEO} are the mole fractions of DPPC and PBd-PEO.

$$r_{ideal} = x_{DPPC} r_{DPPC} + x_{PBdPEO} r_{PBdPEO} \quad \text{(S5)}$$

The deviation of observed anisotropy values from ideal values, $\Delta r/r$, was calculated as shown in Equation (S6) and plotted as a function of vesicle composition across a range of temperatures (Figure 2 in the main text). Positive values of $\Delta r/r$ suggest the LUV membrane is less fluid than

would be expected if it were ideally mixed, as membrane fluidity is inversely proportional to DPH anisotropy values.

$$\frac{\Delta r}{r} = \frac{r_{actual} - r_{ideal}}{r_{ideal}} \quad \text{(S6)}$$

A plot of *Δr/r* for DPPC/DOPC vesicles (Figure S7) also displays visible trends differentiating temperatures above and below $T_{completion}$, though not always as distinct as those observed for the DPPC/PBd-PEO system. Below $T_{completion}$, where solid and fluid DPPC-rich and DOPC-rich phases coexist for a wide range of vesicle compositions, primarily positive deviations from ideality are observed, similarly to the DPPC/PBd-PEO system. Larger negative deviations from ideality are also observed at temperatures close to $T_{completion}$ for most compositions in both DPPC/DOPC and DPPC/PBd-PEO vesicles. Above $T_{completion}$, however, primarily smaller, negative deviations from ideal anisotropy values are observed for DPPC/DOPC vesicles (as opposed to the clearly negative deviations from ideality observed for DPPC/PBd-PEO vesicles). This difference is likely due to the similarity of the fluidities of DPPC and DOPC above their T_{mid}, which would limit the dependence of *Δr/r* on vesicle composition. Indeed, the anisotropy values of pure DPPC and pure DOPC are within ~0.01 anisotropy units of each other above 50 °C (

Figure S1). DPPC/DOPC membrane fluidity might thus be expected to display only weak deviations from ideality above $T_{completion}$. Conversely, DPPC and PBd-PEO display appreciably different anisotropy values even above the T_{mid} of DPPC (ranging from 0.04-0.02 for pure DPPC and 0.09-0.05 for pure PBd-PEO as the temperature varies from 50-70 °C), indicating PBd-PEO is more ordered than fluid DPPC. Greater dependence of fluidity on composition and thus potentially larger deviations from ideality would therefore be possible for DPPC/PBd-PEO LUVs.

This could contribute to the more distinct trends in $\Delta r/r$ observed above $T_{completion}$ for DPPC/PBd-PEO vesicles as compared to DPPC/DOPC vesicles.

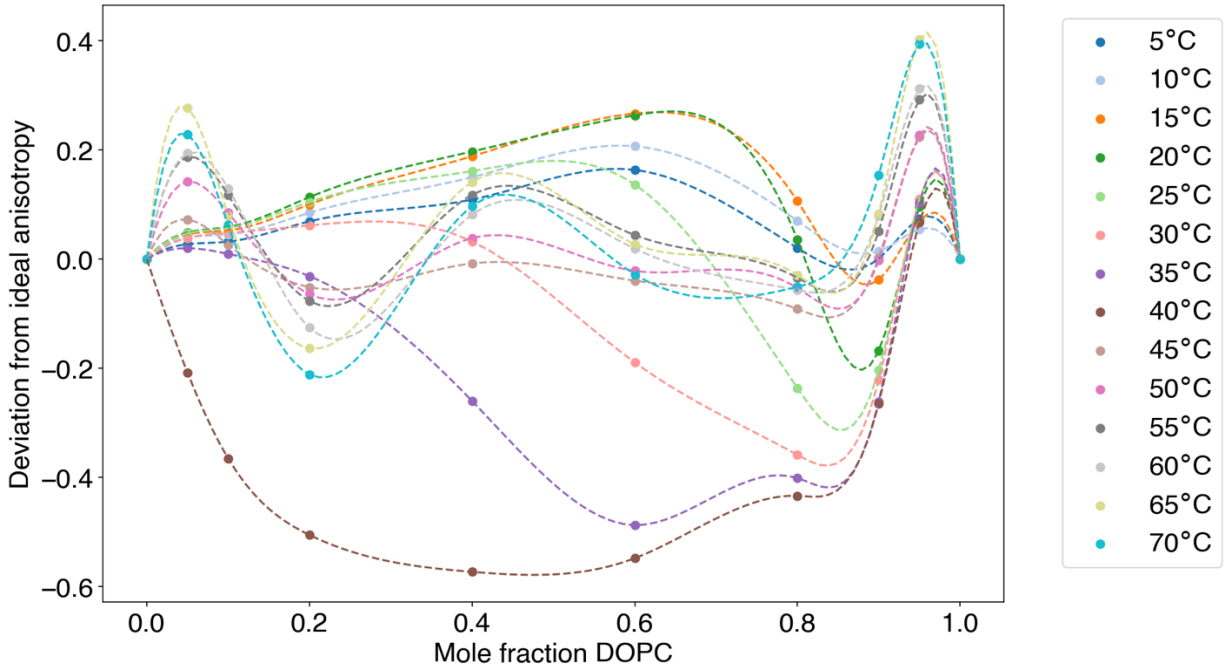

Figure S7. Deviations from ideal anisotropy (Δr/r) for DPPC/DOPC LUVs. Points were calculated as described above (with PBd-PEO replaced by DOPC); dashed lines are cubic splines fit to calculated values.

2.8.4 Effects of fluorescent probe Rh-DOPE on T_{mid}

To investigate the potential of Rh-DOPE to impact the T_{mid} reported by FRET, DPH anisotropy and laurdan GP were used to evaluate T_{mid} for LUVs containing 1% or 2% Rh-DOPE (to match the concentrations used for FRET experiments), as shown in Figure S8. T_{mid} values were relatively similar in LUVs made with and without Rh-DOPE (Table S2), especially in comparison to the significant differences between T_{mid} reported by FRET and by DPH anisotropy/laurdan GP. T_{mid} values increased slightly upon inclusion of Rh-DOPE.

The differences in the shapes of the anisotropy and GP curves between LUVs made with and without Rh-DOPE may be the result of FRET, as both DPH and laurdan can participate in FRET with Rh-DOPE. GP may be especially strongly impacted by this, as GP values are calculated by

comparing laurdan emission intensities at two different wavelengths (440 nm and 490 nm). The latter is closer to the excitation peak of rhodamine, so laurdan emission at 490 nm may be more strongly quenched by participation in FRET with rhodamine than at 440 nm. This would result in elevated GP values, as greater differences between laurdan emission intensity values at 440 nm and 490 nm correspond to higher GP.

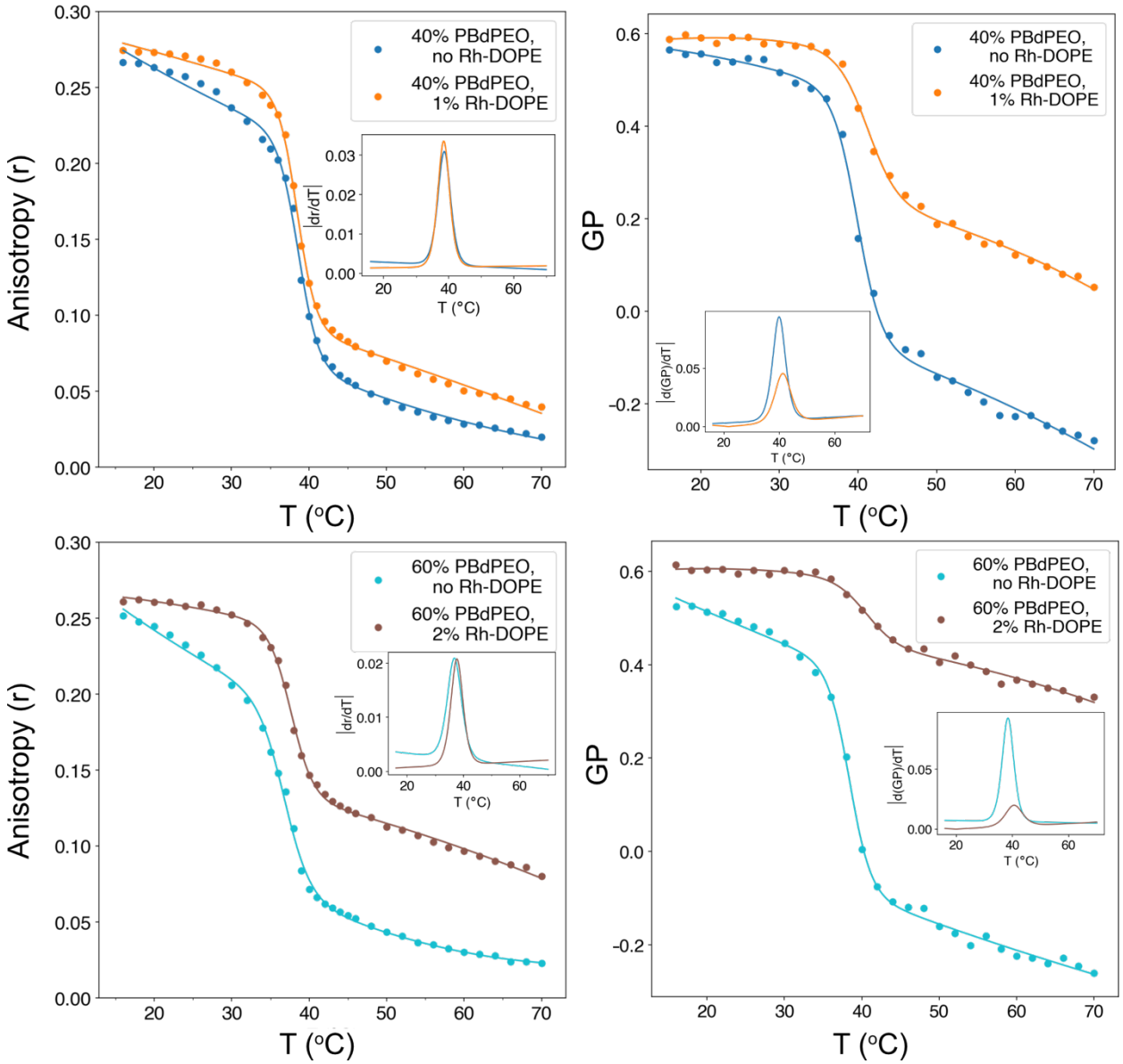

Figure S8. DPH anisotropy and laurdan GP in 60:40 and 40:60 DPPC:PBd-PEO LUVs in the presence and absence of 1% and 2% Rh-DOPE, respectively (matching the percentage used for FRET experiments with vesicles of each composition). Insets show the absolute values of the derivatives of the DPH anisotropy and laurdan GP curves with

respect to temperature. DPH anisotropy and laurdan GP curves were fit using the sigmoidal expressions described in "Methods" in the main text (section 2.3).

Table S2. Comparison of T_{mid} values reported by DPH anisotropy and laurdan GP in LUVs made with and without Rh-DOPE. ΔT_{mid} refers to the differences in T_{mid} for LUVs made with and without the indicated amount of Rh-DOPE; positive values indicate T_{mid} was greater for LUVs containing Rh-DOPE.

	DPH anisotropy ΔT_{mid} (°C)	**Laurdan GP ΔT_{mid} (°C)**
1% Rh-DOPE	+0.5	+1.34
2% Rh-DOPE	+0.9	+2.2

2.8.5 Light scattering measurements of LUV size

The average diameters of extruded hybrid LUVs were determined by dynamic light scattering and are shown in Table S3.

Table S3. Diameters of DPPC/PBd-PEO LUVs indicated by DLS. Uncertainty represents standard deviation of at least 4 measurements.

Mole fraction PBd-PEO	LUV diameter (nm)
0	113±9
0.05	120±12
0.2	86±9
0.4	98±11
0.6	80±5
0.8	96±13
0.9	90±10
0.95	117±3
1	95±18

2.8.6 Assessment of T_{onset}, T_{mid}, $T_{completion}$

2.8.6.1 DPH anisotropy

T_{mid} was determined from DPH anisotropy values by least squares regression to a sigmoidal function in Python as described in "Methods" in the main text (Section 2.3). T_{onset} and $T_{completion}$ correspond to the start and end of the peak in the absolute value of the derivative of this function with respect to temperature (Figure S9). The baseline was determined by fitting a straight line along the base of either side of the peak. Tangent lines were constructed against the steepest point of the sides of each peak and against the points of greatest curvature (visually determined) as the derivative returned to its baseline on each side. The points at which these tangent lines intersect with the baseline were averaged to obtain T_{onset} and $T_{completion}$. The error bounds on T_{onset} and $T_{completion}$ were then the differences between the points at which the lines on each side of the peak intersects with the baseline (i.e. for T_{onset}, the difference between the points at which the two green lines constructed along the left side of the peak intersect with the baseline).

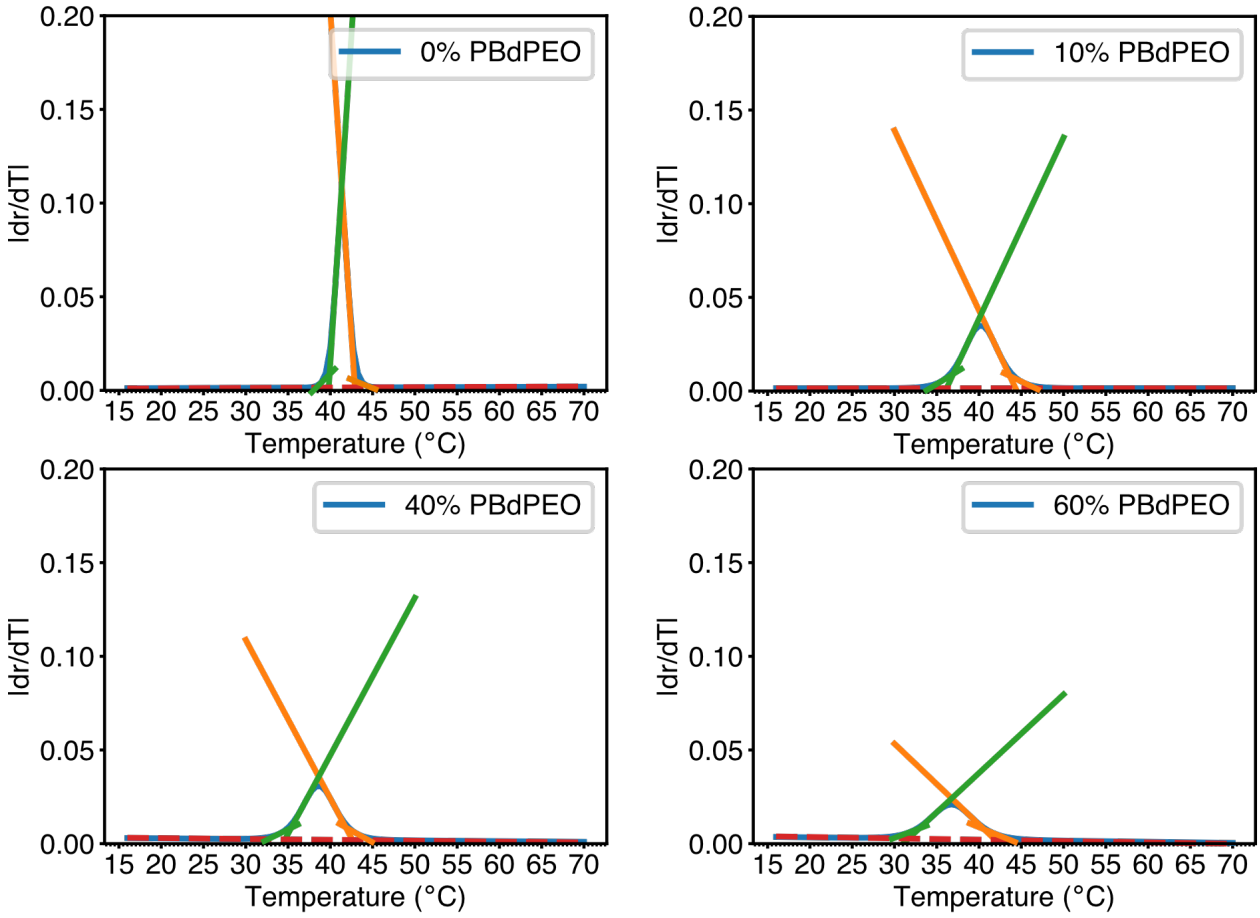

Figure S9. Representative plots of the absolute values of the first derivatives of the sigmoidal function to which DPH anisotropy values were fitted, along with tangent constructions and fitted baseline (red) used to determine T_{onset} and $T_{completion}$. The mean of the intersection with the baseline of lines tangent to the points of steepest slope and of greatest curvature was taken as T_{onset} (green) or $T_{completion}$ (orange).

2.8.6.2 Laurdan GP

The observed GP values were regressed against a sigmoidal function as described in "Methods" in the main text (Section 2.3). T_{mid} was thus determined as a regression parameter of the sigmoidal fit. T_{onset} and $T_{completion}$ were evaluated by taking the absolute value of the derivative with respect to temperature of the fit to the observed GP values and constructing tangents as described for DPH anisotropy values. Representative derivatives and tangents are shown in Figure S10.

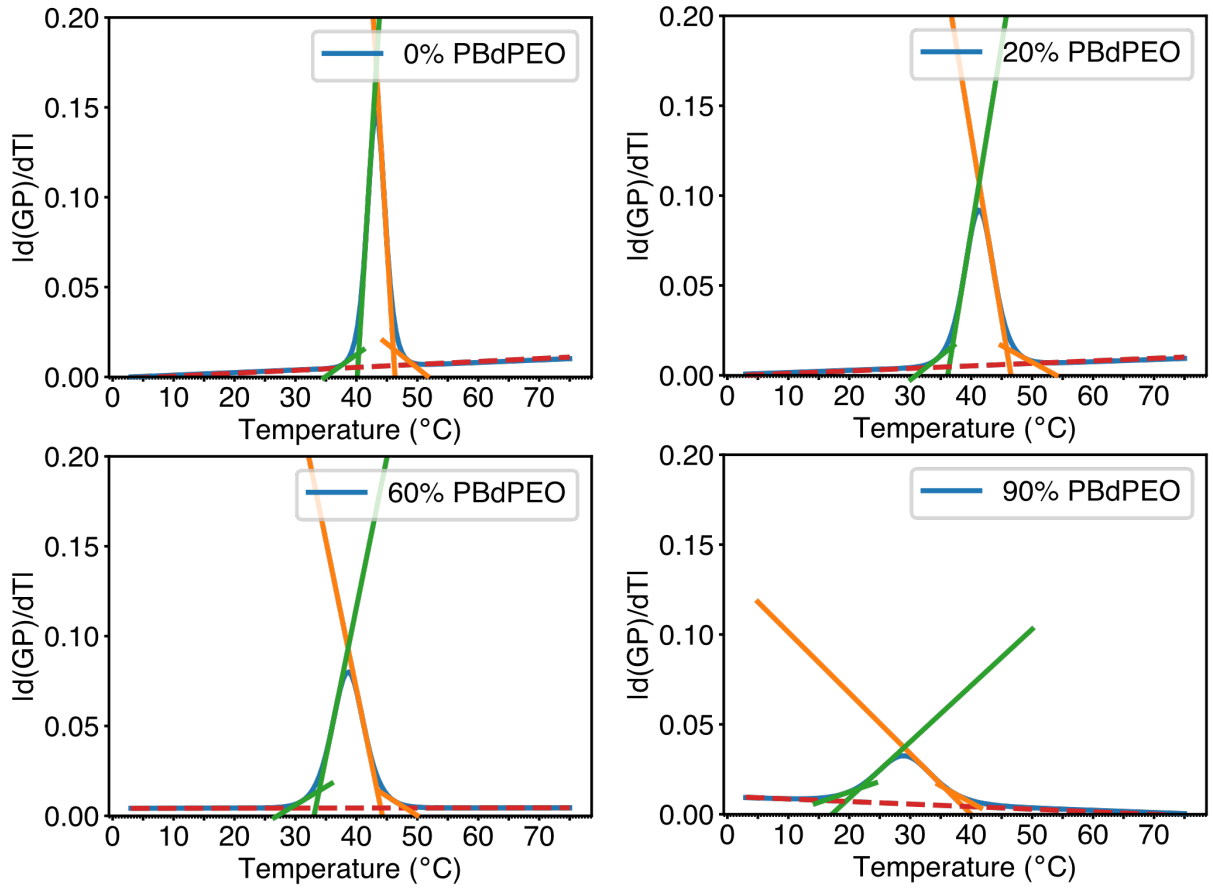

Figure S10. Sample tangent constructions for plots of the absolute value of the derivative of laurdan GP with respect to temperature for DPPC/PBd-PEO LUVs. The mean of the intersection with the baseline of lines tangent to the points of steepest slope and of greatest curvature was taken as T_{onset} (green) or $T_{completion}$ (orange).

2.8.6.3 Statistical analysis

For single samples, T_{mid} uncertainty values were determined by doubling the standard deviation error for T_{mid} obtained by least squares regression of measured anisotropy or GP values against the sigmoidal functions described in "Methods" (Section 2.3 in the main text). If it is specified that multiple samples were measured to obtain a mean T_{mid} and corresponding uncertainty value, the reported T_{mid} is the average obtained from at least 3 independent samples, each independently regressed against a sigmoidal function. The uncertainty in this average T_{mid} is the propagated error in the average using the standard deviation errors of T_{mid} across at least 3 samples. This propagated error was doubled for error bounds and error bars.

Although multiple anisotropy measurements were taken per sample per temperature, the uncertainties arising from variation in multiple measurements on the same sample were not included because the standard deviation of anisotropy measurements on the same sample was typically ~2 orders of magnitude smaller than the standard deviation across samples.

2.9 Supplementary References

[1] M.L. Schmidt, L. Ziani, M. Boudreau, J.H. Davis, Phase equilibria in DOPC/DPPC: Conversion from gel to subgel in two component mixtures, The Journal of Chemical Physics. 131 (2009) 175103. https://doi.org/10.1063/1.3258077.

[2] B.R. Lentz, Y. Barenholz, T.E. Thompson, Fluorescence depolarization studies of phase transitions and fluidity in phospholipid bilayers. 2. Two-component phosphatidylcholine liposomes, Biochemistry. 15 (1976) 4529–4537. https://doi.org/10.1021/bi00665a030.

[3] M. Shinitzky, Y. Barenholz, Fluidity parameters of lipid regions determined by fluorescence polarization, Biochimica et Biophysica Acta (BBA) - Reviews on Biomembranes. 515 (1978) 367–394. https://doi.org/10.1016/0304-4157(78)90010-2.

[4] R.L. Knorr, J. Steinkühler, R. Dimova, Micron-sized domains in quasi single-component giant vesicles, Biochimica et Biophysica Acta (BBA) - Biomembranes. 1860 (2018) 1957–1964. https://doi.org/10.1016/j.bbamem.2018.06.015.

[5] H. Bouvrais, L. Duelund, J.H. Ipsen, Buffers Affect the Bending Rigidity of Model Lipid Membranes, Langmuir. 30 (2014) 13–16. https://doi.org/10.1021/la403565f.

[6] M.A. Kreutzberger, E. Tejada, Y. Wang, P.F. Almeida, GUVs Melt Like LUVs: The Large Heat Capacity of MLVs Is Not Due to Large Size or Small Curvature, Biophysical Journal. 108 (2015) 2619–2622. https://doi.org/10.1016/j.bpj.2015.04.034.

[7] N. Kučerka, J. Pencer, J.N. Sachs, J.F. Nagle, J. Katsaras, Curvature Effect on the Structure of Phospholipid Bilayers, Langmuir. 23 (2007) 1292–1299. https://doi.org/10.1021/la062455t.

[8] M.M. Lozano, M.L. Longo, Complex formation and other phase transformations mapped in saturated phosphatidylcholine/DSPE-PEG2000 monolayers, Soft Matter. 5 (2009) 1822. https://doi.org/10.1039/b820070j.

Chapter 3 - Characterization of phase separation phenomena in hybrid lipid/block copolymer/cholesterol bilayers using laurdan fluorescence with log-normal multipeak analysis

Previously published in Biochimica et Biophysica Acta – Biomembranes 2022

(https://doi.org/10.1016/j.bbamem.2022.183887)

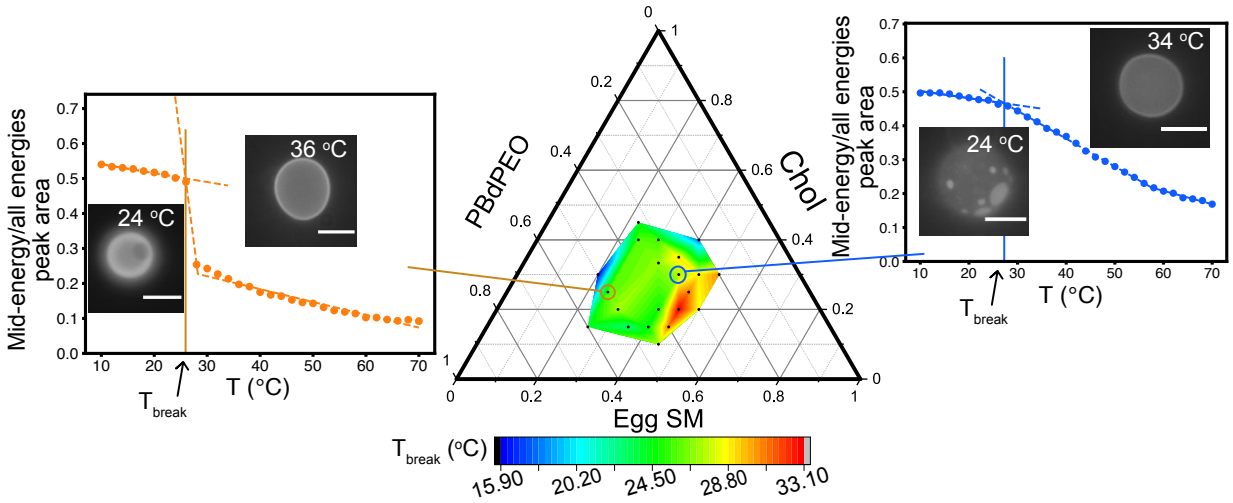

Abstract

Phase separation phenomena in hybrid lipid/block copolymer/cholesterol bilayers combining polybutadiene-*block*-polyethylene oxide (PBdPEO), egg sphingomyelin (egg SM), and cholesterol were studied with fluorescence spectroscopy and microscopy for comparison to lipid bilayers composed of palmitoyl oleoyl phosphatidylcholine (POPC), egg SM, and cholesterol. Laurdan emission spectra were decomposed into three lognormal curves. The temperature dependence of the ratios of the areas of the middle and lowest energy peaks revealed temperature break-point (T_{break}) values that were in better agreement, compared to generalized polarization inflection

temperatures, with phase transition temperatures in giant unilamellar vesicles (GUVs). Agreement between GUV and spectroscopy results was further improved for hybrid vesicles by using the ratio of the area of the middle peak to the sum of the areas all three peaks to find the T_{break} values. For the hybrid vesicles, trends at T_{break} are hypothesized to be correlated with the mechanisms by which the phase transition takes place, supported by the compositional range as well as the morphologies of domains observed in GUVs. Low miscibility of PBdPEO and egg SM is suggested by the finding of relatively high T_{break} values at cholesterol contents greater than 30 mol%. Further, GUV phase behavior suggests stronger partitioning of cholesterol into PBdPEO than into POPC, and less miscibility of PBdPEO than POPC with egg SM. These results, summarized using a heat-map, contribute to the limited body of knowledge regarding the effect of cholesterol on hybrid membranes, with potential application toward the development of such materials for drug delivery or membrane protein reconstitution.

3.1 Introduction

Hybrid membranes combining lipids and amphiphilic block copolymers have been a recent area of scientific interest, especially because of their potential value toward biomedical applications. Both lipid membranes and block copolymer membranes individually offer unique advantages, motivating the study of hybrid membranes. While the biocompatibility of lipid membranes has facilitated their usage in the areas of liposomal drug delivery and membrane protein reconstitution, the wide range of chemical functionality and increased mechanical stability of block copolymer membranes are also desirable [1]. Such hybrid membranes are thus appealing because they combine the favorable properties of both lipid and block copolymer membranes. In comparison to

lipid-only or polymer-only membranes, hybrid membranes have been demonstrated to extend the functional lifetime of an incorporated membrane protein [2] and to increase the yield of cell-free expression of a membrane protein [3]. Hybridization of polymer vesicles with lipids has also been demonstrated to increase the efficacy of targeted vesicle binding to tumors in mice [4].

To further inform the application of hybrid membranes, it is important to understand their phase behavior, as this may have implications toward their function. For example, in lipid vesicles the formation of domains enriched in a cationic lipid has been suggested to enhance intracellular delivery of macromolecules [5,6]. The phase behavior of lipid membranes has been studied extensively. It is well documented that in the presence of cholesterol, certain lipid mixtures can display solid/fluid or fluid/fluid phase separation depending upon the mixture composition [7–9]. Similarly, phase separation in hybrid membranes has been reported for a variety of compositions [1,10]. However, the effect of cholesterol on the phase behavior of block copolymer and hybrid membranes has been explored to only a limited extent [10,11]. There thus exists a need for continued investigation of the phase behavior of hybrid membranes.

Fluorescent probes, including diphenylhexatriene (DPH) [12] and laurdan [13], have been used to study the phase behavior of both lipid-only [12–15] and hybrid membranes [16,17] . For this work, laurdan was chosen due to its greater sensitivity to the phase behavior of hybrid dipalmitoylphosphatidylcholine (DPPC)/polybutadiene-*block*-polyethylene oxide (PBdPEO) vesicles which we demonstrated in recent work [16]. Laurdan displays a red shift in its emission spectrum as the polarity of its local environment increases [13]. This is directly related to the hydration of the membrane, which is in turn dependent on the extent of the ordering of the membrane. The relative membrane polarity indicated by laurdan is quantified by calculation of

generalized polarization (GP) values. Trends in laurdan GP values thus provide information regarding the phase behavior of the membrane [13]. To gain further insight into the phase behavior of lipid membranes, decomposition of laurdan emission spectra into multiple peaks has been proposed as an additional tool [18–20]. For the case of cholesterol-containing lipid membranes in particular, multipeak analysis has been proposed to provide greater insight into phase behavior than calculation of GP values [18]. Because the emission wavelength of laurdan depends strongly on the polarity of the membrane, trends observed in the relative areas of the peaks returned by such decomposition approaches have been reported to correspond with the phase behavior of the membrane [18,19].

Here, we apply multipeak analysis to laurdan emission spectra, taken at sequential temperatures, of 3-component vesicles composed of the block copolymer PBdPEO or the lipid palmitoyl oleoyl phosphatidylcholine (POPC), egg sphingomyelin (egg SM), and cholesterol. This technique has not been used with hybrid membranes before, to the best of our knowledge, but presents a means of studying their phase behavior in greater depth than possible with the more general information provided by trends in laurdan GP values. A PBdPEO block copolymer with an average molecular weight of 950 g/mol, expected to form a relatively fluid membrane at room temperature [21], was used. Vesicles combining either POPC (solid-fluid transition temperature of -2 ^{o}C) or PBdPEO (glass transition temperature of ~-22 ^{o}C) and egg SM (solid-fluid transition temperature of ~39 ^{o}C [7]) are first compared as POPC and PBdPEO are expected to be fluid and egg SM is expected to be solid at room temperature. Then, analysis of laurdan emission spectra for lipid-only vesicles containing POPC, egg SM, and cholesterol is presented for a limited range of compositions. Subsequently for a broad range of compositions, laurdan emission spectra for hybrid vesicles containing PBdPEO, egg SM, and cholesterol are presented. For both hybrid and lipid-only

vesicles with cholesterol, the phase behavior indicated by multipeak analysis is found to be in better agreement with fluorescence microscopy results in giant unilamellar vesicles (GUVs) than that indicated by laurdan GP values. Similar to the phase behavior reported for lipid-only vesicles [7], both solid/fluid and fluid/fluid phase separation are observed for hybrid GUVs containing cholesterol. Overall, our results suggest stronger partitioning of cholesterol into the copolymer PBdPEO than into POPC, and less miscibility of PBdPEO with egg SM in comparison to POPC and egg SM.

3.2 Materials and Methods

3.2.1 Materials

Egg sphingomyelin (egg SM), palmitoyl oleoyl phosphatidylcholine (POPC), egg lissamine rhodamine B phosphatidylethanolamine (egg rhod PE), and cholesterol were purchased from Avanti Polar Lipids, Inc. The diblock copolymer poly(1,2-butadiene)-*block*-poly(ethylene oxide) (PBdPEO), with an average molecular weight of 950 g/mol, (P41807C-BdEO, Bd(600)-*b*-EO(350), PDI = 1.06) was purchased from Polymer Source, Inc. 6-dodecanoyl-2-dimethylaminonaphthalene (laurdan) was purchased from AdipoGen Life Sciences. Texas Red 1,2-dihexadecanoyl-sn-glycero-3-phosphoethanolamine (Texas Red DHPE) was purchased from Biotium. All water used for experiments was purified with a Barnstead Nanopure System (Barnstead Thermolyne) and had a resistivity ≥17.8 MΩ·cm.

3.2.2 Preparation of large unilamellar vesicles (LUVs)

Appropriate volumes of lipid, polymer, and cholesterol stock solutions in chloroform and laurdan stock solution in ethanol were combined in clean glass vials. A gentle stream of nitrogen was used to evaporate the solvent, leaving a uniform film. To remove any residual solvent, the vials were then kept under vacuum for 2-24 hours. The dried film was heated in a water bath of at least 50 ºC and rehydrated with water to a final lipid/polymer concentration of 2 mM. This solution was then passed 11 times through a polycarbonate membrane with 0.1 μm pores using a mini extruder (Avanti).

3.2.3 Preparation of giant unilamellar vesicles (GUVs)

Appropriate volumes of lipid, polymer, and cholesterol stock solutions in chloroform were combined in a clean glass vial and further diluted with chloroform to yield a final lipid/polymer concentration of 0.5 mg/mL. 0.2 mol% of egg rhodamine PE was incorporated into lipid-only giant unilamellar vesicles (GUVs); the same concentration of Texas Red DHPE was used instead for hybrid GUVs. The mole percentage of the lower melting temperature component (POPC or PBdPEO) was reduced in compensation. GUVs were prepared in a custom built electroformation chamber consisting of parallel platinum electrodes in a polytetrafluoroethylene housing. 25 μL of the prepared stock solution was spread over each electrode with a gastight Hamilton glass syringe, and a gentle stream of nitrogen was used to dry the electrodes. The chamber was then placed under vacuum for 2-24 hours to remove any residual solvent. Immediately prior to vesicle formation, glass coverslips were fixed over the openings of the chamber with vacuum grease and the sealed chamber was filled with water. The chamber temperature was maintained at 45 ºC (lipid-only GUVs) or 50 ºC (hybrid GUVs) with an external heating element. A sinusoidal wave with an

amplitude of 3 V was applied at a frequency of 10 Hz for 30 minutes; then, the frequency was reduced to 3 Hz for 15 minutes. After this, 2 V/1 Hz were applied for 7.5 minutes, and then 2 V/0.5 Hz for 7.5 minutes. Prior to collection of GUVs, the chamber was allowed to cool freely to room temperature, typically requiring roughly 90 minutes. GUVs were stored in a plastic conical tube and imaged the same day.

To prepare a sample for imaging, a small aliquot of GUV suspension was added to a chamber formed by a glass slide, vacuum grease, and no. 1.5 cover slip. Images were collected using a Nikon Eclipse 80i equipped with either a 60x oil immersion or 60x air objective. The air objective was used for all images collected above or below room temperature to avoid thermal coupling of the sample and objective. A heated microscope stage (BoliOptics) was used to control the sample temperature. Sample temperatures were recorded as the average of the temperatures at the upper surfaces of the cover slip and glass slide, as measured by two resistance temperature detectors (Minco). To assess transition temperatures, GUVs were heated to 5-10 ^{o}C above the expected transition temperature, then cooled in increments of 2 ^{o}C while far from the expected transition temperature. The temperature was then reduced in increments of 1 ^{o}C as the expected transition temperature was approached. Lipid-only GUVs were allowed to equilibrate for a minimum of 7 minutes at each temperature, while hybrid GUVs were allowed at least 10 minutes. The transition temperature was identified as the temperature at which domains first appeared upon cooling. Experimental uncertainty in T_m was determined to be roughly a range of 1.5 ^{o}C, based on repeated experiments with selected compositions of GUVs.

3.2.4 Collection and analysis of laurdan emission spectra

LUVs containing laurdan were prepared as described above, using a lipid:probe ratio of 200:1. The prepared LUVs were diluted with water to a final lipid concentration of 200 μM immediately prior to fluorescence spectroscopy experiments. Laurdan emission spectra were collected from 370-600 nm with a Jasco spectrofluorometer using an excitation wavelength of 355 nm. Samples were heated to the highest temperature of interest, allowed to equilibrate for 30 minutes, then cooled in increments of 2 °C with an incubation time of 3 minutes at each temperature. Each sample was subjected to only one heating/cooling cycle prior to being discarded.

Laurdan generalized polarization (GP) provides insight into membrane polarity, with higher GP values corresponding to a more polar membrane. GP values were calculated using Equation (1), where I_{440} and I_{490} are the respective intensities of the laurdan emission spectrum at 440 nm and 490 nm.

$$GP = \frac{I_{440} - I_{490}}{I_{440} + I_{490}} \quad (1)$$

Least squares regression was also applied to fit a sigmoidal equation to calculated GP values (Equation (2)) [18]. GP_{max} and GP_{min} represent the upper and lower limits of the GP curve, while n is a fitting parameter related to the slope of the curve in the vicinity of T_{mid}. T_{mid} represents the inflection point of the curve. Uncertainty values for T_{mid} were expressed as the standard deviation error for the fitting of this parameter.

$$GP(T) = \frac{GP_{max} - GP_{min}}{1 + e^{(T-T_{mid})n}} + GP_{min} \quad (2)$$

Decomposition of laurdan emission spectra into multiple peaks was also carried out to gain further insight into membrane phase behavior. Emission spectra were fit in Python with the sum of multiple lognormal curves using least squares regression as described in Puff et al. [18], with each lognormal curve characterized by an equation of the following form:

$$y = A_0 + A_1 exp\left[-\left(\frac{\ln\left(\frac{x}{A_2}\right)}{A_3}\right)^2\right] \quad (3)$$

A_0 represents the baseline, A_1 the amplitude, A_2 the position, and A_3 the width of the fitted curve. All parameters besides A_0 were constrained to be greater than 0 when performing the fit. Additionally, the peak position A_2 was constrained to the range of measured wavelengths, which spans the observed emission spectrum of laurdan in the membrane. Prior to spectral decomposition, emission intensities were expressed as a function of energy at each wavelength using the relationship ($h*c/E^2$), where h is Planck's constant, c is the speed of light in a vacuum, and E is the energy corresponding to each wavelength (calculated as $h*c/\lambda$, where λ is the wavelength) [18,22,23].

When three-peak fits to laurdan emission spectra were used, peak area ratios were calculated at each temperature studied as the area of the middle energy peak divided by the area of the lowest energy peak unless otherwise specified. Peak area ratio plots were fit with a three-piece linear function in Python to identify the temperature at which the first two lines met, which is expected

to be within the range the phase transition temperature of the membrane, as described in Puff et al [18]. Uncertainty values for this position were reported as the standard deviation error in the intersection of these lines as calculated from the standard deviation error of the piecewise linear fit applied to each peak area ratio plot.

3.3 Results and Discussion

A combination of fluorescence spectroscopy and microscopy was used to study phase behavior in large unilamellar vesicles (LUVs) and giant unilamellar vesicles (GUVs) composed of palmitoyl oleoyl phosphatidylcholine (POPC) or polybutadiene-*block*-polyethylene oxide (PBdPEO), egg sphingomyelin (egg SM), and cholesterol. Compositions are reported as mole percentages.

3.3.1 Cholesterol-free vesicles

First, a selected 40-60 mol% composition of POPC-egg SM and PBdPEO-egg SM LUVs was compared. Calculating the generalized polarization (GP) of laurdan in these LUVs as described in Equation (1) yielded the plot in Figure 1A. Both curves display a sigmoidal dependence of GP on temperature, with the inflection point (T_{mid}) of each curve representing the approximate midpoint temperature for the formation of solid phase domains [24]. For the POPC-egg SM LUVs, laurdan GP indicated a T_{mid} of 27.5±0.2 ^{o}C. For the PBdPEO-egg SM LUVs, T_{mid} was 33.9±0.2 ^{o}C. Figure 1B shows fluorescence images of 40-60 mol% POPC-egg SM and PBdPEO-egg SM GUVs. After heating GUVs so that a single phase was observed, dark domains formed upon cooling. The temperature at which domains first appeared upon cooling (T_m), 32.0±1.5 ^{o}C for POPC-egg SM

and 33.0±1.5 ºC for PBdPEO-egg SM, was within a few degrees of T_{mid} measured by laurdan GP. In both cases, irregularly shaped domains were observed as shown in Figure 1B, indicative of solid/fluid phase separation.

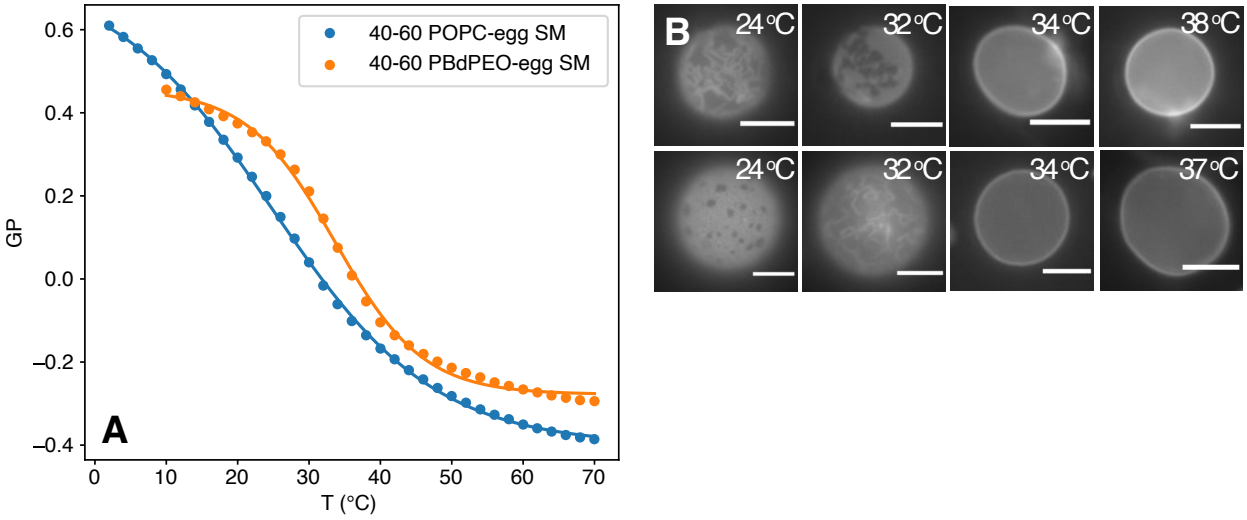

Figure 1. Comparison of POPC-egg SM and PBdPEO-egg SM vesicles. A. GP of laurdan in LUVs obtained upon cooling. The inflection point, T_{mid}, for the POPC-egg SM LUVs is 27.5±0.2 ºC, and for the PBdPEO-egg SM LUVs is 33.9±0.2 ºC. Plotted points show calculated GP values, while lines show a fit to Equation (2). B. Fluorescence microscopy of GUVs. Top row, 40-60 mol% POPC-egg SM GUVs; bottom row, 40-60 mol% PBdPEO-egg SM. The temperature at which domains in GUV populations first appeared upon cooling, T_m, is 32.0±1.5 ºC for the POPC-egg SM GUVs and 33.0±1.5 ºC for the PBdPEO-egg SM GUVs. Scale bar is 10 µm.

3.3.2 Analysis of laurdan spectroscopy results for POPC-egg SM-cholesterol LUVs

These methods were then applied to POPC-egg SM-cholesterol vesicles containing sufficient cholesterol to promote liquid/liquid phase separation. Laurdan GP values in POPC-egg SM-cholesterol LUVs are shown in Figure 2A. The shapes of the GP curves are generally sigmoidal, suggesting a phase transition takes place within the temperature range studied. However, the shallow slopes of the GP curves contrast especially with the results shown in Figure 1A for vesicles containing no cholesterol, for which a less broad phase transition is expected. This can make clear assessment of the inflection point difficult. For egg phosphatidylcholine-egg SM-cholesterol LUVs containing less cholesterol, good agreement between GP analysis and GUV phase

transitions has been reported [18]. However, for the POPC-egg SM-cholesterol compositions shown in Figure 2A, the T_{mid} values indicated by laurdan GP range from roughly 40-50 ^{o}C. These temperatures are significantly above the range of 20-35 ^{o}C expected for miscibility of the two liquid phases for similar vesicle compositions [9,18].

Decomposition of laurdan emission spectra into multiple peaks [18] was therefore carried out in an attempt to gain further insight into the phase behavior of cholesterol-containing membranes beyond the information provided by GP values. Three lognormal peaks characterized by Equation (3) were used to fit laurdan emission spectra as described in Puff et al [18]. An example of such a decomposition for 30-40-30 mol% POPC-egg SM-chol at 20 ^{o}C is shown in Figure S1.

For the three-peak fits of laurdan emission spectra in POPC-egg SM-cholesterol vesicles, the peak positions typically ranged from ~2.89-2.92 eV (425-430 nm, high-eV peak), ~2.67-2.79 eV (445-465 nm, mid-eV peak), and ~2.48-2.58 eV (480-500 nm, low-eV peak) across the range of temperatures studied. This is comparable to the ranges reported for similar multipeak analyses of laurdan [18,25] and BADAN [26], a probe with the same fluorescent moiety as laurdan. These peaks are hypothesized to respectively correspond to a non-hydrogen bonded state, an immobilized hydrogen bonded state, and a mobile hydrogen bonded state [26]. The ratio of the areas of the mid-eV peak and low-eV peak has thus been proposed as a metric of the relative amount of the liquid ordered phase in cholesterol-containing vesicles [18].

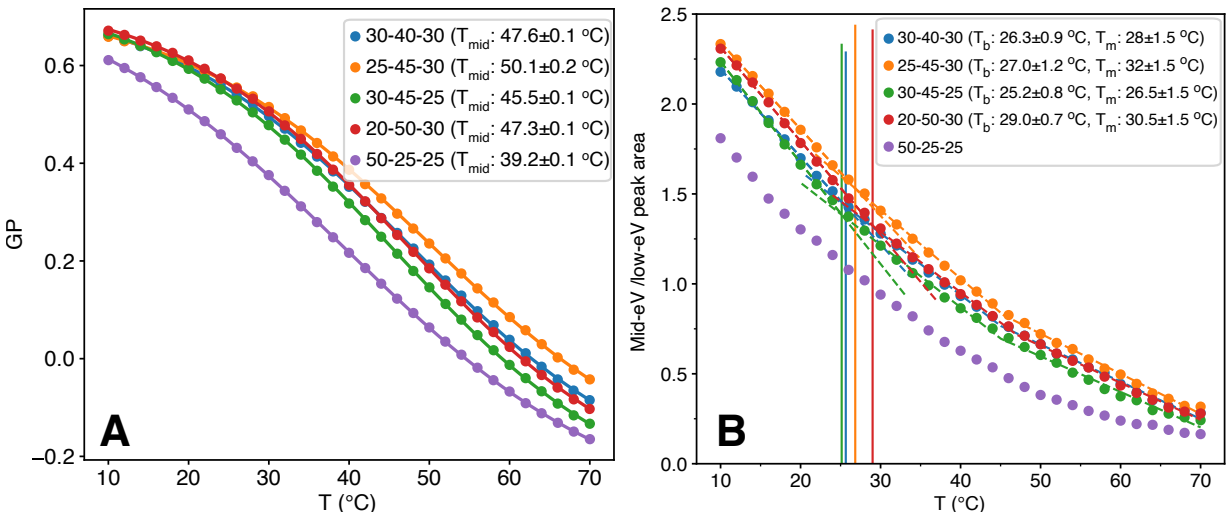

Figure 2. A. GP of laurdan in POPC-egg SM-cholesterol LUVs of the specified mole percentages. Lines represent fits to an equation for a sigmoidal curve, as described in Equation (2), and T_{mid} is the inflection point of this fit. B. Plot of the ratios of the mid-eV and low-eV peak areas resulting from the decomposition of laurdan emission spectrum into three peaks. Dashed lines indicate the piecewise linear function used to evaluate T_{break}. Vertical lines indicate T_{break}, the temperature at which the slope of the plot changes (T_b in the legend). T_m in the legend refers to the temperature at which domains first appeared upon cooling indicated by fluorescence microscopy images of GUVs.

The results of carrying out three-peak laurdan emission spectra decomposition for POPC-egg SM-cholesterol LUVs are therefore plotted in Figure 2B as the area of the mid-eV peak divided by the area of the low-eV peak [18]. As described in Puff et al. [18], this resulted in concave plots. A three-piece linear fit was applied to each plot, and the temperatures at which the first line and second line meet (T_{break}, indicated by the vertical lines in Figure 2B) lie within the range of the miscibility transition expected based on previous literature [9,18]. Moreover, plotting these transitions as a heat map in Figure S2 on a 3-component triangle yielded expected trends [9]. Therefore, multipeak analysis may be a more accurate approach than GP analysis to interpreting this laurdan spectral data.

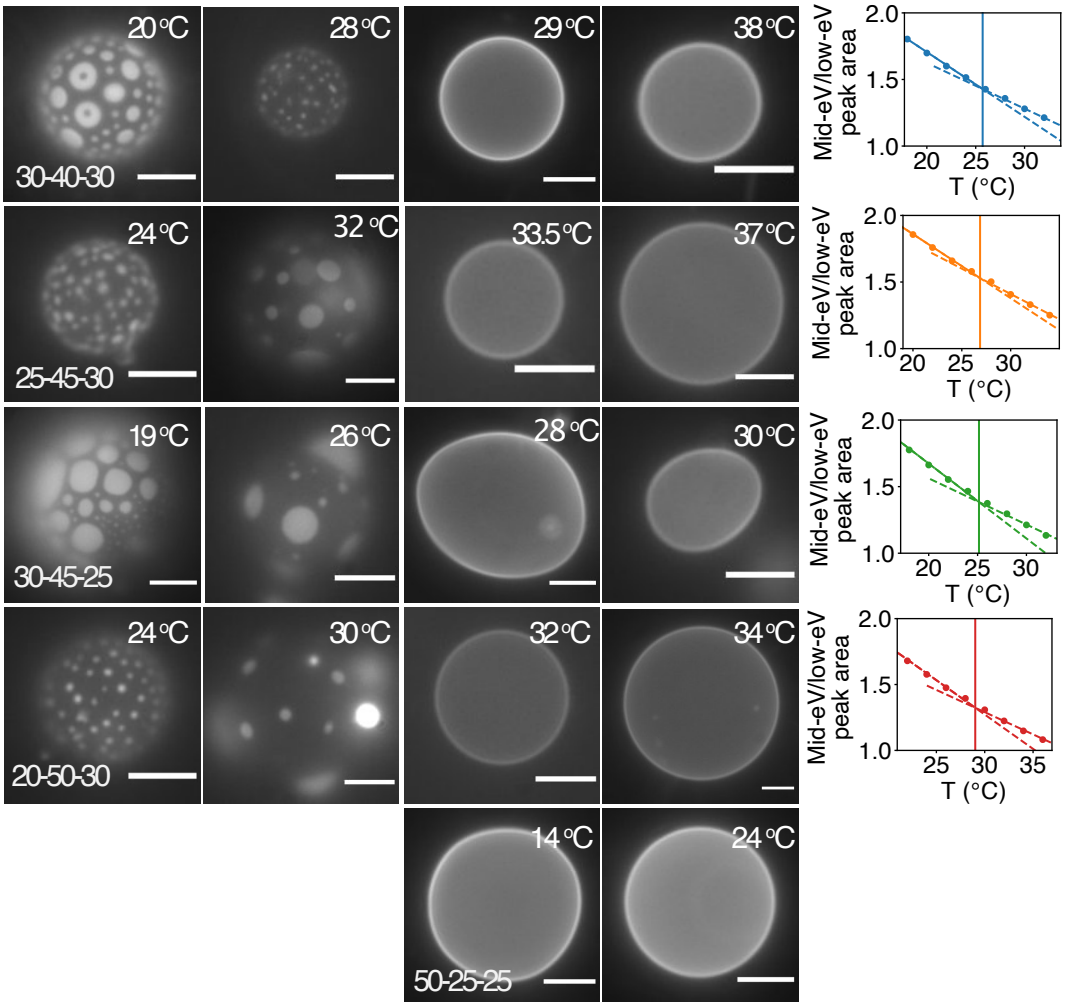

Figure 3. Fluorescence microscopy images of POPC-egg SM-cholesterol GUVs of the specified mole percentages across a range of temperatures. Some deformation of GUVs is evident at higher temperatures, likely due to a combination of the increased fluidity of the membrane and convection within the sample volume. Scale bar represents 10 µm. Rightmost panels show portions of Figure 2B for individual compositions in the vicinity of T_{break}. Dashed lines indicate the piecewise linear function used to evaluate T_{break}. Vertical line denotes T_{break}.

3.3.3 POPC-egg SM-cholesterol GUV behavior

For comparison, GUVs of the same compositions were examined, as shown in Figure 3. The temperatures at which domains first appeared upon cooling (T_m) were in good agreement with T_{break} (see plots in Figure 3, and Table S1) but not T_{mid} laurdan GP results (see legends of Figure 2). T_m values were also in good agreement with previously published work regarding GUVs composed of a similar lipid mixture (which instead incorporated palmitoyl sphingomyelin (PSM),

the primary component of egg SM) [9]. GUVs typically displayed bright, round domains on a dark background, suggesting the presence of both the liquid disordered (POPC-rich) and liquid ordered (egg SM-rich) phases. For the 50-25-25 mol% POPC-egg SM-cholesterol GUVs, domains were not observed at room temperature or at the lowest temperature accessible to us (~13 ºC). This composition lies at the very edge of the previously reported two-phase region for POPC-PSM-cholesterol GUVs [9], so it is possible the slight compositional differences between egg SM and PSM may have resulted in the observation of only one phase for this composition.

3.3.4 Analysis of laurdan spectroscopy results for PBdPEO-egg SM-cholesterol LUVs

Given the consistent results of the three-peak decomposition for lipid-only membranes containing cholesterol (i.e., good agreement of T_{break} with T_m), we then applied the same approach to hybrid membranes containing the block copolymer polybutadiene-*block*-polyethylene oxide instead of POPC. Results of laurdan GP calculation and laurdan emission spectrum decomposition are shown in Figure 4. As for the POPC-egg SM-cholesterol vesicles, the shallow slopes of the laurdan GP curves suggest a broad phase transition. T_{mid} values ranged from ~35-56 ºC (legend of Figure 4A) by fitting to Equation (2), similar to those indicated by laurdan GP for POPC-egg SM-cholesterol LUVs.

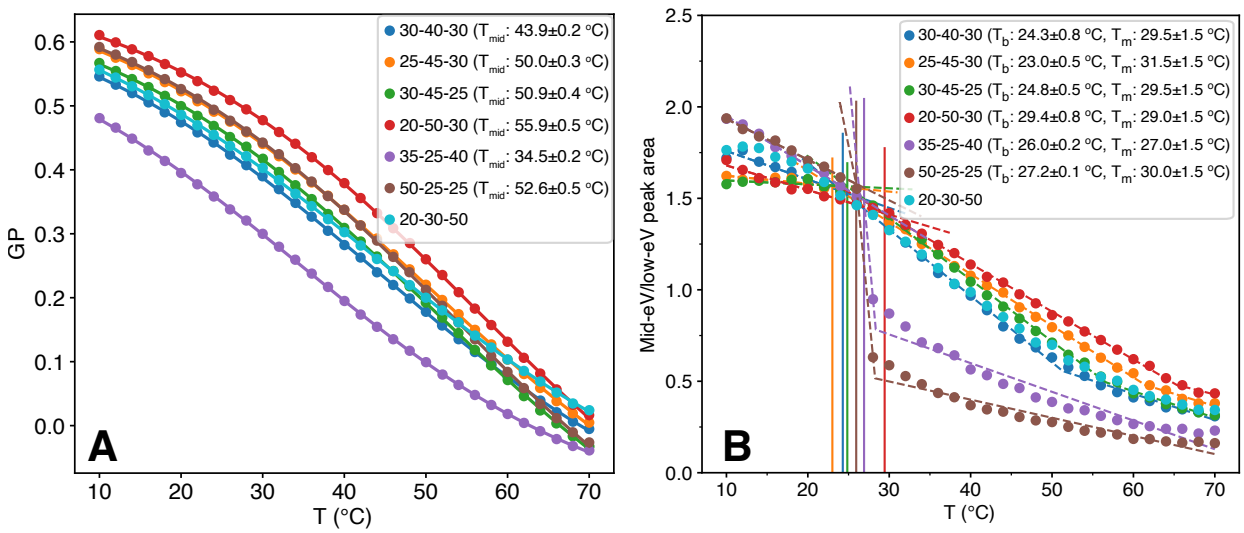

Figure 4. A. GP of laurdan in PBdPEO-egg SM-chol LUVs of the specified mole percentages. T_{mid} is the inflection point indicated by fitting to Equation (2). B. Ratio of the areas beneath the mid-eV and low-eV peaks resulting from the decomposition into three curves of laurdan emission spectra in PBdPEO-egg SM-chol LUVs of the specified mole percentages. Vertical lines indicate the first change in slope at temperature T_{break}. In the legend, T_b refers to T_{break}. T_m in the legend refers to the temperature at which domains first appeared upon cooling indicated by fluorescence microscopy images of GUVs. Dashed lines indicate the piecewise linear function used to evaluate T_{break}.

Figure S3 shows an example of a three-peak fit to a laurdan emission spectrum for 30-40-30 mol% PBdPEO-egg SM-chol at 20 °C. The small values of the residuals and relatively Gaussian distribution suggest a good fit is achieved with three peaks. A difference in the shapes of the peak area ratio profiles is clear between the hybrid (Figure 4B) and lipid-only (Figure 2B) membranes. While the lipid-only membranes had concave peak area ratio plots, those for the hybrid membranes appeared roughly sigmoidal, with some compositions displaying a discontinuity at T_{break} and others displaying a change in slope. Additionally, T_{break} values were in a similar range, ~23-29 °C (legend of Figure 4B), to those indicated for POPC-egg SM-cholesterol LUVs.

To further investigate, peak area ratio plots were constructed for a broad range of compositions of hybrid LUVs (Figure 5). At T_{break}, either a discontinuity (Figure 5A) or only a change in slope (Figure 5B) was observed depending on the composition. The peak area ratio is expected to correlate with the relative amount of the liquid ordered phase—more specifically, with the relative

amount of hydrogen-bound but immobile laurdan [18,26]. This suggests that for the compositions plotted in Figure 5A, once the temperature decreases below T_{break}, the liquid-ordered lipid population increases sharply. For the compositions in Figure 5B, after the temperature decreases below T_{break}, the size of this population increases gradually.

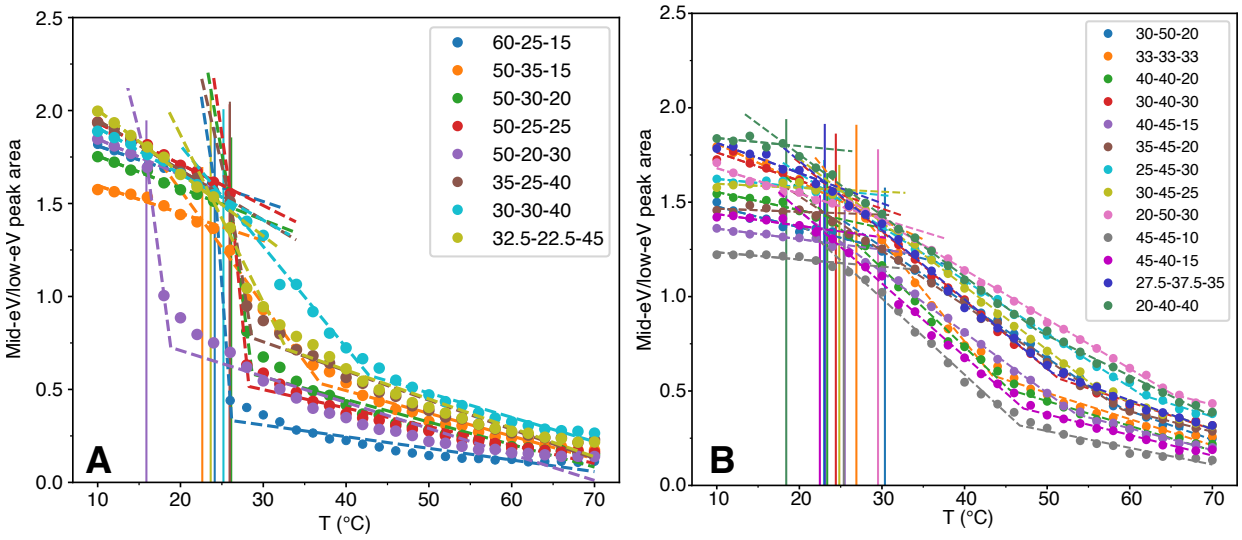

Figure 5. Comparison of trends in the temperature dependence of the peak area ratio plots for PBdPEO-egg SM-chol LUVs of the specified mole percentages. Dashed lines indicate the piecewise linear function used to evaluate T_{break}. A. Compositions for which the peak area ratio plot shows a discontinuity at T_{break}. B. Compositions for which the peak area ratio plot shows only a change in slope at T_{break}.

To better visualize any compositional trends in T_{break} and in the peak area ratio plots for hybrid LUVs, a 3-component triangle (Figure 6A) was used. T_{break} values are plotted as a heat map on the 3-component triangle. In Figure 6A, red circles indicate compositions displaying a discontinuity in their peak area ratio plot. This is not a phase diagram, as the results are not shown at a single temperature, but instead represents an overview of the data presented above. For comparison, a similar figure was constructed for the POPC-egg SM-cholesterol LUVs discussed above (Figure S2).

The T_{break} values shown on the heat maps in Figure 6 tend to increase as the amount of egg SM is increased and the amount of cholesterol is decreased, similar to the trends reported for lipid vesicles [9]. The range of temperatures observed for T_{break} (~15-30 ºC for the compositions studied here) is also similar to the miscibility transitions reported in POPC-PSM-cholesterol GUVs of comparable compositions [9]. For the hybrid vesicles, however, T_{break} is significantly higher at high cholesterol contents (>30%) indicating relatively less miscibility between PBdPEO and egg SM. In this respect, some similarity is shared with the phase coexistence region of dioleoylphosphatidylcholine (DOPC)-PSM-cholesterol vesicles, which displays miscibility temperature values near room temperature at ~40 mol% cholesterol [9].

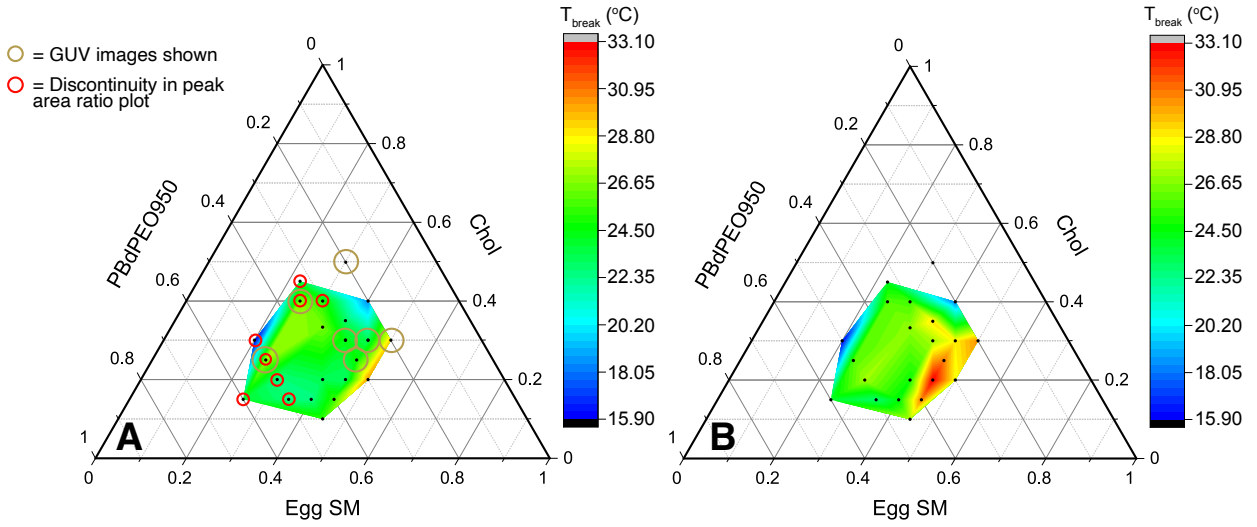

Figure 6. Heat maps of T_{break} values indicated by laurdan in PBdPEO-egg SM-cholesterol LUVs. A. T_{break} values calculated from the ratio of the mid-eV and low-eV peak areas. Gold circles mark compositions for which images of GUVs are shown. Compositions for which a discontinuity is observed in the laurdan peak area ratio plots are indicated with a red circle. For the single point plotted outside the edges of the heat map, only a single phase was observed for GUVs at the lowest accessible temperature (~13 ºC). However, the edges of the heat map do not indicate the boundaries of a phase coexistence region. B. T_{break} values recalculated based on the ratio of the mid-eV peak area to the sum of the areas of all three peaks. T_{break} was obtained from the meeting point of the first and second lines of a piecewise linear fit to the peak area ratios, as in part A.

For two-phase lipid GUVs, phase separation by spinodal decomposition has been reported for compositions with the average area fraction of one phase ranging from 0.3-0.7 (i.e., similar proportions of each phase) [27]. Outside of this range, phase separation is initiated by nucleation and growth, which takes place when there is a discontinuity in the composition associated with the new phase. Therefore, it is not too surprising that the compositions for which a discontinuity in the peak area ratio plot was observed are all positioned roughly on the left side of the phase space explored, which is perhaps in the compositional range for nucleation and growth. The lack of discontinuities in the peak area ratio plots for the remainder of the compositions suggests that they phase separate by spinodal composition, which may be visible somewhat in the domain morphologies observed in GUVs.

3.3.5 PBdPEO-egg SM-cholesterol GUVs and further analysis of laurdan spectroscopy results

For comparison, GUVs of compositions from Figure 4 were imaged. The temperatures at which domains first appeared upon cooling (T_m) were in better agreement with T_{break} than with the T_{mid} laurdan results (see legends of Figure 4). To attempt to gain better agreement between T_{break} and T_m, an additional fitting approach was used. The relative amount of the mid-eV peak, reported to be correlated with the relative abundance of the liquid ordered phase [18], was recalculated by comparing the area of the mid-eV peak to the area of all three peaks (Table S2). Interestingly, this resulted in better agreement for the compositions with larger (~>4-5 ^oC) discrepancies between T_{break} and T_m. For the compositions for which there was little difference between T_{break} and T_m, this recalculation did not significantly change T_{break} (typically less than a ~1 ^oC difference after recalculation).

For the hybrid membranes, certain compositions displayed a high-eV peak area that remained relatively consistent at all temperatures studied, both above and below T_m in GUVs. In comparison, for the lipid-only vesicles in this work the area beneath the high-eV peak increased and the area beneath the low-eV peak decreased as the temperature decreased (Figure S4), consistent with the expectation of an increasingly ordered membrane at lower temperatures and with previously reported results [18,19]. DOPC vesicles [19] also unexpectedly displayed high energy peaks of relatively constant area with temperature in another work. The authors attributed the relatively constant area of these peaks to the presence of an energetically unfavorable but still observable population of non-hydrogen bonded laurdan molecules at high temperature, based on their report of a short lifetime at this wavelength. It is possible that such a phenomenon is taking place in the hybrid membranes as well. In such a case, considering the recalculation of the peak area ratios as described above may provide more accurate insight into the phase transition temperatures of hybrid vesicles.

Recalculating peak area ratios as the area of the mid-eV peak divided by the sum of the areas of the high-eV, mid-eV, and low-eV peaks and evaluating T_{break} resulted in the heat map shown in Figure 6B. Similar trends are observed for vesicles containing lower amounts of egg SM as shown in Figure 6A. However, for vesicles incorporating more than ~40% egg SM, recalculated T_{break} values were ~5-7 ^oC higher, which is more consistent with the trends observed for T_m in GUVs.

It should also be noted that below T_m, it was typically more common to observe bright, single phase GUVs when PBdPEO rather than POPC was incorporated. This may be due to budding away of the dark phase prior to imaging; significant and rapid budding has been previously reported in hybrid GUVs incorporating a different triblock copolymer [28]. Therefore,

discrepancies in T_m and T_{break} may also occur from differences in composition of hybrid GUVs and LUVs respectively attributed to rapid budding before the heating and cooling cycle. Alternatively, such compositional variations could arise from incomplete detachment of GUVs immediately after formation but prior to cooling [29–31]. This would allow domain formation in the interconnected GUV buds prior to their separation and collection, resulting in subsequent compositional differences amongst individual GUVs.

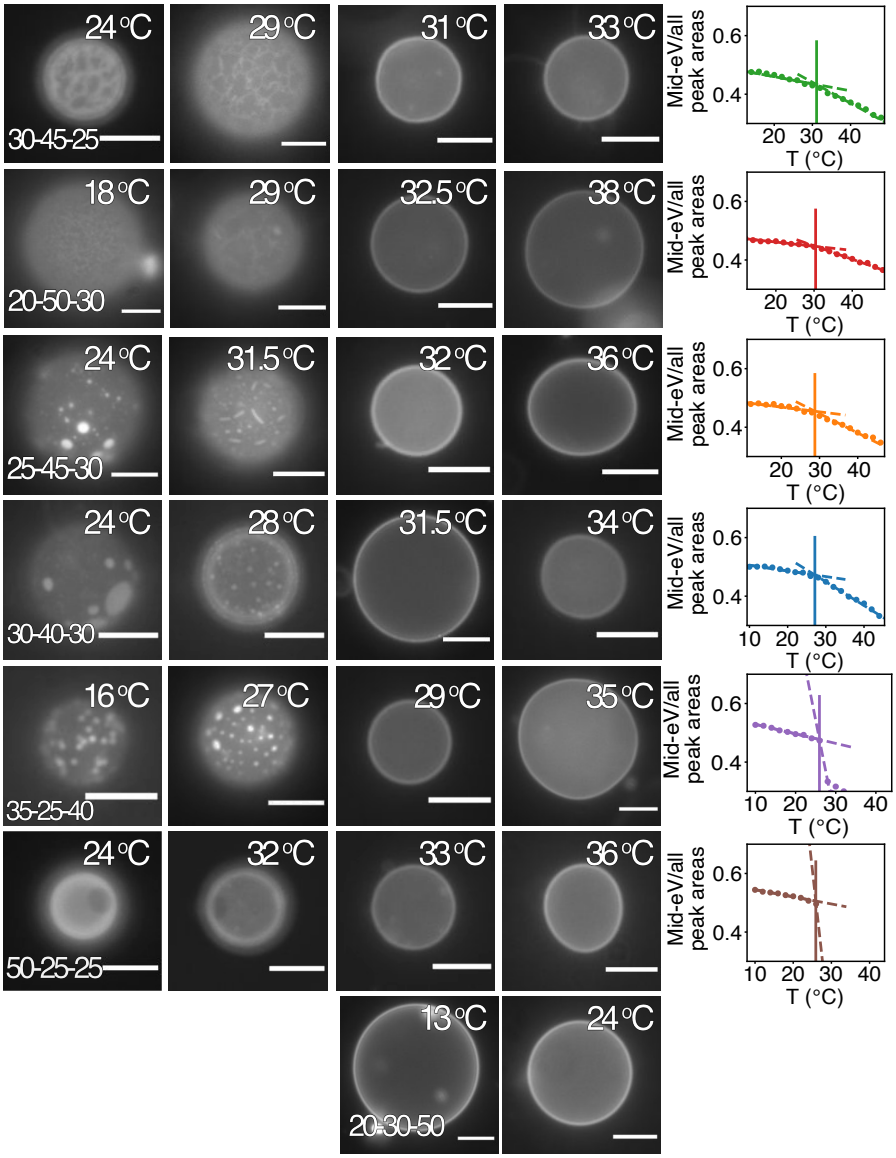

Figure 7. Fluorescence microscopy images of giant unilamellar vesicles consisting of PBdPEO-egg SM-cholesterol at the specified mole percentages across a range of temperatures. For the vesicles containing 50 mol% cholesterol, domains were not observed even at the lowest accessible temperature. For the 50-25-25 mol% sample, T_m was assessed by heating rather than cooling the vesicles, as excessive budding away of domains upon cooling complicated assessment of T_m. Scale bar represents 10 μm. Rightmost panels show portions of peak area ratio plots recalculated by dividing the area of the mid-eV peak by the sum of the areas of all three peaks for individual compositions in the vicinity of T_{break}. Dashed lines indicate the piecewise linear function used to evaluate T_{break}. Vertical line denotes T_{break}.

Fluorescence images of GUVs of compositions from Figure 4 are shown in Figure 7. The panels on the far right of Figure 7 show selected regions of mid eV/all eV peaks near the refitted T_{break} values for each composition. The compositions in rows 3-6 of Figure 7 (25-45-30, 30-40-30, 35-

25-40, and 50-25-25 mol% PBdPEO-egg SM-cholesterol) appear to display coexisting fluid phases, based on the presence of round domains. In this case, the dark phase is likely rich in egg SM, given that below T_m this dark phase makes up the majority of the vesicle surface area for compositions richer in egg SM and less of the surface area when less egg SM is included. Circular domains have been previously reported in hybrid membranes upon inclusion of cholesterol and were hypothesized to be a liquid ordered-like phase [10].

In contrast to POPC-egg SM-cholesterol GUVs of the same compositions (Figure 3), the GUVs in rows 1 and 2 of Figure 7 (30-45-25 and 20-50-30 mol% PBdPEO-egg SM-cholesterol) appear to display predominantly solid/fluid instead of fluid/fluid phase separation, based on the irregularity of the domain shapes. This indicates greater amounts of cholesterol may be required to induce fluid/fluid phase separation in hybrid membranes as compared to lipid membranes. This result suggests that cholesterol partitions to a greater extent into PBdPEO in comparison to fluid lipids such as POPC. Of note, for POPC-PSM-cholesterol compositions with greater amounts of PSM, a three-phase region consisting of solid, liquid ordered, and liquid disordered phases with an upper bound delineated by the observed transition from fluid/fluid to solid/fluid phase separation has been suggested to exist across a range of cholesterol concentrations (~10-25 mol%) [9]. It is possible that one or both of the compositions of the GUVs in rows 1 and 2 of Figure 7 may lie within such a three-phase region as well, with T_{break} perhaps corresponding to the appearance of the liquid-ordered phase as the sample is cooled.

For the 20-30-50 mol% PBdPEO-egg SM-cholesterol GUVs, no phase separated vesicles were observed at 13 ^oC or above, consistent with the observation that greater amounts of cholesterol were required to induce fluid/fluid phase separation in hybrid membranes than in lipid-only

membranes. For comparison, a phase diagram for POPC-PSM-cholesterol GUVs indicates a single fluid phase exists above ~35 mol % cholesterol at temperatures greater than 15 ^{o}C [9]. Similarly, while 50-25-25 mol% PBdPEO-egg SM-cholesterol GUVs displayed dark, round domains up to ~32 ^{o}C, phase separation was not observed for POPC-egg SM-cholesterol GUVs of the same composition at or above ~13 ^{o}C, the lowest accessible temperature (Figure 3).

Rows 2-3 of Figure 7 (20-50-30 and 25-45-30 mol% PBdPEO-egg SM-cholesterol) show hybrid GUVs that displayed domain morphologies suggestive of spinodal decomposition below T_m. For the 20-50-30 mol% GUVs, at low temperatures the widespread, grainy appearance of the domains and the low contrast between light and dark phases resemble the early stages of spinodal decomposition. Similarly, for the 25-45-30 mol% PBdPEO-egg SM-cholesterol GUVs elongation of domains is observed just below T_m. Such morphologies have been observed in GUVs undergoing spinodal decomposition [7,32] and are attributed to reduced line tension near a critical point [7]. Additionally, these GUVs as well as those in rows 1 and 4 of Figure 7 (30-45-25 and 30-40-30 mol% PBdPEO-egg SM-cholesterol) display relatively low contrast in the brightness of light and dark domains—especially just below T_m. This is indicative of a gradual change in composition, and thus weak partitioning of the probe. In agreement with these observations, these mixtures fall within the compositional region that was hypothesized to phase separate by gradual spinodal decomposition based upon laurdan multipeak analysis.

Of note, the length scales of the domains observed in GUVs and in LUVs are inherently different. Fluorescence microscopy enables observation of micron-scale domains in GUVs. While there may be temperatures at which stable nanodomains exist in GUVs but for some reason do not coalesce, this phenomenon occurs at a length scale unresolvable by fluorescence microscopy. LUVs,

however, have diameters of ~100 nm; any domains that form in LUVs accordingly have sizes on the order of 100 nm or less. The laurdan experiments performed with LUVs would therefore detect the formation of such nanoscale domains. Theoretically, the same laurdan experiments could be carried out using GUVs, although our preliminary attempts to do so were limited by the low concentration of GUVs in solution yielded by electroformation. Further optimization of such experiments could allow for comparison between spectroscopy and microscopy results in GUVs.

To gauge the possible usefulness of multipeak analysis applied to cholesterol-free membranes, T_{break} was evaluated for 40-60 mol% PBdPEO-egg SM vesicles based on the ratio of areas of the mid-eV peaks to the sum of the areas of all three peaks (Figure S5). A discontinuity in the vicinity of T_{break} was observed, suggesting a significant difference in the compositions of the solid and fluid phases at T_{break}. T_{break} was 29.6±0.4 ºC, less than both the GP T_{mid} of 33.9±0.2 ºC and the GUV T_m of 33.0±1.5 ºC. T_{break} resulting from analysis of the ratios of the areas of the mid-eV and low-eV peaks for 40-60 mol% POPC-egg SM vesicles (Figure S5) was 36.7±0.8 ºC, greater than both the GP T_{mid} of 27.5±0.2 ºC and the GUV T_m of 32.0±1.5 ºC. For POPC-egg SM LUVs, a gradual change in slope is observed in the vicinity of T_{break}, similar to the trends observed for POPC-egg SM-cholesterol LUVs and suggestive of more gradual changes in the compositions of the two phases as the temperature is decreased. For cholesterol-free vesicles, which undergo a solid to fluid phase transition, laurdan GP analysis could potentially be used to more accurately determine the temperature at which solidification begins and the temperature at which half of the lipids have transitioned to the solid phase, as described in our previous work [16]. GUV T_m values would then be expected to lie within the range of these temperatures. Conversely, multipeak analysis of laurdan emission spectra indicates a single temperature, T_{break}. This may correspond

more accurately to the behavior observed for GUVs in which the liquid ordered phase is present, typically resulting in domains that coalesce rapidly even just below T_m.

3.4 Conclusions

Fluorescence spectroscopy and microscopy were employed to study the phase behavior of POPC-egg SM-cholesterol and PBdPEO-egg SM-cholesterol vesicles. While laurdan GP indicated phase behavior consistent with observations of GUVs for POPC-egg SM and PBdPEO-egg SM vesicles, multipeak analysis of laurdan emission spectra was found to provide more accurate insight into phase behavior than analysis of laurdan GP values for cholesterol-containing lipid-only and hybrid vesicles. For hybrid vesicles, taking the ratio of the area of the middle energy peak to the sum of the areas of all peaks improved the temperature-dependent agreement with GUV behavior in comparison to the ratio of the area of the middle peak to the area of the lowest energy peak. Either a more gradual change in slope or a discontinuity around the break-point of this ratio was observed for the hybrid vesicles. We hypothesize that these trends correspond to the mechanism by which phase separation proceeds (spinodal decomposition or nucleation and growth) based on the characteristic shapes of the peak area ratio plots, the compositions for which each profile was observed, and the morphologies of domains in GUVs of corresponding compositions. The relatively high T_{break} values at cholesterol contents greater than 30 mol% are suggestive of low miscibility of PBdPEO and egg SM. Additionally, greater amounts of cholesterol were observed to be required to induce fluid/fluid phase separation in hybrid GUVs than in lipid-only GUVs. This suggests stronger partitioning of cholesterol into PBdPEO than into POPC. These results, which

we summarized on a heat map, may inform the further investigation of the phase behavior of hybrid vesicles toward applications such as drug delivery.

3.5 Acknowledgements

This material is based upon work supported by the National Science Foundation under Grant No. DMR – 1806366.

Appendix A. Supplementary data

Supplementary data to this article can be found online.

3.6 References

[1] D. Chen, M.M. Santore, Hybrid copolymer–phospholipid vesicles: phase separation resembling mixed phospholipid lamellae, but with mechanical stability and control, Soft Matter. 11 (2015) 2617–2626. https://doi.org/10.1039/C4SM02502D.

[2] S. Khan, M. Li, S.P. Muench, L.J.C. Jeuken, P.A. Beales, Durable proteo-hybrid vesicles for the extended functional lifetime of membrane proteins in bionanotechnology, Chem. Commun. 52 (2016) 11020–11023. https://doi.org/10.1039/C6CC04207D.

[3] M.L. Jacobs, M.A. Boyd, N.P. Kamat, Diblock copolymers enhance folding of a mechanosensitive membrane protein during cell-free expression, PNAS. 116 (2019) 4031–4036. https://doi.org/10.1073/pnas.1814775116.

[4] Z. Cheng, D.R. Elias, N.P. Kamat, E.D. Johnston, A. Poloukhtine, V. Popik, D.A. Hammer, A. Tsourkas, Improved Tumor Targeting of Polymer-Based Nanovesicles Using Polymer–Lipid Blends, Bioconjugate Chem. 22 (2011) 2021–2029. https://doi.org/10.1021/bc200214g.

[5] Z.I. Imam, L.E. Kenyon, G. Ashby, F. Nagib, M. Mendicino, C. Zhao, A.K. Gadok, J.C. Stachowiak, Phase-Separated Liposomes Enhance the Efficiency of Macromolecular Delivery to the Cellular Cytoplasm, Cel. Mol. Bioeng. 10 (2017) 387–403. https://doi.org/10.1007/s12195-017-0489-4.

[6] A.N. Trementozzi, Z.I. Imam, M. Mendicino, C.C. Hayden, J.C. Stachowiak, Liposome-Mediated Chemotherapeutic Delivery is Synergistically Enhanced by Ternary Lipid Compositions and Cationic Lipids, Langmuir. 35 (2019) 12532–12542. https://doi.org/10.1021/acs.langmuir.9b01965.

[7] S.L. Veatch, S.L. Keller, Seeing spots: Complex phase behavior in simple membranes, Biochimica et Biophysica Acta (BBA) - Molecular Cell Research. 1746 (2005) 172–185. https://doi.org/10.1016/j.bbamcr.2005.06.010.

[8] D. Marsh, Cholesterol-induced fluid membrane domains: A compendium of lipid-raft ternary phase diagrams, Biochimica et Biophysica Acta (BBA) - Biomembranes. 1788 (2009) 2114–2123. https://doi.org/10.1016/j.bbamem.2009.08.004.

[9] S.L. Veatch, S.L. Keller, Miscibility Phase Diagrams of Giant Vesicles Containing Sphingomyelin, Phys. Rev. Lett. 94 (2005) 148101. https://doi.org/10.1103/PhysRevLett.94.148101.

[10] J. Nam, T.K. Vanderlick, P.A. Beales, Formation and dissolution of phospholipid domains with varying textures in hybrid lipo-polymersomes, Soft Matter. 8 (2012) 7982–7988. https://doi.org/10.1039/c2sm25646k.

[11] S. Winzen, M. Bernhardt, D. Schaeffel, A. Koch, M. Kappl, K. Koynov, K. Landfester, A. Kroeger, Submicron hybrid vesicles consisting of polymer – lipid and polymer – cholesterol blends, Soft Matter. 9 (2013) 5883–5890. https://doi.org/10.1039/C3SM50733E.

[12] B.R. Lentz, Y. Barenholz, T.E. Thompson, Fluorescence depolarization studies of phase transitions and fluidity in phospholipid bilayers. 2. Two-component phosphatidylcholine liposomes, Biochemistry. 15 (1976) 4529–4537. https://doi.org/10.1021/bi00665a030.

[13] T. Parasassi, G. De Stasio, G. Ravagnan, R.M. Rusch, E. Gratton, Quantitation of lipid phases in phospholipid vesicles by the generalized polarization of Laurdan fluorescence, Biophysical Journal. 60 (1991) 179–189. https://doi.org/10.1016/S0006-3495(91)82041-0.

[14] W.F. Zeno, S. Hilt, K.K. Aravagiri, S.H. Risbud, J.C. Voss, A.N. Parikh, M.L. Longo, Analysis of Lipid Phase Behavior and Protein Conformational Changes in Nanolipoprotein Particles upon Entrapment in Sol–Gel-Derived Silica, Langmuir. 30 (2014) 9780–9788. https://doi.org/10.1021/la5025058.

[15] K. Suga, H. Umakoshi, Detection of Nanosized Ordered Domains in DOPC/DPPC and DOPC/Ch Binary Lipid Mixture Systems of Large Unilamellar Vesicles Using a TEMPO Quenching Method, Langmuir. 29 (2013) 4830–4838. https://doi.org/10.1021/la304768f.

[16] N. Hamada, S. Gakhar, M.L. Longo, Hybrid lipid/block copolymer vesicles display broad phase coexistence region, Biochimica et Biophysica Acta (BBA) - Biomembranes. 1863 (2021) 183552. https://doi.org/10.1016/j.bbamem.2021.183552.

[17] K. Flandez, S. Bonardd, M. Soto-Arriaza, Physicochemical properties of L-alpha dipalmitoyl phosphatidylcholine large unilamellar vesicles: Effect of hydrophobic block

(PLA/PCL) of amphipathic diblock copolymers, Chemistry and Physics of Lipids. 230 (2020) 104927. https://doi.org/10.1016/j.chemphyslip.2020.104927.

[18] N. Puff, G. Staneva, M.I. Angelova, M. Seigneuret, Improved Characterization of Raft-Mimicking Phase-Separation Phenomena in Lipid Bilayers Using Laurdan Fluorescence with Log-Normal Multipeak Analysis, Langmuir. 36 (2020) 4347–4356. https://doi.org/10.1021/acs.langmuir.0c00412.

[19] N. Watanabe, Y. Goto, K. Suga, T.K.M. Nyholm, J.P. Slotte, H. Umakoshi, Solvatochromic Modeling of Laurdan for Multiple Polarity Analysis of Dihydrosphingomyelin Bilayer, Biophysical Journal. 116 (2019) 874–883. https://doi.org/10.1016/j.bpj.2019.01.030.

[20] M. Bacalum, B. Zorilă, M. Radu, Fluorescence spectra decomposition by asymmetric functions: Laurdan spectrum revisited, Anal Biochem. 440 (2013) 123–129. https://doi.org/10.1016/j.ab.2013.05.031.

[21] J.C.-M. Lee, M. Santore, F.S. Bates, D.E. Discher, From Membranes to Melts, Rouse to Reptation: Diffusion in Polymersome versus Lipid Bilayers, Macromolecules. 35 (2002) 323–326. https://doi.org/10.1021/ma0112063.

[22] J. Mooney, P. Kambhampati, Get the Basics Right: Jacobian Conversion of Wavelength and Energy Scales for Quantitative Analysis of Emission Spectra, J. Phys. Chem. Lett. 4 (2013) 3316–3318. https://doi.org/10.1021/jz401508t.

[23] A.D. Lúcio, C.C. Vequi-Suplicy, R.M. Fernandez, M.T. Lamy, Laurdan Spectrum Decomposition as a Tool for the Analysis of Surface Bilayer Structure and Polarity: a Study with DMPG, Peptides and Cholesterol, J Fluoresc. 20 (2010) 473–482. https://doi.org/10.1007/s10895-009-0569-5.

[24] B. Kubsch, T. Robinson, R. Lipowsky, R. Dimova, Solution Asymmetry and Salt Expand Fluid-Fluid Coexistence Regions of Charged Membranes, Biophysical Journal. 110 (2016) 2581–2584. https://doi.org/10.1016/j.bpj.2016.05.028.

[25] N. Watanabe, K. Suga, J.P. Slotte, T.K.M. Nyholm, H. Umakoshi, Lipid-Surrounding Water Molecules Probed by Time-Resolved Emission Spectra of Laurdan, Langmuir. 35 (2019) 6762–6770. https://doi.org/10.1021/acs.langmuir.9b00303.

[26] R.B.M. Koehorst, R.B. Spruijt, M.A. Hemminga, Site-Directed Fluorescence Labeling of a Membrane Protein with BADAN: Probing Protein Topology and Local Environment, Biophysical Journal. 94 (2008) 3945–3955. https://doi.org/10.1529/biophysj.107.125807.

[27] C.A. Stanich, A.R. Honerkamp-Smith, G.G. Putzel, C.S. Warth, A.K. Lamprecht, P. Mandal, E. Mann, T.-A.D. Hua, S.L. Keller, Coarsening Dynamics of Domains in Lipid Membranes, Biophysical Journal. 105 (2013) 444–454. https://doi.org/10.1016/j.bpj.2013.06.013.

[28] T.P.T. Dao, F. Fernandes, E. Ibarboure, K. Ferji, M. Prieto, O. Sandre, J.-F. Le Meins, Modulation of phase separation at the micron scale and nanoscale in giant polymer/lipid hybrid unilamellar vesicles (GHUVs), Soft Matter. 13 (2017) 627–637. https://doi.org/10.1039/C6SM01625A.

[29] D.J. Estes, M. Mayer, Giant liposomes in physiological buffer using electroformation in a flow chamber, Biochimica et Biophysica Acta (BBA) - Biomembranes. 1712 (2005) 152–160. https://doi.org/10.1016/j.bbamem.2005.03.012.

[30] A. Li, J. Pazzi, M. Xu, A.B. Subramaniam, Cellulose Abetted Assembly and Temporally Decoupled Loading of Cargo into Vesicles Synthesized from Functionally Diverse Lamellar Phase Forming Amphiphiles, Biomacromolecules. 19 (2018) 849–859. https://doi.org/10.1021/acs.biomac.7b01645.

[31] J. Pazzi, A.B. Subramaniam, Nanoscale Curvature Promotes High Yield Spontaneous Formation of Cell-Mimetic Giant Vesicles on Nanocellulose Paper, ACS Appl. Mater. Interfaces. 12 (2020) 56549–56561. https://doi.org/10.1021/acsami.0c14485.

[32] S.L. Veatch, S.L. Keller, Separation of Liquid Phases in Giant Vesicles of Ternary Mixtures of Phospholipids and Cholesterol, Biophysical Journal. 85 (2003) 3074–3083. https://doi.org/10.1016/S0006-3495(03)74726-2.

3.7 Supplementary Material

3.7.1 Supplementary Figures

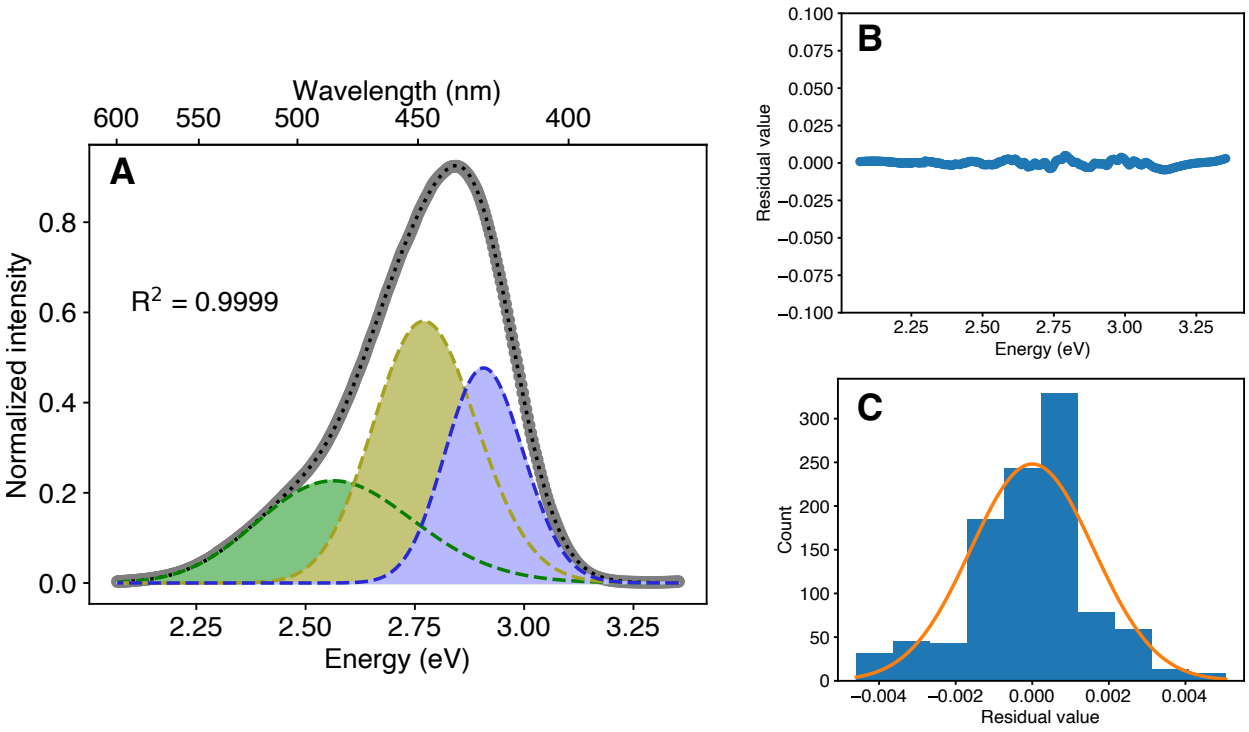

Figure S1. A. Example of a three-peak fit to the emission spectrum of laurdan in 30-40-30 mol% POPC-egg SM-cholesterol LUVs at 20 ºC. Green peak is low-eV, yellow peak is mid-eV, purple peak is high-eV. B. Residual values for the peak fit. C. Residual histogram and corresponding distribution (orange overlay). Relatively small residual values and Gaussian residual distribution suggest a reasonably accurate fit.

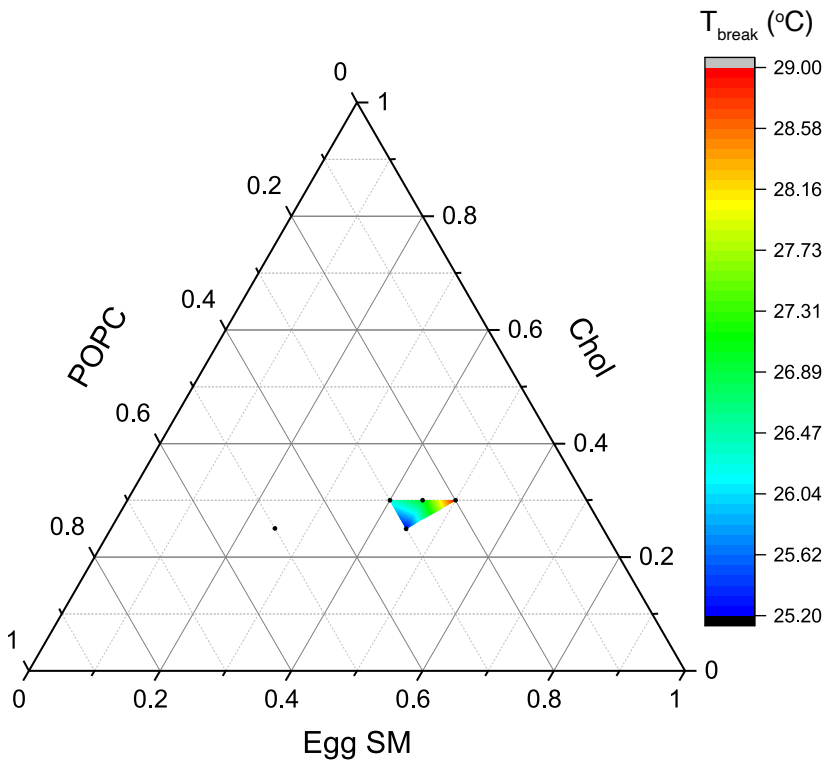

Figure S2. Heat map of T_{break} values indicated by three-peak decomposition of laurdan emission spectra in POPC-egg SM-cholesterol LUVs. For the single point plotted outside the edges of the heat map, only a single phase was observed for GUVs at the lowest accessible temperature (~13 ºC).

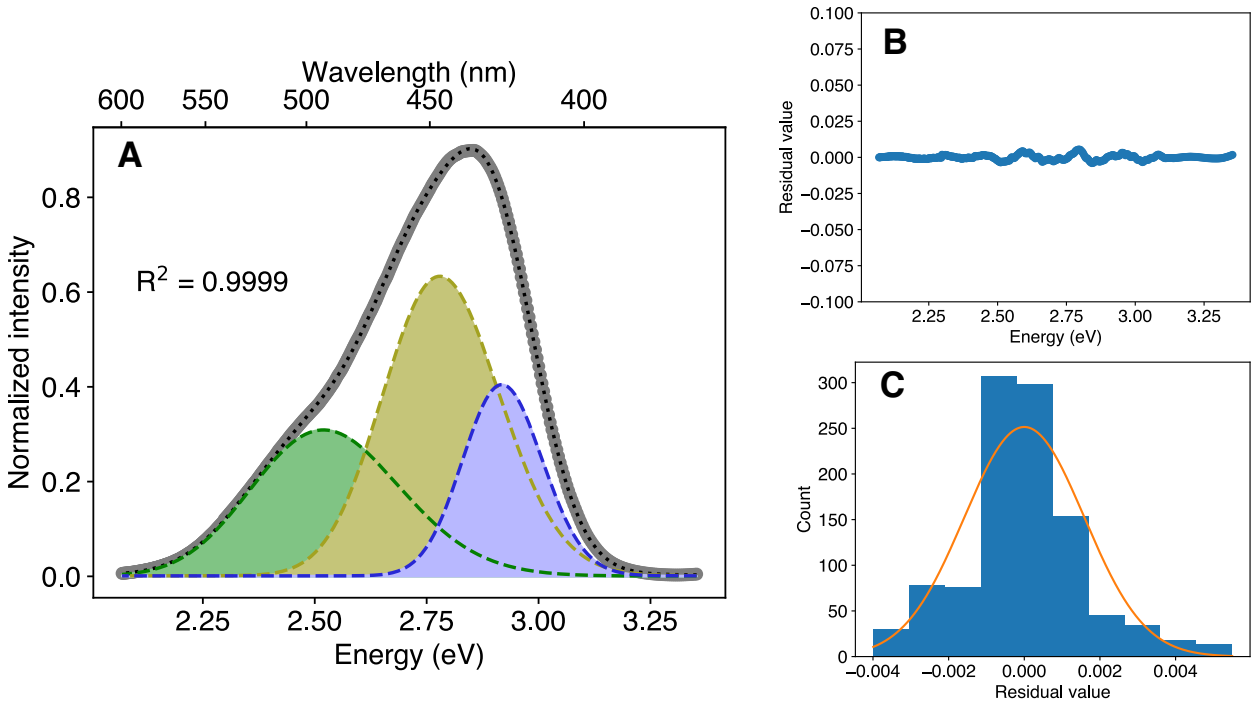

Figure S3. A. Three peak fit of laurdan emission spectrum in 30-40-30 mol% PBdPEO-egg SM-chol LUVs at 20 ºC. Green peak is low-eV, yellow peak is mid-eV, purple peak is high-eV. B. Residual values as a function of position. C. Residual histogram and corresponding distribution (orange overlay). Relatively small residual values and Gaussian residual distribution suggest a reasonably accurate fit.

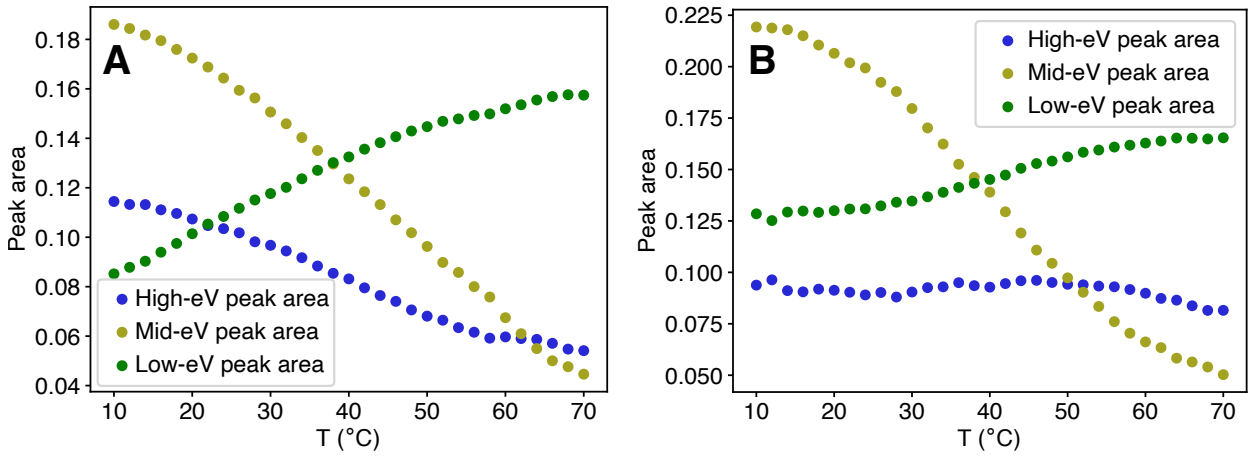

Figure S4. A. Temperature dependence of the areas of peaks returned from decomposition of laurdan emission spectra in 30-40-30 mol% POPC-egg SM-cholesterol LUVs. Steady decrease of the area of the high-eV peak with increasing temperature is evident. B. Peak areas returned from laurdan emission spectra decomposition for 30-40-30 mol% PBdPEO-egg SM-cholesterol LUVs. The area of the high-eV peak remains relatively constant with temperature, unlike the trend observed for the lipid-only vesicles.

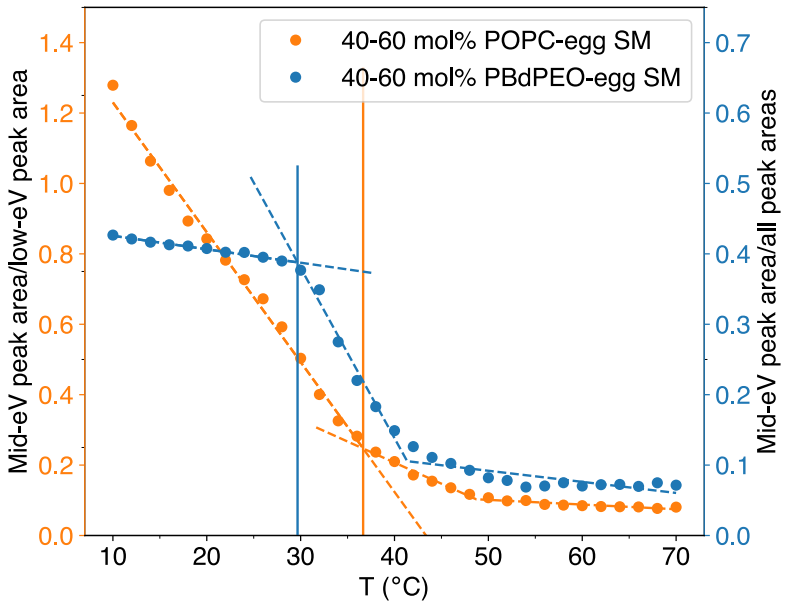

Figure S5. Comparison of three-peak analysis of laurdan emission spectra for cholesterol-free vesicles composed of either 40-60 mol% POPC-egg SM or 40-60 mol% PBdPEO-egg SM. The ratios of the areas of the mid-eV and low-eV peaks (left y-axis) are plotted for POPC-egg SM vesicles. For PBdPEO-egg SM vesicles, the areas of the mid-eV peaks are compared to the sum of the areas of all peaks (right y-axis), based on the finding that this yielded a T_{break} more consistent with GUV T_m results for hybrid vesicles. Dashed lines indicate the piecewise linear function used to evaluate T_{break}.

3.8 Supplementary Tables

Table S1. Comparison of the miscibility temperatures observed in GUVs (T_m) and indicated by laurdan in POPC-egg SM-cholesterol LUVs (T_{break}). T_{break} was determined from the ratios of the areas of the mid-eV and low-eV peaks resulting from decomposition of laurdan emission spectra into three peaks. Experimental uncertainty in T_m was determined to be roughly a range of 1.5 ºC, based on repeated experiments with selected compositions of GUV. Uncertainty values in T_{break} are obtained from the standard deviation error in the piecewise linear fit to the peak area ratio values.

POPC-egg SM-chol (mol%)	**T_m (ºC)**	**T_{break} (ºC)**
30-40-30	28.0±1.5	26.3±0.9
25-45-30	32.0±1.5	27.0±1.2
30-45-25	26.5±1.5	25.2±0.8
20-50-30	30.5±1.5	29.0±0.7

Table S2. Comparison of the miscibility temperatures observed in GUVs (T_m) and indicated by laurdan in PBdPEO-egg SM-cholesterol LUVs (T_{break}). T_{break} was determined from the ratios of the areas of the mid-eV and low-eV peaks resulting from decomposition of laurdan emission spectra into three peaks; T_{break} was also refitted by calculating the ratio of the area of the mid-eV peak to the total area of all three peaks. Asterisk (*) indicates T_m was determined upon heating rather than cooling. Experimental uncertainty in T_m was determined to be roughly a range of 1.5 °C, based on repeated experiments with selected compositions of GUV. Uncertainty values in T_{break} are obtained from the standard deviation error in the piecewise linear fit to the peak area ratio values.

PBdPEO-egg SM-chol (mol%)	**T_m (°C)**	**T_{break} (°C)**	**T_{break}, refitted (°C)**
30-40-30	29.5±1.5	24.3±0.8	27.2±0.4
25-45-30	31.5±1.5	23.0±0.5	28.8+0.9
30-45-25	29.5±1.5	24.8±0.5	29.1±1.0
20-50-30	29.0±1.5	29.4±0.8	30.1±0.9
35-25-40	27.0±1.5	26.0±0.2	25.9±0.2
20-30-50	None observed.	-	-
50-25-25	30-32*	27.2±0.1	27.2±0.1

Chapter 4 - Charged hybrid block copolymer-lipid-cholesterol vesicles: pH, ionic environment, and composition dependence of phase transitions

Previously published in Biochimica et Biophysica Acta – Biomembranes 2022

(https://doi.org/10.1016/j.bbamem.2022.184026)

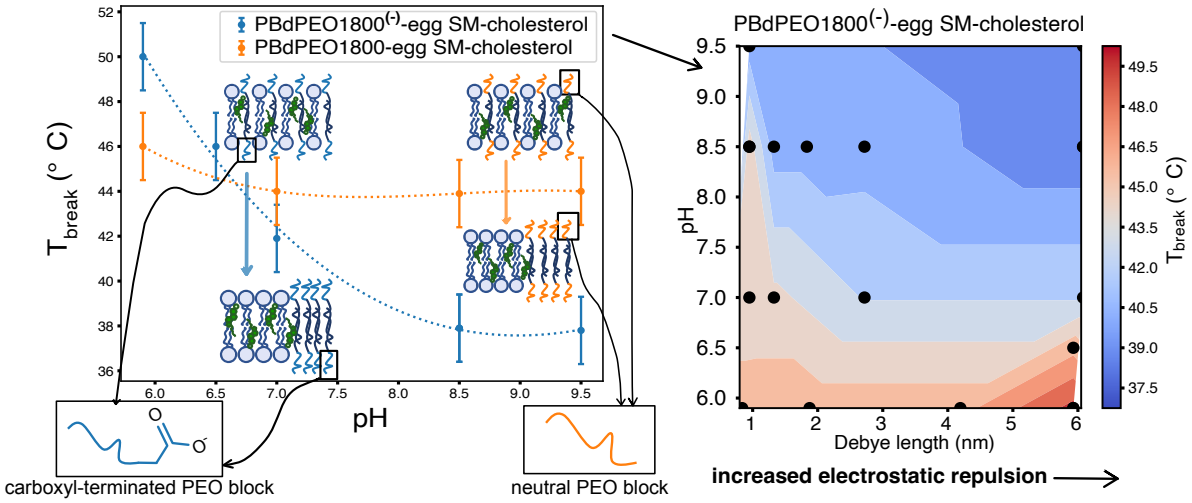

Abstract

The impacts of pH, salt concentration (expressed as Debye length), and composition on the phase behavior of hybrid block copolymer-lipid-cholesterol bilayers incorporating carboxyl-terminated poly(butadiene)-block-poly(ethylene oxide) copolymer (PBdPEO1800$^{(-)}$) or/and non-carboxyl-terminated PBdPEO (PBdPEO1800 or/and PBdPEO950), egg sphingomyelin (egg SM), and cholesterol were examined using fluorescence spectroscopy of laurdan. Laurdan emission spectra were decomposed into three lognormal curves as functions of energy. The ratio of the area of the mid-energy peak to the sum of the areas of all three peaks was evaluated as vesicles were cooled, yielding temperature breakpoint values (T_{break}) expected to be within the range of the phase

transition temperature. T_{break} values displayed dependence on pH, Debye length, and vesicle composition consistent with an electrostatic repulsion contribution to vesicle phase behavior. Increased pH and Debye length, for which a greater dissociated fraction of PBdPEO1800$^{(-)}$ and a greater energy of electrostatic repulsion would be expected, resulted in T_{break} values as much as 10 ^{o}C less than at low pH or short Debye lengths. Additionally, at Debye lengths comparable to those at physiologically relevant ionic strength, T_{break} at pH 5.9 was observed to be slightly higher than at pH 7.0 for vesicles containing 50 mol% PBdPEO1800$^{(-)}$. Electrostatic effects observed for hybrid vesicles incorporating significant amounts of carboxyl-terminated polymer may have the ability to drive phase separation in response to pH drops—such as those observed after endocytosis—in physiologically relevant conditions, suggesting the utility of such materials for drug delivery.

4.1 Introduction

Hybrid membranes formed of lipids and amphiphilic block copolymers are of interest as a means of combining the biocompatibility of lipids with the tunability and diversity of block copolymers. Such hybrid membranes may have biomedical applications as drug delivery vehicles or hosts for membrane protein reconstitution. Hybrid membranes have already displayed promise toward such applications. For example, the yield of certain membrane proteins produced by cell-free expression has been reported to be increased when vesicles composed of dioleoylphosphatidylcholine (DOPC) and poly(butadiene)-block-poly(ethylene oxide) (PBdPEO) instead of DOPC alone were used [1]. Similarly, the functional lifetime of a different membrane protein residing in a palmitoyl

oleoyl phosphatidylcholine (POPC)/PBdPEO membrane was reported to be extended in comparison to when lipid-only or polymer-only vesicles were used [2]. The incorporation of biodegradable polymers to facilitate release of cargo from hybrid vesicles for drug delivery has also been explored, highlighting the potential diversity of function offered by block copolymers [3].

Exploring the conditions under which phase separation arises in hybrid membranes is of use to further inform their biomedical application. Previous works have demonstrated that domain formation in lipid vesicles can be harnessed to concentrate functional groups within given regions of the membrane, impacting their function in biomedical contexts. In one such example, phase separation of lipid vesicles, resulting in localized concentration within domains of an apoptosis-inducing anticancer protein, was demonstrated to enhance cytotoxicity in certain cell lines, underscoring the potential effectiveness of this method toward vesicle-mediated delivery of certain proteins for cancer treatment [4]. Similarly, increased efficacy of cargo delivery to the cell cytoplasm by phase-separated vesicles, concentrating a cationic lipid within domains, has also been reported [5].

Like lipid membranes [6], hybrid membranes have been reported to demonstrate composition- and temperature-dependent separation into domains, expected to be enriched in either lipid or polymer [7–10]. Such phase separation has been observed to exist across a broader range of compositions and temperatures for certain hybrid membranes in comparison to their lipid-only counterparts [10,11]. However, there exists only limited knowledge regarding the impact of factors such as cholesterol content or charged components on hybrid membrane phase behavior.

Fluorescence spectroscopy is a valuable tool for the investigation of membrane phase behavior, often involving the incorporation of a fluorescent probe into small lipid vesicles. Laurdan is a commonly used fluorescent probe which displays a red shift in its emission spectrum upon incorporation into environments of increasing polarity [12]. This can be quantified as a generalized polarization (GP) value, typically determined by comparison of the intensities of laurdan emission spectra at 440 and 490 nm [12]. Increases in membrane polarity typically arise from increased hydration, permitted by increasing disorder of the membrane.

The decomposition of laurdan emission spectra into three peaks has also been suggested to provide further insight into membrane phase behavior, beyond the information provided by laurdan GP, based on trends in the evolution of the areas of the peaks returned [13,14]. This has been found to be especially useful when studying cholesterol-containing membranes, for which laurdan GP is often only of limited utility due to the breadth of the phase transitions observed [13]. Similar analysis of BADAN, a probe with the same fluorescent moiety as laurdan, has suggested the three peaks may correspond to non-hydrogen bonded, immobilized hydrogen bonded, and mobile hydrogen bonded states [15]. We have previously applied multipeak analysis to study hybrid vesicles composed of PBdPEO of molecular weight 950 g/mol (PBdPEO950), egg sphingomyelin (egg SM), and cholesterol [16]. For this case, we found that the first change in slope of the temperature dependence of the ratio of the area of the middle peak and the area of all three peaks (T_{break}) obtained by multipeak analysis of laurdan emission spectra resulted in good agreement with the temperature of first appearance of domains of an ordered phase in giant unilamellar vesicles (GUVs).

In this work, we apply multipeak analysis to laurdan fluorescence emission spectra to explore the effects of pH, salt concentration (expressed as Debye length), and vesicle composition on the phase behavior of hybrid vesicles of carboxyl-terminated (PBdPEO1800$^{(-)}$) or/and non-carboxyl-terminated (PBdPEO1800 or/and PBdPEO950) block copolymer, egg sphingomyelin (egg SM), and cholesterol. The carboxyl group terminates the hydrophilic PEO block, allowing PBdPEO1800$^{(-)}$ to bear a single negative charge at sufficiently high pH and consequently introducing electrostatic repulsion between individual charged polymer molecules.

We find clear dependence of T_{break}, the one-phase to two-phase transition temperature, on pH, Debye length, and vesicle composition. For vesicles incorporating PBdPEO1800$^{(-)}$, T_{break} decreased ~5-10 ºC as the Debye length and pH increased. Longer Debye lengths are present at decreased ionic strength and correspond to the effects of electrostatic repulsion being observed over greater length scales. Increased pH would facilitate dissociation of a greater fraction of PBdPEO1800$^{(-)}$ molecules, also resulting in increased electrostatic repulsion. This is consistent with previous reports of the inclusion of anionic lipids in GUVs having slight impacts on phase behavior in low ionic strength conditions [17]. We compare these findings with the decrease in T_{break} with decreasing molecular weight of the PBdPEO component. Interestingly, for vesicles containing 50 mol% PBdPEO1800$^{(-)}$, a ~4 ºC increase in T_{break} values was also observed as the pH decreased from 7.0 to 5.9 in solutions with a Debye length of roughly 0.9 nm—comparable to the Debye length of ~0.8 nm in solutions with physiological ionic strength. This suggests the inclusion of negatively charged block copolymers in hybrid vesicles may be able to drive membrane phase separation even in physiologically relevant conditions.

4.2 Materials and Methods

4.2.1 Materials

Egg sphingomyelin (egg SM) and cholesterol were purchased from Avanti Polar Lipids, Inc. Poly(1,2-butadiene)-block poly(ethylene oxide) with average molecular weights of 950 g/mol (PBdPEO950) and 1800 g/mol (PBdPEO1800) were purchased from Polymer Source, Inc. (P41807C-BdEO, Bd(600)-EO(350) and P41745-BdEO, Bd(1200)-EO(600), respectively). Poly(1,2-butadiene)-block-poly(ethylene oxide) with a carboxylic acid terminating the poly(ethylene oxide) chain and an average molecular weight of 1800 g/mol ($PBdPEO1800^{(-)}$) was also purchased from Polymer Source, Inc. (P40537-BdEOCOOH, Bd(1200)-EO(600)).

6-dodecanoyl-2-dimethylaminonaphthalene (laurdan) was purchased from AdipoGen Life Sciences.

4.2.2 Methods

4.2.2.1 Preparation of large unilamellar vesicles (LUVs)

Appropriate volumes of lipid, polymer, and cholesterol stock solutions in chloroform and laurdan stock solution in ethanol were combined in a clean glass vial. The solvent was evaporated under a gentle stream of nitrogen, and the resulting film was allowed to further dry under vacuum for 2-24 hours to remove any residual solvent. The films were then resuspended in a buffer solution at a concentration of 2 mM with respect to the lipid and polymer. This mixture was passed through a polycarbonate membrane with 0.1 μm pores 11 times, using a mini-extruder (Avanti), over a

water bath of at least 50°C. Dynamic light scattering measurements indicated LUV hydrodynamic diameter distributions centered around ~110-150 nm (Tables S1, S2).

4.2.2.2 Collection and evaluation of laurdan fluorescence emission spectra

LUVs containing laurdan at a lipid/polymer:probe ratio of 200:1 were diluted to a final concentration of 200 μM with respect to the lipid and polymer in a buffer matching the interior solution of the vesicles. Buffers included 0-100 mM NaCl added to 5 mM HEPES/0.5 mM EDTA (pH 7.0), 5 mM Tris/0.5 mM EDTA (pH 8.5), or 5 mM glycine/0.5 mM EDTA (pH 9.5). For low pH measurements, 1-100 mM sodium phosphate/0.5 mM EDTA buffers (pH 5.9 or pH 6.5) were used. Sodium phosphate monobasic (NaH_2PO_4) and sodium phosphate dibasic (Na_2HPO_4) were combined in appropriate ratios to yield desired pH values and ionic strengths.

Laurdan fluorescence emission spectra were collected from 70 °C to 2 °C at intervals of 2 °C, with 3 minutes of equilibration at each temperature. An excitation wavelength of 355 nm was used, and emission spectra were collected from 370-600 nm using a Jasco FP8500 spectrofluorometer. Excitation and emission bandwidths of 5 nm were used.

To gain information regarding the phase behavior of LUVs, multipeak fitting of lognormal curves to laurdan fluorescence emission spectra was carried out, as described previously [13,16]. A Python script applying least-squares regression was used to fit emission spectra with the sum of three lognormal curves, each of which was defined as in Equation (1):

$$y = A_0 + A_1 exp\left[-\left(\frac{\ln\left(\frac{x}{A_2}\right)}{A_3}\right)^2\right] \quad (1)$$

Emission intensities were expressed with respect to electron volts (eV) instead of wavelength by multiplying each intensity by ($h*c/E^2$), where h is Planck's constant, c is the speed of light in a vacuum, and E is the energy corresponding to each wavelength (calculated as $h*c/\lambda$, where λ is the wavelength) [13,16,18,19]. Prior to spectral decomposition, emission intensities were normalized by the greatest intensity observed at the lowest temperature studied in the experiment. When performing fits, all parameters aside from A_0 (the baseline) were constrained to be greater than or equal to 0. A_2 (the peak position) was additionally constrained to be within the range of wavelengths measured, which spanned the observed emission spectrum of laurdan.

The area beneath each of the three lognormal curves was evaluated at each temperature studied to calculate the ratio of the area of the middle peak to the sum of the areas of all three peaks, as we previously found this to result in better agreement with the phase behavior of polymer-containing vesicles [16]. Peak area ratio versus temperature plots were fit with a three-piece linear fit to identify T_{break} (the lower-temperature change in slope of this fit) as described in Puff et. al [13]. T_{break} is expected to be within the range of the phase transition temperature of the membrane. Uncertainty values for T_{break} were assessed as the largest standard deviation (1.5 °C) observed for experiments repeated in triplicate for a few selected compositions.

4.2.2.3 Debye length calculations

For solutions buffered by HEPES, Tris, and glycine, Debye lengths were calculated as

$$\lambda_D = \frac{0.304}{\sqrt{[C_{1:1}]}} \quad (2)$$

where λ_D is the Debye length in nanometers and $[C_{1:1}]$ is the molar concentration of 1:1 electrolyte in the solution [20]. We assumed a 2.5 mM 1:1 electrolyte baseline contribution to the Debye length in addition to the concentration of added NaCl for solutions buffered by HEPES, Tris, and glycine, as all were used near their pK_a, where roughly 50% of the buffer molecules added would be expected to be dissociated. Neither neutral nor zwitterionic [21] molecules are expected to contribute directly to the ionic strength of a solution.

For solutions buffered with sodium phosphate, a mixture of sodium phosphate monobasic (NaH_2PO_4) and sodium phosphate dibasic (Na_2HPO_4) was used at a ratio of roughly 10:1 (pH 5.9) or 5:3 (pH 6.5) sodium phosphate monobasic to sodium phosphate dibasic, as required to achieve the desired pH and ionic strength. The Debye length was therefore calculated as the weighted average

$$\lambda_D = x_1\lambda_{D_1} + x_2\lambda_{D_2} \quad (3)$$

with λ_{D1} calculated as described in Equation 2. λ_{D2} was calculated [20] as

$$\lambda_{D_2} = \frac{0.176}{\sqrt{[C_{2:1}]}} \quad (4)$$

where x_1 and x_2 correspond to the mole fractions of sodium phosphate monobasic and sodium phosphate dibasic, respectively. $[C_{2:1}]$ in Equation 4 refers to the molar concentration of 2:1 electrolyte (in the case of this work, sodium phosphate dibasic).

4.3 Results and Discussion

4.3.1 Multipeak analysis of laurdan emission spectra

Multipeak analysis was applied to fluorescence emission spectra of laurdan in hybrid vesicles to gain insight into the phase behavior of these membranes as we changed pH, salt concentration (expressed as Debye length), and temperature. These large unilamellar vesicles (LUVs) contained either a carboxyl-terminated (PBdPEO1800$^{(-)}$) or/and non-carboxyl-terminated (PBdPEO1800 or/and PBdPEO950) poly(butadiene)-block poly(ethylene oxide) copolymer, egg sphingomyelin (egg SM) and cholesterol. At sufficiently high pH, PBdPEO1800$^{(-)}$ is expected to bear a single negative charge arising from dissociation of the carboxyl group. Multipeak analysis has been previously reported to give further insight into membrane phase behavior than the information provided by laurdan generalized polarization values, especially for cholesterol-containing lipid-only and hybrid vesicles [13,16].

Three lognormal curves were used to fit laurdan emission spectra across the range of temperatures studied. A representative fit is shown in Figure 1A. The ratio of the area beneath the mid-energy curve and the sum of the areas of all three curves was then plotted with respect to temperature and fit with a piecewise linear function (Figure 1B). The lower-temperature change in slope of this plot, referred to as T_{break}, is expected to be within the range of the phase transition temperature. For hybrid vesicles, we previously found that evaluation of T_{break} in this manner resulted in improved agreement between T_{break} and the temperature of first appearance of ordered-phase domains upon cooling in GUVs [16]. For lipid-only vesicles, however, calculation of T_{break} based

on the ratio of the areas of the mid- and lowest-energy peaks has yielded results in good agreement with GUV behavior [13,16].

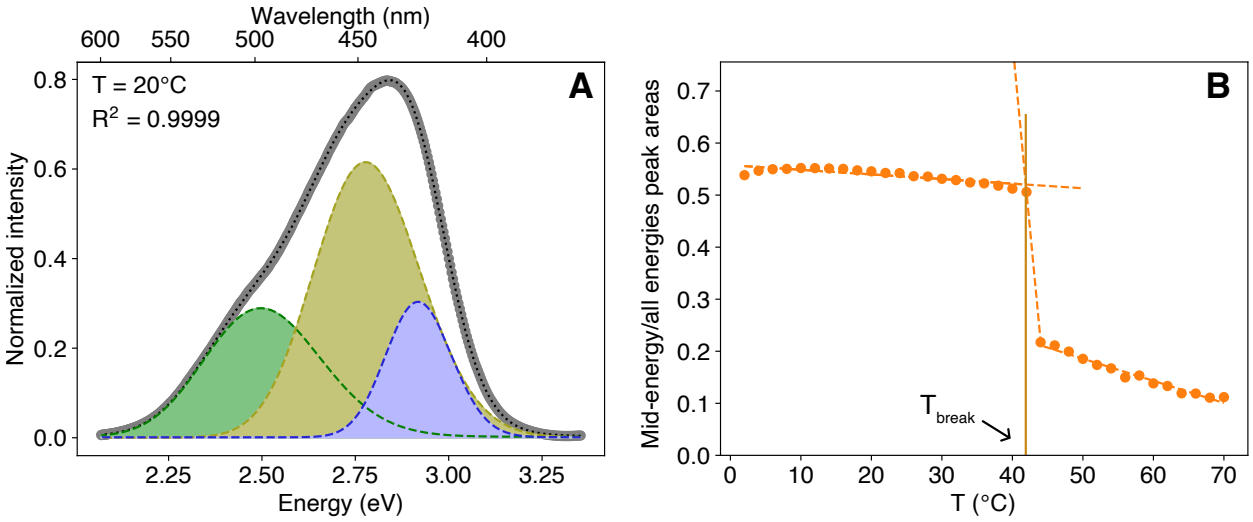

Figure 1. Application of multipeak analysis to laurdan fluorescence emission spectra for vesicles composed of 27.5-37.5-35 mol% PBdPEO1800$^{(-)}$-egg SM-cholesterol in 5 mM HEPES/0.5 mM EDTA, pH 7. A. Sample decomposition of laurdan emission spectrum into three peaks at 20 ºC, showing low (green), mid- (gold), and high energy (blue) peaks. B. Temperature dependence of the ratio of the area of the mid-energy peak to the sum of all three peak areas. Vertical line denotes T_{break}.

For hybrid vesicles, we additionally suggested the slope of the peak area ratio plot (e.g., Figure 1B) in the vicinity of T_{break} provides insight into whether phase separation proceeds by nucleation and growth or spinodal decomposition [16]. Compositions displaying a gradual change in slope around T_{break} showed domains in GUVs that were characteristic of phase separation via spinodal decomposition. On the other hand, a discontinuity around T_{break}, like that shown in Figure 1B, was observed for vesicles hypothesized to undergo phase separation by nucleation and growth [16].

4.3.2 Low salt/long Debye length conditions

T_{break} values were first compared for LUVs composed of 27.5-37.5-35 mol% PBdPEO1800$^{(-)}$- or PBdPEO1800-egg SM-cholesterol across a range of pH values in low salt conditions (Figure 2).

The Debye length in the buffers used ranged from ~5.9-6.1 nm, which is much larger than the distance between adjacent molecules within the membrane. Significant dependence of T_{break} on pH was observed for vesicles containing carboxyl-terminated PBdPEO1800$^{(-)}$, with T_{break} decreasing from ~50 ºC to ~38 ºC as the pH increased from 5.9 to 9.5. This is suggestive of electrostatic repulsion influencing the phase behavior of the membrane. At high pH, a greater fraction of dissociated carboxyl groups would be expected, resulting in electrostatic repulsion introducing competing pressure against the free energy of mixing. A pK_a of ~3-5 is typically expected for carboxylic acids, and this agrees well with the rapid decrease of T_{break} as the pH increases from 5.9 to 7.

For vesicles containing non-carboxyl-terminated PBdPEO1800, however, significant dependence of T_{break} on pH was not observed.

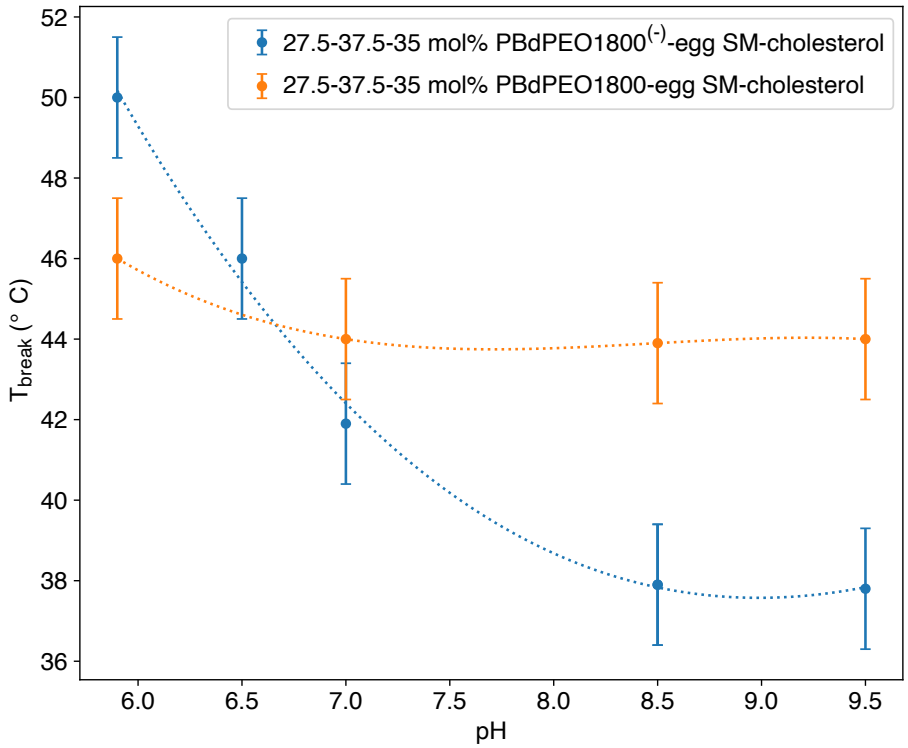

Figure 2. pH dependence of T_{break} values obtained in low salt/long Debye length (~5.9-6.1 nm) conditions for vesicles containing either a carboxyl-terminated (PBdPEO1800$^{(-)}$, blue) or non-carboxyl-terminated (PBdPEO1800, orange) block copolymer. Lines are included only to guide the eye, not as a representation of a fit to any specific equation. Error bars represent the largest standard deviation in T_{break} observed for repeated experiments under selected conditions for selected compositions.

Interestingly, at the lowest pH studied (pH 5.9), T_{break} was higher for vesicles containing PBdPEO1800$^{(-)}$ than for vesicles containing PBdPEO1800. We speculate that this may be due to hydrogen bonding between protonated carboxyl groups at the terminus of the PEO block of PBdPEO1800$^{(-)}$. At sufficiently low pH, an increasing fraction of the carboxyl groups should be protonated and may be capable of participating in hydrogen bonding. Enhanced intermolecular hydrogen bonding capabilities have been suggested to contribute to the elevated phase transition temperature of the lipid palmitoyl dihydrosphingomyelin in comparison to palmitoyl sphingomyelin [14,22]. Along these lines, we hypothesize it is possible that hydrogen bonding

between protonated carboxyl groups may be similarly contributing to increases in the observed T_{break} at low pH.

4.3.3 pH, Debye length, and composition varied for PBdPEO1800$^{(-)}$ or PBdPEO1800-egg SM-cholesterol vesicles

To further investigate the effects of pH and salt concentration on vesicle phase behavior, contour plots of T_{break} values were constructed for vesicles composed of 27.5-37.5-35 mol% PBdPEO1800$^{(-)}$- or PBdPEO1800-egg SM-cholesterol (Figure 3).

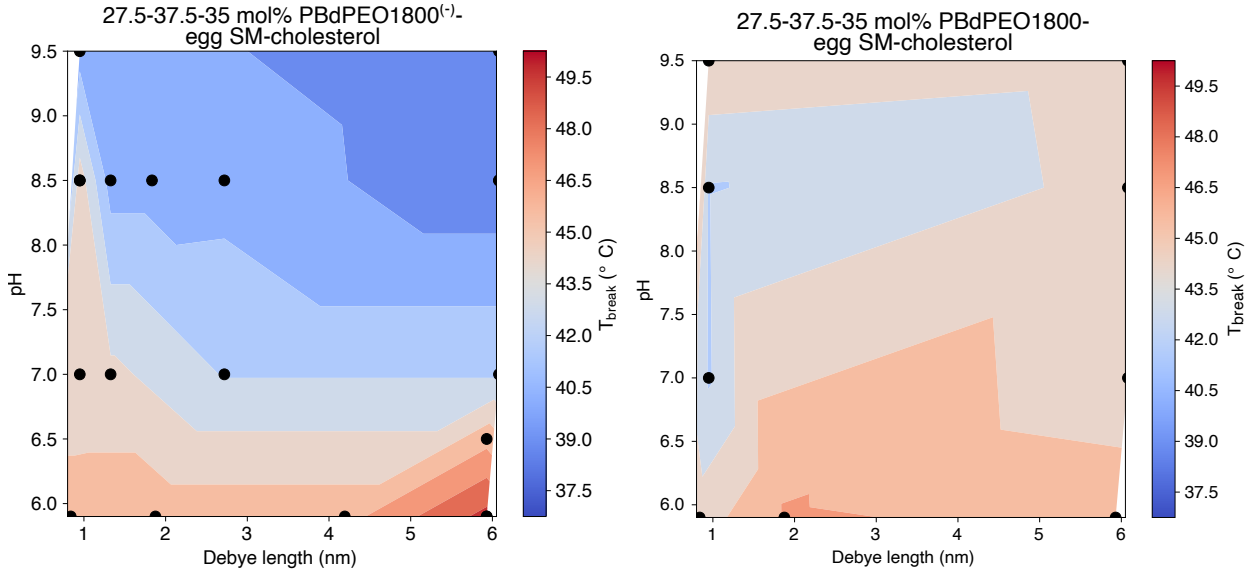

Figure 3. Contour plots of T_{break} values for LUVs composed of 27.5-37.5-35 mol% PBdPEO1800$^{(-)}$-egg SM-cholesterol (left) or PBdPEO1800-egg SM-cholesterol (right) for a range of pH values and Debye lengths. Greater Debye lengths exist at lower salt concentrations. Vesicles contained either a carboxyl-terminated (PBdPEO1800$^{(-)}$) or non-carboxyl-terminated (PBdPEO1800) block copolymer. Black dots represent results from individual experiments. The uncertainty in T_{break} values is expected to be ±1.5 °C.

For vesicles containing PBdPEO1800$^{(-)}$, both pH and salt concentration were observed to influence T_{break} (Figure 3, left). In the case of greater Debye lengths (i.e., in low salt conditions), T_{break} displayed significant dependence on pH, spanning a range of ~10 °C. At high pH and long Debye

lengths, where the effects of electrostatic repulsion between dissociated carboxyl groups should be maximally realized, T_{break} values were low. As the pH was decreased while maintaining constant Debye lengths, T_{break} values increased. Interestingly, at pH 5.9, T_{break} increased instead of decreased as the Debye length increased. As previously discussed, we speculate this may be the result of hydrogen bonding between protonated carboxyl groups.

At the shortest Debye lengths studied (i.e., in high salt conditions), the dependence of observed T_{break} values on pH was weaker, with T_{break} spanning ~5 ºC. In high salt conditions, it is possible that interactions between sodium ions and lipids may be taking place to some extent. This is only expected to have a significant effect on membrane properties (e.g., increasing the order of the lipids and potentially increasing T_{break}) above a sodium concentration of 50 mM, corresponding to a Debye length less than ~1.4 nm [23]. As pH was varied for the shortest Debye length conditions, the same general trends were still observed as for the longer Debye length conditions, however, with T_{break} decreasing slightly as the pH increased.

Vesicles containing PBdPEO1800 instead of PBdPEO1800$^{(-)}$ did not appear to display clear trends in the pH and Debye length dependence of T_{break} (Figure 3, right). For vesicles containing PBdPEO1800, T_{break} spanned a range of approximately 4 ºC across the conditions studied, suggesting weak dependence, if any, on pH or salt concentration. This is similar to the range observed for vesicles containing PBdPEO1800$^{(-)}$ in short Debye length conditions, where electrostatic effects might be expected to contribute minimally to vesicle phase behavior.

The pH and Debye length dependences of T_{break} for vesicles containing PBdPEO1800$^{(-)}$ suggest that electrostatic repulsion between charged polymer molecules contributes to decreasing T_{break}

values. At the shortest Debye lengths studied (~0.84-0.95 nm), the Debye length is on the order of the distance between adjacent molecules within the membrane. At the lowest electrolyte concentrations shown in Figure 3, however, the Debye length ranges from 4-6 nm. The effects of electrostatic repulsion would therefore be expected to be observed much more strongly in conditions with long Debye lengths. Additionally, carboxylic acids typically have a pKa of ~3-5, although this has been reported to be higher, closer to pH 5.5, for carboxyl groups in proximity to the hydrophobic membrane core [24]. The fraction of dissociated carboxyl groups may therefore be changing as the pH changes across the range studied here. At high pH, a larger fraction of carboxyl groups would be expected to be dissociated. However, the lowest pH (5.9) studied is likely approaching the pK_a of the carboxyl group, where far fewer charged PBdPEO1800$^{(-)}$ molecules would exist.

The individual peak area ratio plots used to assess the T_{break} values plotted in Figure 3 displayed discontinuities around T_{break} for all conditions studied for this composition; a selection of representative peak area ratio plots is shown in Figure S1. We previously suggested that such discontinuities are indicative of phase separation by nucleation and growth [16]. Phase separation has also been speculated to proceed by nucleation and growth for GUVs composed of a 5:3:2 ratio of PBdPEO of 3800 g/mol average molecular weight, DPPC, and cholesterol [7]. Interestingly, we previously found that vesicles of the same polymer-egg SM-cholesterol ratio as those shown in Figure 1, which incorporated the lower molecular weight polymer PBdPEO950 instead of PBdPEO1800, demonstrated a gradual change in slope rather than a discontinuity around T_{break} [16]. This suggests differences in the phase behavior of hybrid vesicles incorporating block

copolymers of differing molecular weights, likely due to the resultant difference in hydrophobic mismatch between the lipid and polymer membranes [25].

Similar trends in T_{break} values were observed for vesicles composed of 50-25-25 mol% PBdPEO1800$^{(-)}$- or PBdPEO1800-egg SM-cholesterol (Figure 4). This composition was selected to investigate whether the electrostatic effects observed for the first composition would present more strongly upon increasing the ratio of carboxyl-terminated copolymer to egg SM/cholesterol. For vesicles containing PBdPEO1800$^{(-)}$, T_{break} decreased with increasing pH for conditions with longer Debye lengths. A much weaker dependence of T_{break} on pH was observed for conditions with shorter Debye lengths, likely due to screening of electrostatic interactions between charged PBdPEO1800$^{(-)}$ molecules. As in Figure 3, clear trends in pH or Debye length dependence of T_{break} were not observed for vesicles composed of 50-25-25 PBdPEO1800-egg SM-cholesterol.

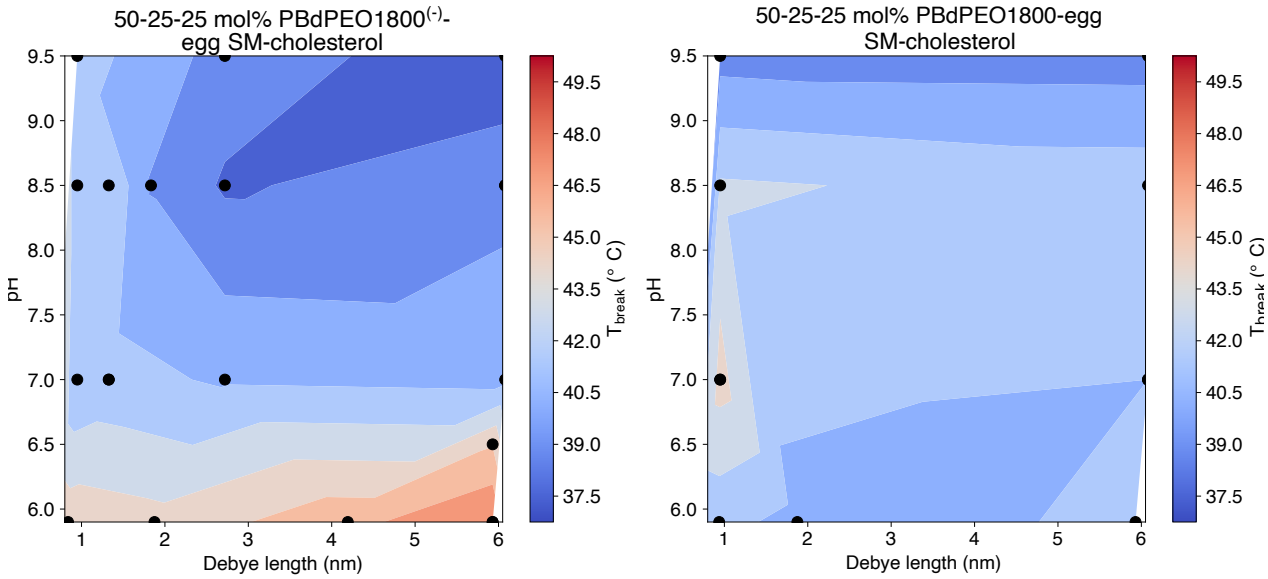

Figure 4. Contour plots for LUVs composed of 50-25-25 mol% PBdPEO1800$^{(-)}$-egg SM-cholesterol (left) or PBdPEO1800-egg SM-cholesterol (right). Black dots represent results from individual experiments. The uncertainty in T_{break} values is expected to be ±1.5 ºC.

Generally, T_{break} values were lower than observed for the 27.5-37.5-35 mol% composition for vesicles containing either PBdPEO1800$^{(-)}$ or PBdPEO1800. For the 27.5-37.5-35 mol% PBdPEO1800$^{(-)}$-egg SM-cholesterol vesicles, PBdPEO1800$^{(-)}$ makes up two of every five non-cholesterol molecules at the hydrophilic surface of the membrane; this is increased to roughly two of every three non-cholesterol molecules for the 50-25-25 mol% PBdPEO1800$^{(-)}$-egg SM-cholesterol vesicles resulting in greater electrostatic repulsion.

Peak area ratio plots for 50-25-25 mol% PBdPEO1800$^{(-)}$-egg SM-cholesterol at longer and shorter Debye lengths are additionally compared in Figure S2. These display discontinuities around T_{break}, indicative of nucleation and growth, as we have found for all conditions studied for this composition with both carboxylated and non-carboxylated PBdPEO1800. We also previously observed a similar discontinuity in the vicinity of T_{break} for vesicles composed of 50-25-25 mol% PBdPEO950-egg SM-cholesterol, as well as for samples in the nearby compositional space [16].

Significant dependence of T_{break} on pH was observed in long Debye length conditions for both 27.5-37.5-35 mol% and 50-25-25 mol% PBdPEO1800$^{(-)}$-egg SM-cholesterol (Figure 5). T_{break} displayed a rapid decrease as the pH increased from 5.9 to 8.5. However, T_{break} did not display significant dependence on pH between pH 8.5 and pH 9.5. This could suggest an increasing fraction of PBdPEO1800$^{(-)}$ being deprotonated as the pH increases, with this fraction reaching saturation between pH 7 and 8.5. As mentioned previously, carboxylic acids typically have pK_a values of ~3-5 and it is possible that the closer proximity of the PBdPEO1800$^{(-)}$ carboxyl group to the hydrophobic membrane core could increase this; for example, the carboxyl in the headgroup of the lipid DMPS has been reported to have a pK_a of ~5.5, likely for this reason [24].

The observation of pH dependence of T_{break} in the pH range 5.9-7 may be of especial interest for biomedical applications such as the design of pH-responsive drug delivery vehicles. Even in conditions with a short Debye length, a small increase in T_{break} beyond the expected uncertainty value was observed for the 50-25-25 mol% PBdPEO1800$^{(-)}$-egg SM-cholesterol vesicles as the pH decreased from 7 to 5.9 (Figure 5). Physiological salt concentration (~150 mM NaCl) corresponds to a Debye length of ~ 0.8 nm, comparable to the ~0.84-0.95 nm Debye lengths studied here. This suggests the inclusion of relatively large amounts of charged molecules might have the ability to drive phase separation of vesicles in response to a change in pH, such as that experienced during endosomal acidification, even in biologically relevant ionic strength conditions.

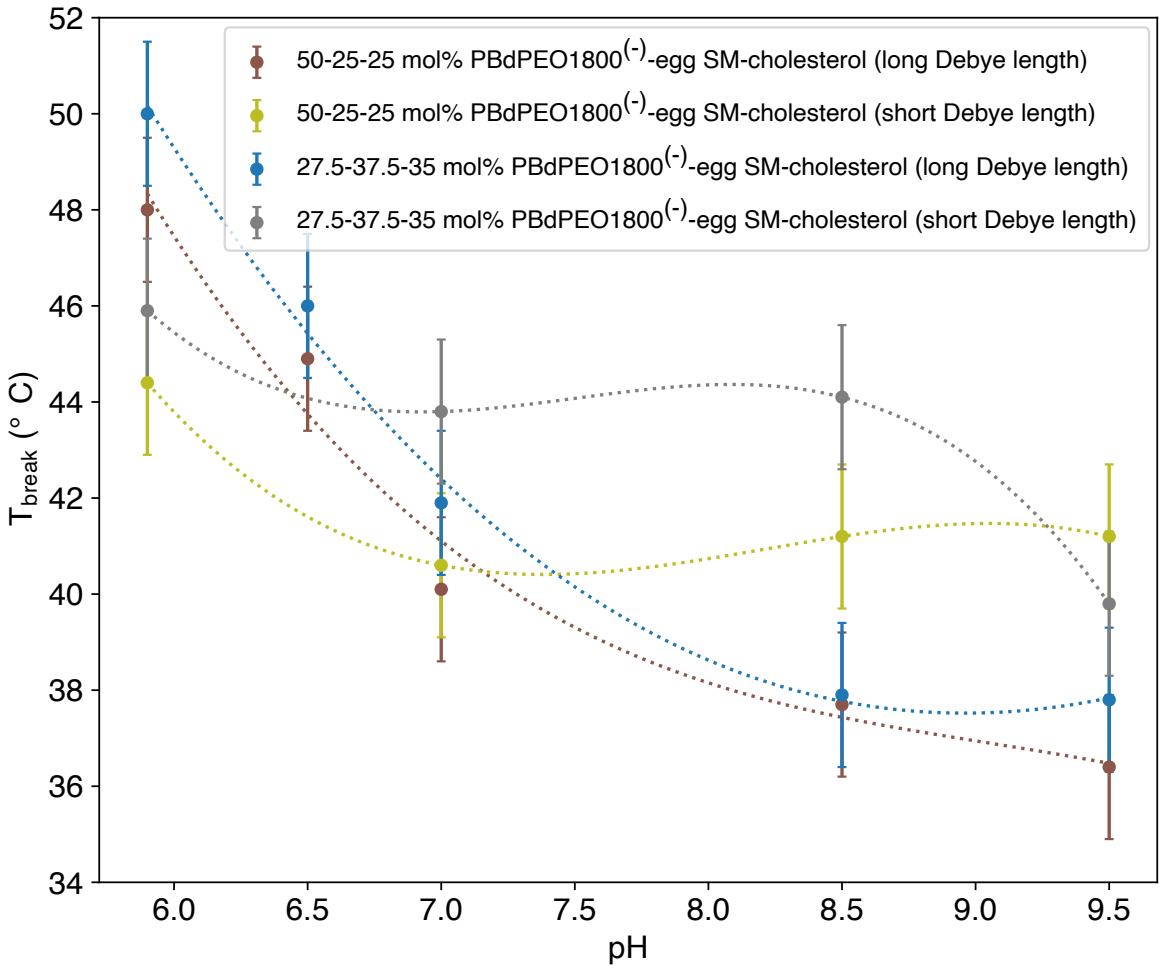

Figure 5. Comparison of pH dependence of T_{break} in conditions with long (~6 nm) and short (~0.84-0.95 nm) Debye lengths for vesicles containing either 50-25-25 (green) or 27.5-37.5-35 (blue) mol% PBdPEO1800$^{(-)}$-egg SM-cholesterol. Error bars represent the largest standard deviation in T_{break} observed for repeated experiments under selected conditions for selected compositions.

4.3.4 Ratio of PBdPEO1800$^{(-)}$ to PBdPEO1800 and molecular weight of PBdPEO varied

We additionally examined the effects of replacing PBdPEO1800 with increasing amounts of PBdPEO1800$^{(-)}$ while maintaining the overall vesicle composition (i.e., the ratios of polymer, lipid, and cholesterol). Figure 6 shows T_{break} values for 27.5-37.5-35 mol% PBdPEO1800-egg SM-cholesterol with increasing amounts of PBdPEO1800$^{(-)}$ replacing PBdPEO1800 in a pH 9.5 buffer

with either 0 mM NaCl added (long Debye length) or 100 mM NaCl added (short Debye length). Generally, T_{break} decreased more rapidly upon addition of increasing amounts of PBdPEO1800$^{(-)}$ in the low salt condition. It is interesting to note that upon the incorporation of 10 mol% PBdPEO1800$^{(-)}$, a small increase in T_{break} was observed for both 0 mM and 100 mM NaCl conditions, although still less than the uncertainty value. It is possible that this does represent a genuine effect, perhaps arising from differences in the molecular weight distributions of PBdPEO1800 and PBdPEO1800$^{(-)}$; the latter has a broader distribution, so the presence of larger molecular weight PBdPEO1800$^{(-)}$ molecules might result in slightly increased T_{break} values before the effects of electrostatic repulsion were significant enough to compete with the energy of mixing. Upon incorporation of 20 mol% PBdPEO1800$^{(-)}$, however, a significantly lower T_{break} value was observed for the 0 mM NaCl condition than for the 100 mM NaCl condition. This is consistent with the greater strength of electrostatic effects at lower ionic strength and longer Debye lengths.

Interestingly, the replacement of a similar non-carboxyl-terminated PBdPEO with carboxyl-terminated PBdPEO in hybrid DOPC/dioleoylphosphatidylserine/PBdPEO vesicles has been recently observed to result in a moderate decrease in zeta potential at pH 7.4 [26]. Conversely, the zeta potential at pH 7 of vesicles combining diphytanoylphosphatidylcholine and 1000 g/mol carboxyl-terminated PBdPEO has been reported not to display significant dependence on the mole percentage of carboxyl-terminated PBdPEO [27]. One key difference between these studies is that the solution salt concentration, which strongly impacts the magnitude and therefore the observable dynamic range of the zeta potential, is roughly doubled in the latter, emphasizing the importance of Debye length in the consideration of charge-related phenomena. Additionally, the weaker effects observed at pH 7 in both studies are consistent with our observation of the absence of a

significant difference in T_{break} for vesicles containing either PBdPEO1800$^{(-)}$ or PBdPEO1800 at pH 7 (Figure 2).

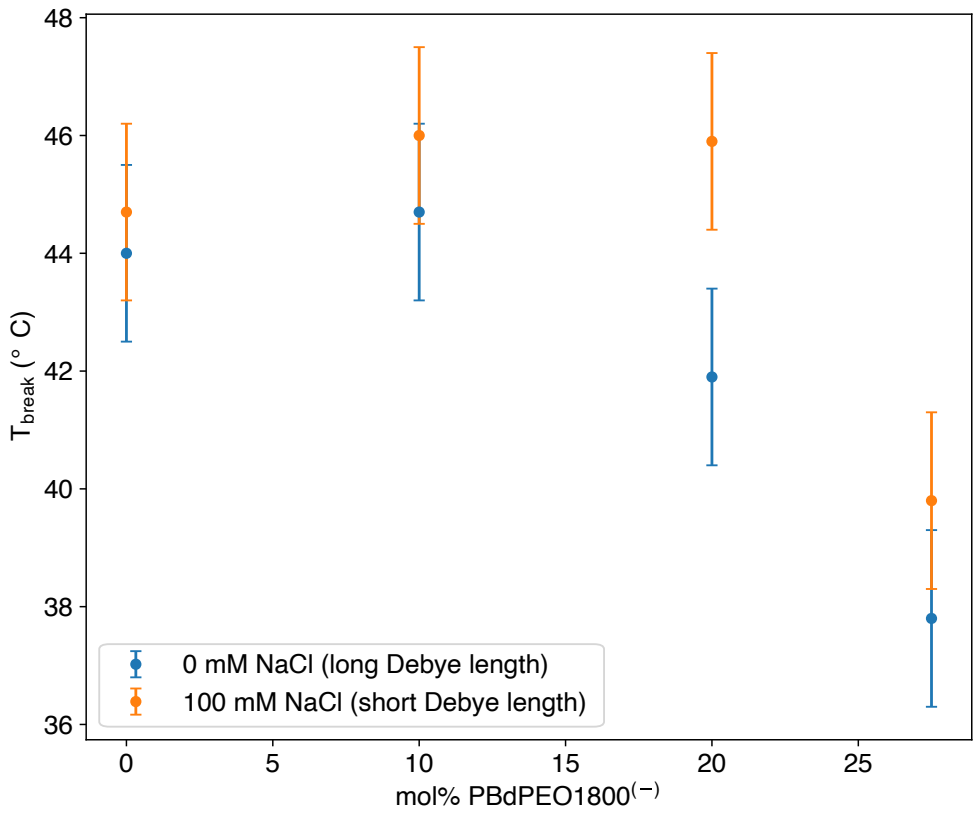

Figure 6. T_{break} values for 27.5-37.5-35 mol% PBdPEO1800-egg SM-cholesterol with increasing amounts of PBdPEO1800$^{(-)}$ replacing PBdPEO1800 in 5 mM glycine/0.5 mM EDTA at pH 9.5, with either 0 mM NaCl added (long Debye length) or 100 mM NaCl added (short Debye length). The overall composition was maintained at 27.5 mol% polymer. Error bars represent the largest standard deviation in T_{break} observed for repeated experiments under selected conditions for selected compositions.

Contour plots showing the effects of composition and pH while maintaining similar Debye lengths are shown in Figures S3 and S4. For conditions with longer Debye lengths, clear decreases in T_{break} are evident, especially at higher pH, as more PBdPEO1800$^{(-)}$ is introduced. However, for conditions with shorter Debye lengths, trends in T_{break} are not clearly associated with either pH or composition, consistent with the effects of increased charge screening.

Finally, we examined the effects of incorporating either PBdPEO1800 or PBdPEO1800$^{(-)}$ into hybrid vesicles containing a lower molecular weight PBdPEO copolymer (PBdPEO950, average molecular weight 950 g/mol) at pH 7 and long Debye length. The specified mole percentages (Figure 7) of PBdPEO950 were replaced by PBdPEO1800 or PBdPEO1800$^{(-)}$ in 27.5-37.5-35 mol% PBdPEO950-egg SM-cholesterol vesicles. While vesicles containing only PBdPEO950, egg SM, and cholesterol displayed T_{break} values around 25 ^{o}C, incorporation of either PBdPEO1800 or PBdPEO1800$^{(-)}$ resulted in rapid and significant increases in T_{break}. Vesicles for which 10 mol% of PBdPEO950 was replaced with either PBdPEO1800 or PBdPEO1800$^{(-)}$ had T_{break} values very similar to vesicles whose polymer composition consisted entirely of PBdPEO1800 or PBdPEO1800$^{(-)}$. Interestingly, significant differences were not observed between T_{break} values for vesicles containing either PBdPEO1800 or PBdPEO1800$^{(-)}$, suggesting that at pH 7, the molecular weight difference between PBdPEO950 and PBdPEO1800/PBdPEO1800$^{(-)}$ is the primary factor affecting T_{break}, rather than electrostatic effects. This is also consistent with the similar T_{break} values observed at pH 7 in solutions with long Debye lengths (Figure 2).

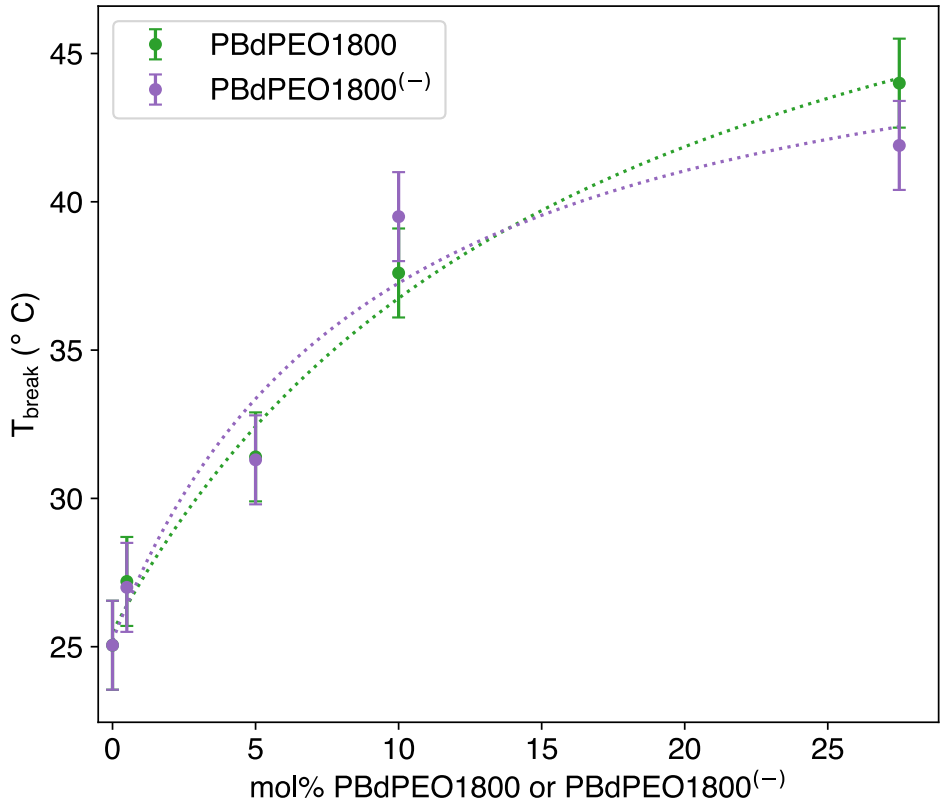

Figure 7. 27.5-37.5-35 mol% PBdPEO950-egg SM-cholesterol with increasing amounts of PBdPEO1800 (green) or PBdPEO1800$^{(-)}$ (purple) replacing PBdPEO950 at pH 7 in a long Debye length (5 mM HEPES/0.5 mM EDTA) buffer. Lines included only to guide the eye. Error bars represent the largest standard deviation in T_{break} observed for repeated experiments under selected conditions for selected compositions.

Significant changes have been reported in the physical properties of polymer membranes as the molecular weight increases, and likely contribute to the prominent dependence of T_{break} on polymer molecular weight observed in Figure 7. PBdPEO with an average molecular weight of 1800 g/mol has been observed to result in a significant decrease of the diffusion coefficient within the membrane upon combination with POPC compared to PBdPEO with an average molecular weight of 1150 g/mol [28]. Indeed, the viscosity of GUVs composed of 1800 g/mol PBdPEO has been reported to be nearly 50 times greater than that of GUVs composed of 1050 g/mol PBdPEO (which had a viscosity only slightly higher than pure POPC GUVs) [29]. An increase in membrane

hydrophobic thickness of ~1.7 nm is predicted for poly(ethylethylene)-PEO block copolymers as the hydrophobic block molecular weight increases from 500 to 1000 g/mol [30]. This is comparable to the difference in the hydrophobic block molecular weights of PBdPEO950 and PBdPEO1800 (600 g/mol and 1200 g/mol, respectively). Poly(ethylethylene) shares a nearly identical structure to poly(1,2-butadiene). The only difference is saturation of the pendant carbon-carbon double bond in the former, so it is likely that a similar difference in hydrophobic thickness would be expected between PBdPEO950 and PBdPEO1800. Hybrid lipid/polymer vesicles incorporating PEO-PDMS-PEO triblock copolymers of varying molecular weights have also previously displayed phase behavior that depended strongly on the polymer molecular weight, which the authors attributed to the effects of molecular weight on domain line tension and membrane fluidity [25].

4.4 Conclusions

The pH, salt concentration, and compositional dependence of the phase behavior of hybrid vesicles was examined via multipeak analysis of laurdan emission spectra. The analysis yielded temperature breakpoint values (T_{break}) expected to be within the range of phase transition temperatures. While in long Debye length conditions (i.e., at low salt concentrations), the observed T_{break} values depended strongly on pH for vesicles containing carboxyl-terminated PBdPEO1800$^{(-)}$, only weak variation was observed in short Debye length conditions. This variation in T_{break} at short Debye length was similar to the range of variation observed for vesicles containing neutral PBdPEO1800, which did not display strong dependence of T_{break} on pH or Debye length. However,

polymer molecular weight appeared to have a greater impact on T_{break} than either pH or Debye length did. Interestingly, though, an increase of 2-4 ^{o}C was still observed for T_{break} as the pH was reduced from 7 to 5.9 even in physiologically relevant ionic strength conditions for vesicles containing significant amounts of PBdPEO1800$^{(-)}$. This work has potential applications toward the design of pH-sensitive vesicles for drug delivery and contributes to the relatively limited body of work regarding the phase behavior of cholesterol-containing hybrid membranes.

4.5 Acknowledgements

This material is based upon work supported by the National Science Foundation under Grant No. DMR – 1806366.

Appendix A. Supplementary data

Supplementary data to this article can be found online.

4.6 References

[1] M.L. Jacobs, M.A. Boyd, N.P. Kamat, Diblock copolymers enhance folding of a mechanosensitive membrane protein during cell-free expression, Proc. Natl. Acad. Sci. 116 (2019) veatch kl. https://doi.org/10.1073/pnas.1814775116.

[2] S. Khan, M. Li, S.P. Muench, L.J.C. Jeuken, P.A. Beales, Durable proteo-hybrid vesicles for the extended functional lifetime of membrane proteins in bionanotechnology, Chem. Commun. 52 (2016) 11020–11023. https://doi.org/10.1039/C6CC04207D.

[3] S. Khan, J. McCabe, K. Hill, P.A. Beales, Biodegradable hybrid block copolymer – lipid vesicles as potential drug delivery systems, J. Colloid Interface Sci. 562 (2020) 418–428. https://doi.org/10.1016/j.jcis.2019.11.101.

[4] T.Q. Vu, J.A. Peruzzi, L.E. Sant'Anna, E.W. Roth, N.P. Kamat, Lipid Phase Separation in Vesicles Enhances TRAIL-Mediated Cytotoxicity, Nano Lett. (2022). https://doi.org/10.1021/acs.nanolett.1c04365.

[5] Z.I. Imam, L.E. Kenyon, G. Ashby, F. Nagib, M. Mendicino, C. Zhao, A.K. Gadok, J.C. Stachowiak, Phase-Separated Liposomes Enhance the Efficiency of Macromolecular Delivery to the Cellular Cytoplasm, Cell. Mol. Bioeng. 10 (2017) 387–403. https://doi.org/10.1007/s12195-017-0489-4.

[6] S.L. Veatch, S.L. Keller, Seeing spots: Complex phase behavior in simple membranes, Biochim. Biophys. Acta BBA - Mol. Cell Res. 1746 (2005) 172–185. https://doi.org/10.1016/j.bbamcr.2005.06.010.

[7] J. Nam, T.K. Vanderlick, P.A. Beales, Formation and dissolution of phospholipid domains with varying textures in hybrid lipo-polymersomes, Soft Matter. 8 (2012) 7982–7988. https://doi.org/10.1039/c2sm25646k.

[8] T.P.T. Dao, F. Fernandes, M. Er-Rafik, R. Salva, M. Schmutz, A. Brûlet, M. Prieto, O. Sandre, J.-F. Le Meins, Phase Separation and Nanodomain Formation in Hybrid Polymer/Lipid Vesicles, ACS Macro Lett. 4 (2015) 182–186. https://doi.org/10.1021/mz500748f.

[9] C. Magnani, C. Montis, G. Mangiapia, A.-F. Mingotaud, C. Mingotaud, C. Roux, P. Joseph, D. Berti, B. Lonetti, Hybrid vesicles from lipids and block copolymers: Phase behavior from the micro- to the nano-scale, Colloids Surf. B Biointerfaces. 168 (2018) 18–28. https://doi.org/10.1016/j.colsurfb.2018.01.042.

[10] D. Chen, M.M. Santore, Hybrid copolymer–phospholipid vesicles: phase separation resembling mixed phospholipid lamellae, but with mechanical stability and control, Soft Matter. 11 (2015) 2617–2626. https://doi.org/10.1039/C4SM02502D.

[11] N. Hamada, S. Gakhar, M.L. Longo, Hybrid lipid/block copolymer vesicles display broad phase coexistence region, Biochim. Biophys. Acta BBA - Biomembr. 1863 (2021) 183552. https://doi.org/10.1016/j.bbamem.2021.183552.

[12] T. Parasassi, E.K. Krasnowska, L. Bagatolli, E. Gratton, Laurdan and Prodan as Polarity-Sensitive Fluorescent Membrane Probes, J. Fluoresc. 8 (1998) 365–373. https://doi.org/10.1023/A:1020528716621.

[13] N. Puff, G. Staneva, M.I. Angelova, M. Seigneuret, Improved Characterization of Raft-Mimicking Phase-Separation Phenomena in Lipid Bilayers Using Laurdan Fluorescence with Log-Normal Multipeak Analysis, Langmuir. 36 (2020) 4347–4356. https://doi.org/10.1021/acs.langmuir.0c00412.

[14] N. Watanabe, Y. Goto, K. Suga, T.K.M. Nyholm, J.P. Slotte, H. Umakoshi, Solvatochromic Modeling of Laurdan for Multiple Polarity Analysis of Dihydrosphingomyelin Bilayer, Biophys. J. 116 (2019) 874–883. https://doi.org/10.1016/j.bpj.2019.01.030.

[15] R.B.M. Koehorst, R.B. Spruijt, M.A. Hemminga, Site-Directed Fluorescence Labeling of a Membrane Protein with BADAN: Probing Protein Topology and Local Environment, Biophys. J. 94 (2008) 3945–3955. https://doi.org/10.1529/biophysj.107.125807.

[16] N. Hamada, M.L. Longo, Characterization of phase separation phenomena in hybrid lipid/block copolymer/cholesterol bilayers using laurdan fluorescence with log-normal multipeak analysis, Biochim. Biophys. Acta BBA - Biomembr. 1864 (2022) 183887. https://doi.org/10.1016/j.bbamem.2022.183887.

[17] M.C. Blosser, J.B. Starr, C.W. Turtle, J. Ashcraft, S.L. Keller, Minimal Effect of Lipid Charge on Membrane Miscibility Phase Behavior in Three Ternary Systems, Biophys. J. 104 (2013) 2629–2638. https://doi.org/10.1016/j.bpj.2013.04.055.

[18] J. Mooney, P. Kambhampati, Get the Basics Right: Jacobian Conversion of Wavelength and Energy Scales for Quantitative Analysis of Emission Spectra, J. Phys. Chem. Lett. 4 (2013) 3316–3318. https://doi.org/10.1021/jz401508t.

[19] A.D. Lúcio, C.C. Vequi-Suplicy, R.M. Fernandez, M.T. Lamy, Laurdan Spectrum Decomposition as a Tool for the Analysis of Surface Bilayer Structure and Polarity: a Study with DMPG, Peptides and Cholesterol, J. Fluoresc. 20 (2010) 473–482. https://doi.org/10.1007/s10895-009-0569-5.

[20] Jacob N. Israelachvili, Intermolecular and Surface Forces, 3rd ed., Academic Press, 2011.

[21] E. Stellwagen, J.D. Prantner, N.C. Stellwagen, Do zwitterions contribute to the ionic strength of a solution?, Anal. Biochem. 373 (2008) 407–409. https://doi.org/10.1016/j.ab.2007.10.038.

[22] T. Nyholm, M. Nylund, A. Söderholm, J.P. Slotte, Properties of Palmitoyl Phosphatidylcholine, Sphingomyelin, and Dihydrosphingomyelin Bilayer Membranes as Reported by Different Fluorescent Reporter Molecules, Biophys. J. 84 (2003) 987–997. https://doi.org/10.1016/S0006-3495(03)74915-7.

[23] S. Garcia-Manyes, G. Oncins, F. Sanz, Effect of Ion-Binding and Chemical Phospholipid Structure on the Nanomechanics of Lipid Bilayers Studied by Force Spectroscopy, Biophys. J. 89 (2005) 1812–1826. https://doi.org/10.1529/biophysj.105.064030.

[24] D. Marsh, Phospholipid pK s, in: Handb. Lipid Bilayers, Routledge Handbooks Online, 2013. https://doi.org/10.1201/9781420088335-8.

[25] T.P.T. Dao, F. Fernandes, E. Ibarboure, K. Ferji, M. Prieto, O. Sandre, J.-F. Le Meins, Modulation of phase separation at the micron scale and nanoscale in giant polymer/lipid hybrid unilamellar vesicles (GHUVs), Soft Matter. 13 (2017) 627–637. https://doi.org/10.1039/C6SM01625A.

[26] K.L. Willes, S.A. McFarland, T.E. Johnson, D.R. Hart, W.F. Paxton, Modulating and Modeling the Surface ζ Potential of Hybrid Lipid/Polymer Nanovesicles: Implications for Surface

Modification and Drug Delivery, ACS Appl. Nano Mater. (2022). https://doi.org/10.1021/acsanm.2c01407.

[27] S. Koner, J. Tawfik, F. Mashali, K.B. Kennison, W.T. McClintic, F.A. Heberle, Y.-M. Tu, M. Kumar, S.A. Sarles, Homogeneous hybrid droplet interface bilayers assembled from binary mixtures of DPhPC phospholipids and PB-b-PEO diblock copolymers, Biochim. Biophys. Acta BBA - Biomembr. 1864 (2022) 183997. https://doi.org/10.1016/j.bbamem.2022.183997.

[28] R. Seneviratne, R. Catania, M. Rappolt, L.J. C. Jeuken, P. A. Beales, Membrane mixing and dynamics in hybrid POPC/poly(1,2-butadiene- block -ethylene oxide) (PBd- b -PEO) lipid/block co-polymer giant vesicles, Soft Matter. 18 (2022) 1294–1301. https://doi.org/10.1039/D1SM01591E.

[29] H.A. Faizi, R. Dimova, P.M. Vlahovska, A vesicle microrheometer for high-throughput viscosity measurements of lipid and polymer membranes, Biophys. J. 121 (2022) 910–918. https://doi.org/10.1016/j.bpj.2022.02.015.

[30] G. Srinivas, D.E. Discher, M.L. Klein, Self-assembly and properties of diblock copolymers by coarse-grain molecular dynamics, Nat. Mater. 3 (2004) 638–644. https://doi.org/10.1038/nmat1185.

4.7 Supplementary Material

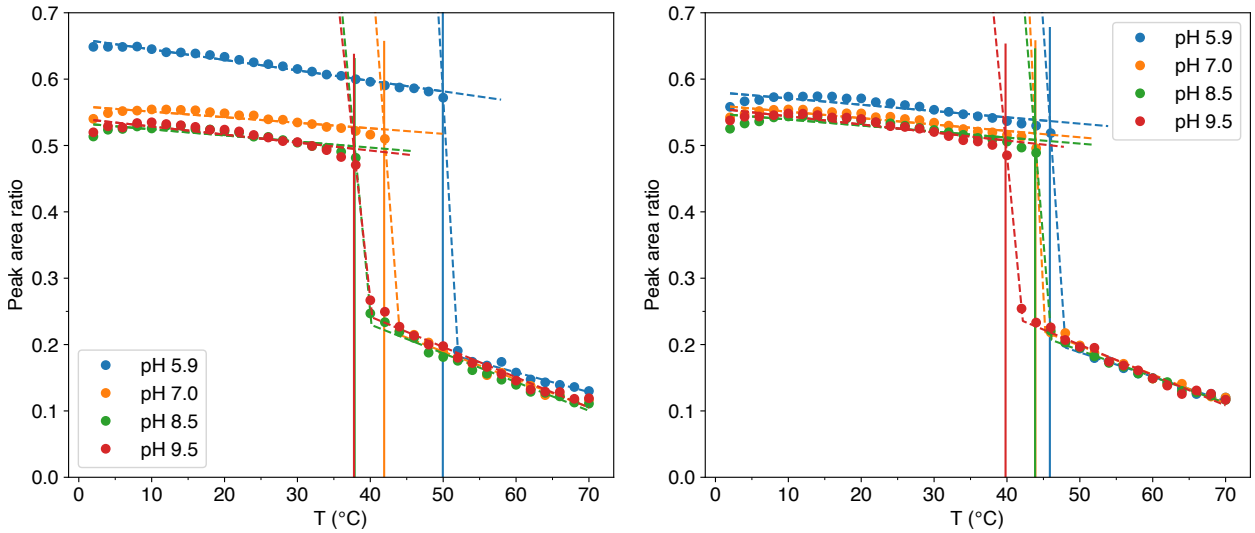

Figure S1. Peak area ratio plots for 27.5-37.5-35 mol% PBdPEO1800$^{(-)}$-egg SM-cholesterol LUVs in long Debye length (left) and short Debye length (right) conditions. "Long Debye length" conditions correspond to Debye lengths of ~5.9-6.1 nm, while "short Debye length" conditions correspond to Debye lengths of ~0.84-0.95 nm.

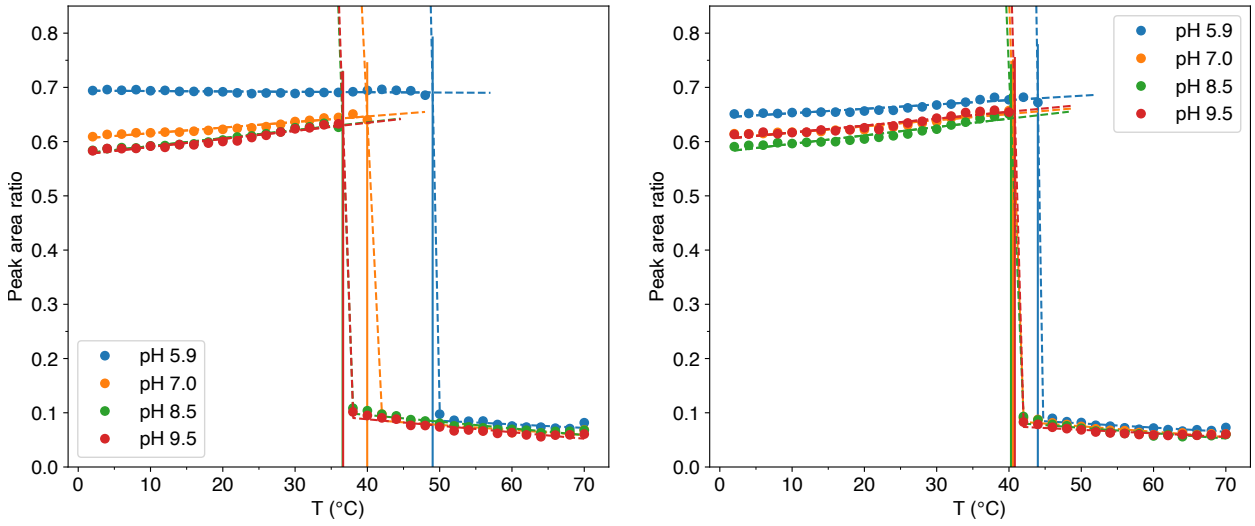

Figure S2. Peak area ratio plots for 50-25-25 mol% PBdPEO1800$^{(-)}$-egg SM-cholesterol LUVs in long Debye length (left) and short Debye length (right) conditions. "Long Debye length" conditions correspond to Debye lengths of ~5.9-6.1 nm, while "short Debye length" conditions correspond to Debye lengths of ~0.84-0.95 nm.

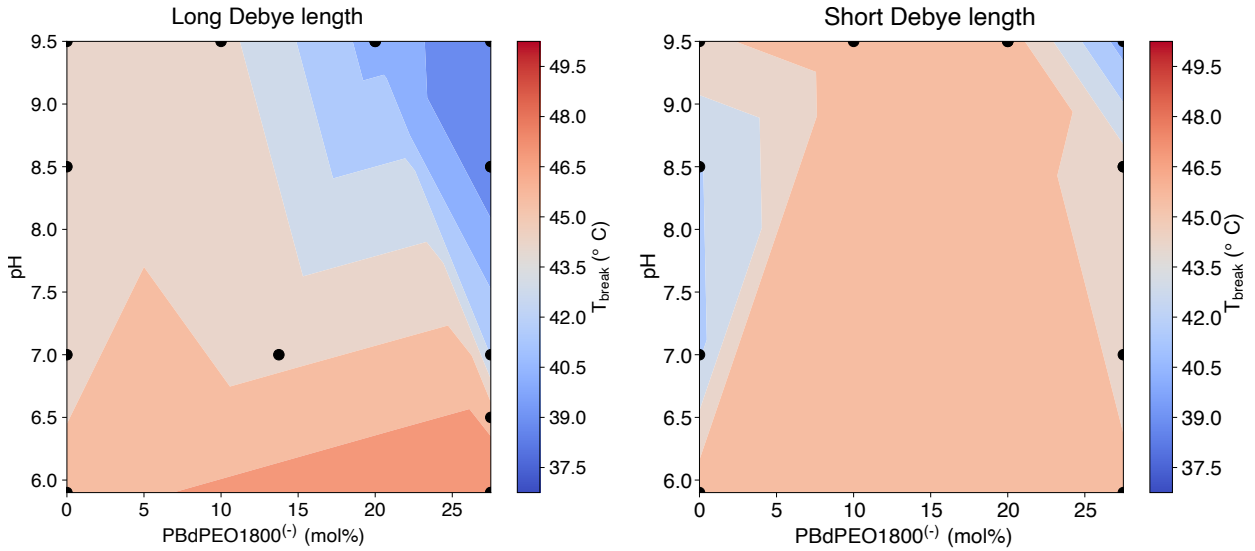

Figure S3. T_{break} values in long and short Debye length conditions as PBdPEO1800 is replaced by increasing amounts of PBdPEO1800$^{(-)}$ in 27.5-37.5-35 mol% PBdPEO1800-egg SM-cholesterol LUVs. "Long Debye length" conditions correspond to Debye lengths of ~5.9-6.1 nm, while "short Debye length" conditions correspond to Debye lengths of ~0.84-0.95 nm.

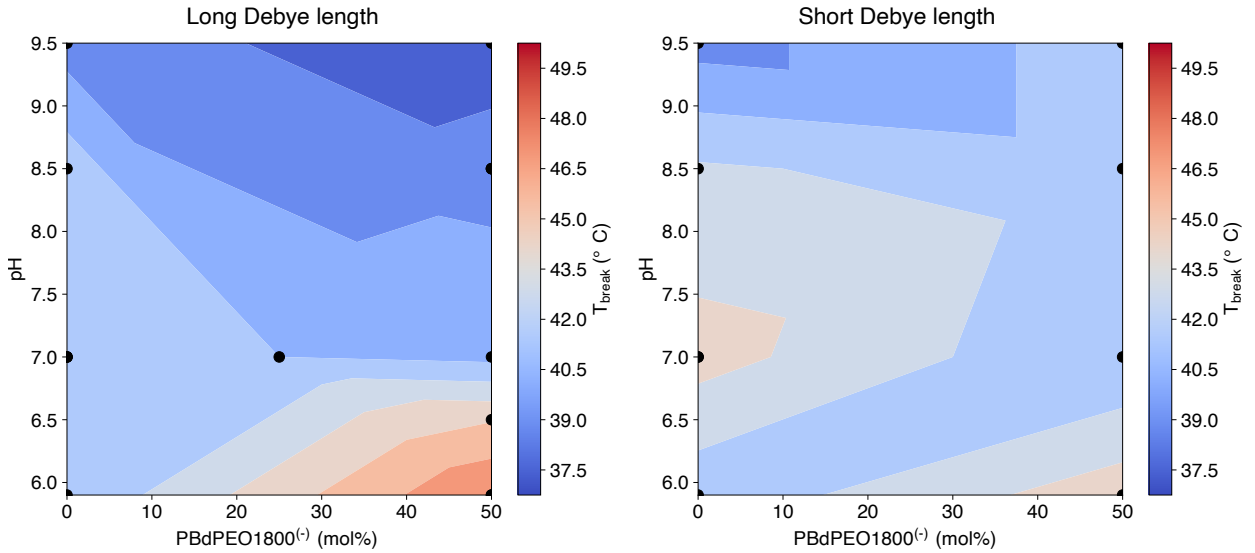

Figure S4. Comparison of T_{break} values in long and short Debye length conditions as PBdPEO1800 is replaced by increasing amounts of PBdPEO1800$^{(-)}$ in 50-25-25 mol% PBdPEO1800-egg SM-cholesterol LUVs. "Long Debye length" conditions correspond to Debye lengths of ~5.9-6.1 nm, while "short Debye length" conditions correspond to Debye lengths of ~0.84-0.95 nm.

Table S1. Hydrodynamic diameters of 27.5-37.5-35 mol% PBdPEO1800$^{(-)}$ or PBdPEO1800-egg SM-cholesterol LUVs as measured by DLS. Mean diameter and one standard deviation were assessed from at least 5 measurements.

Vesicle composition (mol%)	**Buffer**	**Mean diameter (nm)**
27.5-37.5-35 PBdPEO950-egg SM-cholesterol	5 mM HEPES/0.5 mM EDTA/0 mM NaCl, pH 7	113±30
27.5-37.5-35 PBdPEO1800-egg SM-cholesterol	1 mM sodium phosphate/0.5 mM EDTA, pH 5.9	128±25
27.5-37.5-35 PBdPEO1800-egg SM-cholesterol	5 mM HEPES/0.5 mM EDTA/100 mM NaCl, pH 7	115±11
27.5-37.5-35 PBdPEO1800$^{(-)}$-egg SM-cholesterol	1 mM sodium phosphate/0.5 mM EDTA, pH 5.9	116±47
27.5-37.5-35 PBdPEO1800$^{(-)}$-egg SM-cholesterol	5 mM Tris/0.5 mM EDTA/0 mM NaCl, pH 8.5	120±7
27.5-37.5-35 PBdPEO1800$^{(-)}$-egg SM-cholesterol	5 mM Tris/0.5 mM EDTA/100 mM NaCl, pH 8.5	116±14
27.5-37.5-35 PBdPEO1800$^{(-)}$-egg SM-cholesterol	5 mM glycine/0.5 mM EDTA/0 mM NaCl, pH 9.5	117±14

Table S2. Hydrodynamic diameters of 50-25-25 mol% PBdPEO1800$^{(-)}$ or PBdPEO1800-egg SM-cholesterol LUVs as measured by DLS. Mean diameter and one standard deviation were assessed from at least 5 measurements.

Vesicle composition (mol%)	**Buffer**	**Mean diameter (nm)**
50-25-25 PBdPEO1800-egg SM-cholesterol	1 mM sodium phosphate/0.5 mM EDTA, pH 5.9	147±40
50-25-25 PBdPEO1800-egg SM-cholesterol	5 mM HEPES/0.5 mM EDTA/0 mM NaCl, pH 7	116±15
50-25-25 PBdPEO1800-egg SM-cholesterol	5 mM HEPES/0.5 mM EDTA/100 mM NaCl, pH 7	109±19
50-25-25 PBdPEO1800$^{(-)}$-egg SM-cholesterol	1 mM sodium phosphate/0.5 mM EDTA, pH 5.9	136±18
50-25-25 PBdPEO1800$^{(-)}$-egg SM-cholesterol	5 mM HEPES/0.5 mM EDTA/0 mM NaCl, pH 7	137±16
50-25-25 PBdPEO1800$^{(-)}$-egg SM-cholesterol	5 mM Tris/0.5 mM EDTA/0 mM NaCl, pH 8.5	109±18
50-25-25 PBdPEO1800$^{(-)}$-egg SM-cholesterol	5 mM glycine/0.5 mM EDTA/0 mM NaCl, pH 9.5	126±26